2017

A Palynostratigraphic Investigation of Holocene Coastal Texas Bays: Implications for Future Coastal Change

Shannon Marie Ferguson
Louisiana State University and Agricultural and Mechanical College

A Palynostratigraphic Investigation of Holocene Coastal Texas Bays: Implications for Future Coastal Change

A Dissertation

Submitted to the Graduate Faculty of the
Louisiana State University and
Agricultural and Mechanical College
in partial fulfillment of the
requirements for the degree of
Doctor of Philosophy

in

The Department of Geology and Geophysics

by

Shannon M. Ferguson
B.S. Georgia Southern University
M.S. Louisiana State University
August 2017

To my family

ACKNOWLEDGMENTS

I'd like to thank my advisor Dr. Sophie Warny for believing in me throughout these years as well as her continued guidance. Without her I would have never have had this opportunity of a lifetime. I'm extremely thankful to have had a caring mentor who was there for me every step of the way, and who always challenged me to be a better scientist.

I am also grateful to Dr. John Anderson at Rice University and Dr. Alexander Simms at University of California, Santa Barbara for allowing me to use their sediment, and for their through revisions of countless drafts. Without them and their incredible expertise none of this would have been possible. I'd also like to thank Dr. Gilles Escarguel at Universite Claude Bernard Lyon 1for his time, patience, and kindness teaching me all things geostatistical throughout my time at LSU. I would also like to thank my committee Dr. Phillip Bart and Dr. Samuel Bentley for being with me since the beginning of this project, and for providing excellent feedback along the way. I'd also like to extend my thanks to Dr. Torbjörn Törnqvist at Tulane University for providing helpful comments and knowledgeable age model insight.

I am also indebted to many great students at LSU for making these years enjoyable, and to all of the CENEX students I've had the privilege of knowing throughout the years. I'm lucky to have made so many wonderful friends, and to have had the funniest and smartest office-mates.

I truly appreciate the financial support from the Louisiana State University Museum of Natural Science. I also thank the Shell Center for Sustainability at Rice University, and the Louisiana State University Center for Excellence in Palynology (CENEX) Chair Professorship for providing support for radiocarbon and palynological sample processing.

Finally, I would like to thank my family and my wonderful husband and best friend, Crawford. Thank you Crawford for being with me every step of the way. Your endless encouragement, comfort, and much needed comic relief throughout these demanding years have been invaluable to me. Thank you to my parents who encouraged my interests in geology and the sciences from a young age, for teaching me the importance of education, and for always believing in me. Finally, thanks to Emily, Michael, Wendy, Dick, Kate, and Daniel for all your help and support throughout these years, I couldn't have done it without you.

TABLE OF CONTENTS

ABSTRACT

Although the Gulf of Mexico is one of the most studied basins in the world, a majority of the focus has been driven by petroleum exploration and/or on seismic and sedimentological facies models. Rarely has the intent of previous studies been to characterize the Holocene climatic record of coastal Texas. Of those studies that discuss Holocene vegetation change, the majority focus on the Mississippi River Delta, the Edwards Plateau or central Florida, leaving an absence of insight to western Gulf of Mexico climate changes. The Texas coastline stretches 595 km across almost 4° of latitude and the strong northwestern precipitation gradient results in a diverse coastal vegetation assemblage. We provide a detailed palynological record of Holocene climate for southeast and coastal Texas, based upon four subaqueous sediment core transects from within Baffin Bay, Corpus Christ Bay, and Trinity Bay, south to north, respectively. Our marine record from dinoflagellates in Corpus Christi Bay, Texas found convincing evidence that the bay's coastal barrier island was compromised for several hundred years due to a rapid pulse of sea-level rise. Statistical results of combined marine (dinoflagellate) and terrestrial (pollen and spores) records from Trinity Bay, Texas and Corpus Christi Bay, Texas show that they had similarly-composed assemblages, but that these assemblages first appeared at different times. These environments transitioned through the Holocene from herbaceous-dominated assemblages to arboreal-dominated, as early as 8.4 ka within Corpus Christi Bay, and 3.8 ka within Trinity Bay. Furthermore, our results indicate that coastal Texas' climate operated semi-independently from central Texas regions during the Holocene, and is primarily driven by a coast-wise gradient of precipitation and evapotranspiration. A final study of Baffin Bay, Texas shows that it experienced similarly timed vegetative shifts as seen in Corpus Christi Bay, located < 60 km to

the north. Sample-to-sample shifts in arboreal-herbaceous abundances in this record were shown to be likely correlated with the climatic effects of changing solar irradiance.

CHAPTER 1
INTRODUCTION

1.1 Dissertation Context

Worldwide, coastal and low-lying regions face the challenge of rising sea levels in the coming centuries. These areas are some of the most densely populated on Earth, and understanding how they will react is paramount to mitigating the high cost of increased coastal hazards. Studies of how these environments responded to sea level rise following the Last Glacial Maximum (LGM) can offer timely insight. These are much needed considering what we know of past Holocene sea level rise and what is expected for the next century. When controlling for variability from subsidence and potential glacial-isostatic adjustments across the region, the average late Holocene rate of sea level rise for the western Gulf of Mexico has been estimated to range between 0.4 and 0.6 mm/yr (Törnqvist et al., 2004a; Törnqvist et al., 2004b; Tornqvist et al., 2006; Simms et al., 2007; Milliken, 2008; Livsey and Simms, 2013). Modern rates of sea level rise are as much as an order of magnitude higher, and are expected to double by 2100 (Törnqvist and Hijma, 2012; Bamber and Aspinall, 2013; Church et al., 2013; Anderson et al., 2014). Retreat of the Antarctic Ice Sheet alone due to ocean and atmospheric warming is projected to cause >1 m of eustatic sea-level rise by 2100 and as much as 15 m over the next 500 years (DeConto and Pollard, 2016), likely in episodic pulses (Feldmann and Levermann, 2015) that can have catastrophic effects on coastal infrastructure. This dissertation uses palynostratigraphy to observe and describe the climate, vegetation, and eustatic events of the early- to mid-Holocene along coastal Texas, gaining insight into how we can expect the region to respond to future change.

1.2 Explanation of Palynology as a Discipline

Palynology is the study of palynomorphs, which includes: pollen, spores, dinoflagellates, and other microscopic organic organisms. These organic organisms are generally 20 to 80 μm in diameter (rare forms ranging from 5 μm to more than 200 μm) and are deposited in sediment a variety of sedimentary environments (Heusser, 1978). The durability of palynomorphs is profound due to a chemical compound called sporopollenin (dinosporin for dinoflagellate cysts), probably the most chemically inert of organic compounds, which makes up the palynomorphs' walls (Traverse, 1988). Therefore, palynomorphs ability to be preserved and many have a restricted time range throughout the geologic record (serving as index fossils) allowing for their use in stratigraphy, correlation, paleoecology, and other aspects of geology.

1.3 Palynology of Eastern and Coastal Texas

Although the Gulf of Mexico is one of the most well-studied basins in the world, a majority of the focus has been on oil exploration or on seismic and sedimentological facies models. Rarely has the intent of these studies been to characterize the Holocene climatic record of coastal Texas. Of those studies that discuss Holocene vegetation change, the majority focus on either the Mississippi River Delta (Törnqvist and Hijma, 2012), the Edwards Plateau (Cooke et al., 2003), or central Florida (Grimm et al., 2006; Huang et al., 2006; Donders, 2014), leaving an absence of insight to western Gulf of Mexico climate in the Texas region. The strong precipitation gradient along the northwestern Gulf Coast results in a diverse coastal vegetation assemblage (Longley, 1995; Williams et al., 1999). Differences in precipitation and evapotranspiration have traditionally defined four different climatic regions, ranging from humid near the Louisiana

border to semiarid along the coast and to the Mexican border (Thornthwaite, 1948; Williams et al., 1999).

Less than forty palynological studies of Quaternary Texas deposits have been published since the emergence of the discipline in the 1940s. Many of these studies are old in the context of modern analytical techniques (Potzger and Tharp, 1947; Potzger and Tharp, 1954), frequently omitting or broadly estimating age control and pre-dating the standardization of palynological processing. Indeed, there are only a handful of studies with reasonable age constraints, and therefore relevant to Texas' Holocene climate history (Graham and Heimsch, 1960; Albert, 1981; Holloway and Bryant, 1984; Bousman, 1998), without a clear consensus shared among them. Furthermore, these studies are all based in various peat bogs, lakes, and archaeological sites in central and western Texas; eastern Texas and its associated coastal plains have largely been ignored due to the scarcity of sites promoting palynological preservation. Palynomorph preservation is generally poor due to a combination of factors including high microbial activity in leaf litter on forest floors, sporopollenin damage caused by the constant drying and wetting of soil, and soil oxidation (Bryant and Holloway, 1985). These problems are bypassed by using subaqueous cores in each of our studies.

1.4 Summary of Studies (Chapters 2-4)

This dissertation consists of three principle projects (Chapters 2, 3, & 4) that study climatic and marine events along coastal Texas. Chapter 2 focuses on the marine record from dinoflagellates in Corpus Christi Bay, Texas, and found convincing evidence that the bay's coastal barrier island was compromised for several hundred years due to a rapid pulse of sea-level rise. Chapter 3 combines the marine (dinoflagellate) and terrestrial (pollen and spores)

records from Trinity Bay, Texas and Corpus Christi Bay, Texas and uses statistics to explore trends through time. Both bays had similar assemblages and transitioned through the Holocene from herbaceous-dominated assemblages to arboreal-dominated, as early as 8.4 ka within Corpus Christi Bay, and 3.8 ka within Trinity Bay. Chapter 4 focuses exclusively on Baffin Bay, Texas, which is <60 km south of Corpus Christi Bay and Mustang Island. Baffin Bay experienced a similar vegetative shift as seen in Chapter 2, and we also found that sample-to-sample shifts in arboreal-herbaceous abundances are likely correlated with the climatic effects of changing solar irradiance.

CHAPTER 2
BREAKDOWN OF ANCESTRAL MUSTANG ISLAND-CORPUS CHRISTI BAY COMPLEX IN RESPONSE TO THE 8.2 KA SEA-LEVEL EVENT: IMPLICATIONS FOR FUTURE COASTAL CHANGE

2.1 Introduction

Many wave-dominated passive margins of the world have coastlines dominated by barrier islands and peninsulas associated with back-barrier bays. The past and future stability of these coupled barrier-bay systems is strongly connected, as both are highly sensitive to variations in the rate of relative sea-level rise.

Sea-level curves for the western Gulf of Mexico show an average late Holocene rate of rise between 0.4 and 0.6 mm/yr (Fig. 1; (Törnqvist et al., 2004b; Milliken, 2008; Livsey and Simms, 2013). This rate is based in part on basal peat ages in locations where the role of subsidence is believed to be minimal (Törnqvist et al., 2004a; Törnqvist et al., 2004b; Törnqvist et al., 2006). Other sea-level data used by Milliken (2008) and Livsey and Simms (2013) and shown in Figure 1 exhibit variability that is considered to be due to localized subsidence variations and subtle differences in glacial-isostatic adjustments across the region (Simms et al., 2007). Regardless of this variability, modern rates of rise are as much as an order of magnitude higher than the late Holocene rate and reflects the globally recognized increase in eustatic rise (Church et al., 2013) and anthropogenic influences such as subsurface fluid extraction (Kolker et al., 2011). The rate of eustatic rise is expected to at least double by 2100 (Törnqvist and Hijma, 2012; Church et al., 2013; Bamber and Aspinall, 2013). Indeed, current retreat of the Antarctic Ice Sheet alone due to ocean and atmospheric warming is projected to cause >1 m of global sea-level rise by the end of the century and, according to new modeling efforts, as much as 15 m over the next 500 years

(DeConto and Pollard, 2016). Given what is known about ice sheet behavior, it is possible that future sea-level rise will be punctuated by pulses of rapid rise caused by mass wasting of individual ice streams (e.g. Feldmann and Levermann, 2015).

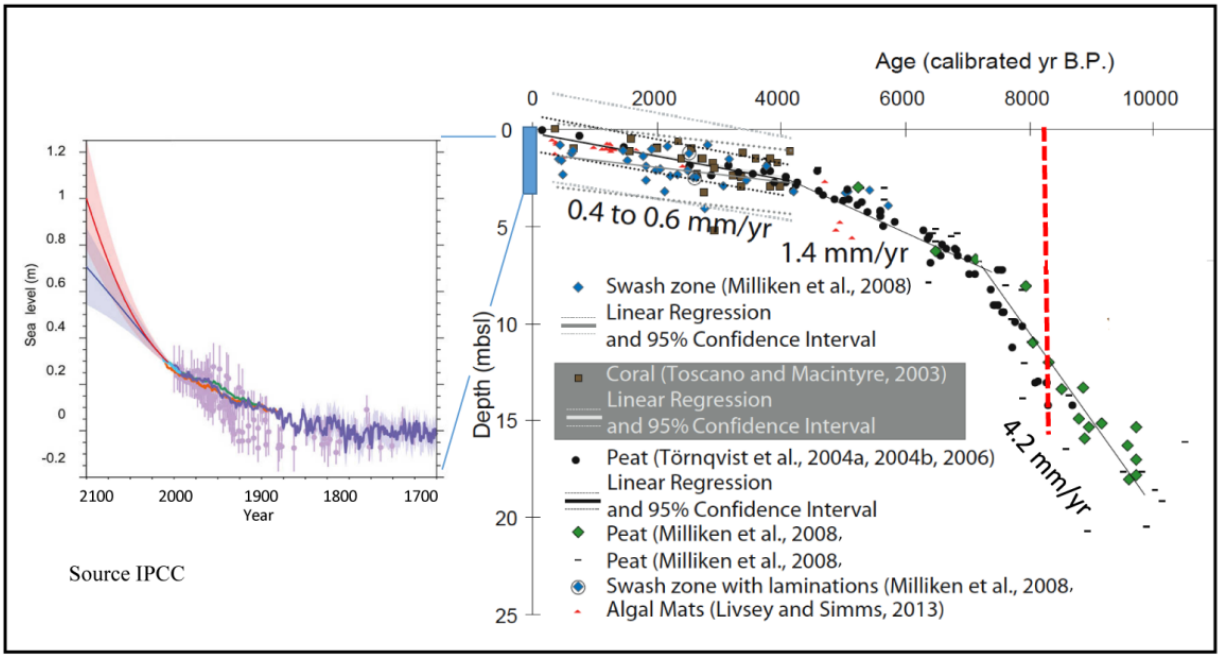

Figure 1. Composite Holocene sea-level curve for the western Gulf of Mexico (modified from Anderson et al., 2014). Also shown is the IPCC sea-level curve showing historic and predicted rates of sea-level rise.

Throughout the early and middle Holocene, North Atlantic and Gulf of Mexico coastlines retreated in response to sea-level rise by stepping landward. In east Texas, this style of coastal evolution has been attributed to episodic sea-level rise (Thomas and Anderson, 1994), which is supported by the apparently contemporaneous nature of flooding events within different bays (Rodriguez et al., 2010; Anderson et al., 2014). This is in stark contrast to the Mustang Island and Corpus Christi Bay complex of central Texas, which has experienced only minor landward migration during the Holocene (Shideler, 1986; Simms et al., 2006).

Improved understanding of how coupled barrier-bay systems respond to changes in sea-level rise can be gained by studying the evolution of these systems during the Holocene, when rates of rise varied by more than an order of magnitude, and particularly the early Holocene when rates were similar to those of the present and to predicted future rates (Fig. 1). However, few studies have examined how coupled barrier and back-barrier systems responded to past variations in the rate of sea-level rise. Here, we present new results from a study of Corpus Christi Bay, which is situated landward of Mustang Island (Fig. 2). To our knowledge, it is the oldest barrier island in Texas, having existed near its current location since ~9.5 ka (Simms et al., 2006; Anderson et al., 2014). The island's early formation and stable shoreline position throughout most of the Holocene makes Mustang Island and Corpus Christi Bay an ideal candidate for yielding an extended record of how changes in the rate of sea-level rise affects coupled barrier island and bay systems. Our results indicate at least one episode of significant morphodynamic change in this bay/barrier complex during the Holocene. We further assess the magnitude and cause of this event.

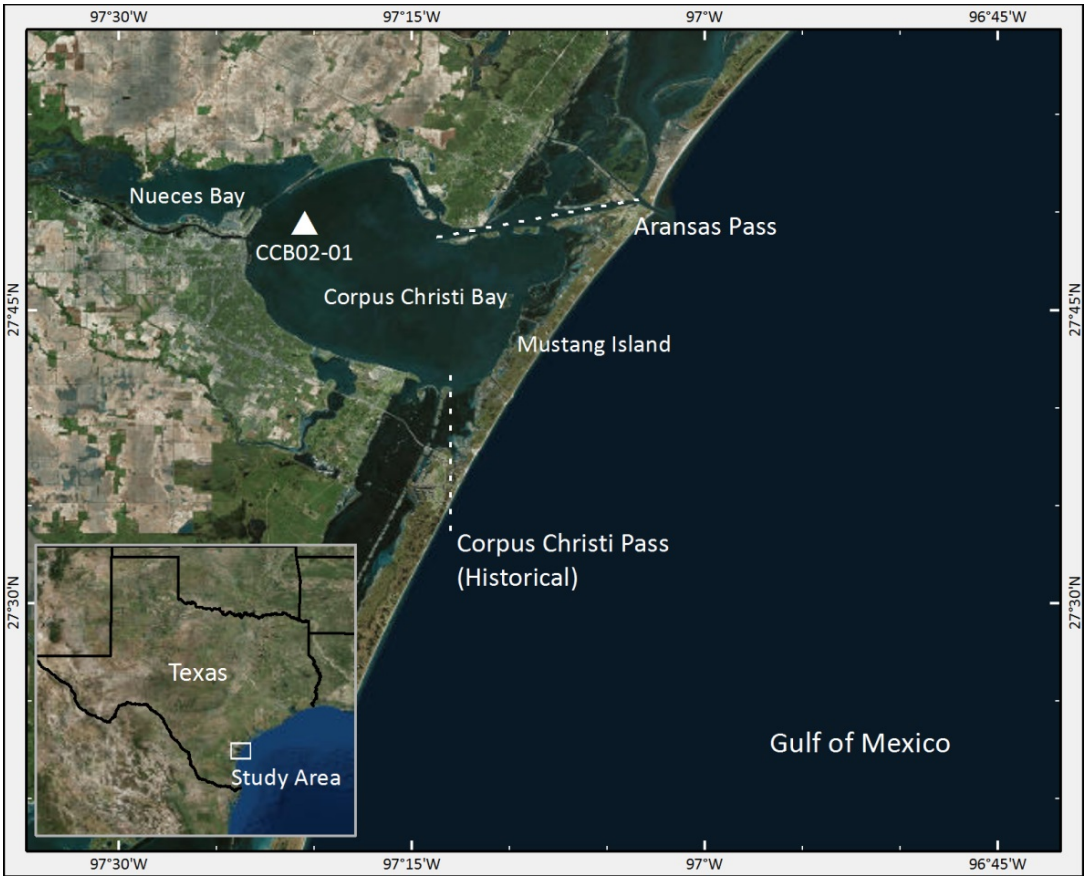

Figure 2. Geographic map of study area showing location of core CCB02-01. Inset shows study area in relation to regional geography.

2.2 Regional Setting and Background

Corpus Christi Bay is a moderate-sized bay located along Texas' central coast with a surface area of roughly 434 km^2 (Fig. 2). The bay is a shallow microtidal estuary typical of other Texas bays, with an average depth of 3 to 4 m and an inner shelf slope of 0.85 m/km (NOAA, 2012). The 525 km-long Nueces River is the bay's largest input of both freshwater and sediment, providing $6.3x10^8$ m^3 yr^{-1} of water and 750,000 tons yr^{-1} of sediment before installation of the Nueces basin dams (constructed in 1958 and 1982) (Henley and Rauschuber, 1981; Simms et al., 2008). The bay is isolated from the Gulf of Mexico by Mustang Island, with the only modern connection between the Gulf and the bay being Aransas Pass, a tidal inlet located at the northern

end of the island (Fig. 2). The island overlies a 38 m deep Pleistocene – Holocene unconformity cut by the Nueces River Marine Isotope Stage (MIS) 2 incised valley (Shideler, 1986; Simms et al., 2006). The island's location overlying the submerged valley of the Nueces River, combined with a steep regional offshore profile and relatively high sand supply to the island, has stabilized the shoreline throughout the Holocene (Simms et al., 2006). However, the island's location above the valley also contributes to local subsidence, which is on average higher over ancestral river valleys because of compaction of relatively thick Holocene sediments that fill these valleys (Anderson et al., 2014). The nearest long-term tide gauge record is at Rockport, Texas, which is located to the west and outside the Nueces River valley. At this location the historical relative sea-level rise has been 5.52 mm/yr (Paine et al., 2016), so the rate of relative sea-level rise at Mustang Island is expected to be higher.

2.3 Methods

2.3.1 Radiocarbon and Age Model

A 21 m-long drill core (CCB02-01) was selected for palynological analysis because of its location in central Corpus Christi Bay and its well-dated sedimentary record based on 9 radiocarbon ages (Simms et al., 2008). The events recorded in this core are tied to changes elsewhere within the bay using the detailed stratigraphic framework of Simms et al. (2008), (Fig. 3).

Depths were related to ages using the Bchron package (Parnell et al., 2008; Haslett and Parnell, 2008) for R and plots were made using SigmaPlot® software. Bchron includes the Marine13 calibration curve (Reimer et al., 2013), assumes a monotonic sedimentation rate and generates several complete chronologies that take into account the uncertainty associated with

our radiocarbon dates (Parnell et al., 2008). These chronologies are reported at the 2.5%, 10%, 50%, 90%, and 97.5% quantiles of the generated probability distribution function for the core, which provide minimum and maximum age estimates for our marine events (ME1—7) within a 95% confidence interval (Table 1). The dates within the text are reported at the Bchron 50% quantile.

Table 1. Radiocarbon ages from drill core CCB02-01 (27.8275 N, 97.3593 W) (Simms et al., 2008). Samples were analyzed by the National Ocean Sciences Accelerator Mass Spectrometry (NOSAMS) laboratory.

Lab Code (NOSAMS)	Species	Core Depth	Depth	Uncalibrated Age	Age error	Marine13 2σ Range (Cal yr BP)		Bchron 2.5%	**Bchron 50%**	Bchron 97.5%
		(m)	(mbsl)	(yr)	(±yr)	**ΔR = 100 ± 300**		(ka)	(ka)	(ka)
OS-38275	*Nuculana concentrica*	3.47	8.04	2310	40	1180	2580	1.08	**1.7**	2.25
OS-38276	*Abra ovalis*	4.78	9.35	2530	45	1370	2770	1.92	**2.45**	2.98
OS-40238	*Nuculana concentrica*	6.22	10.79	3290	35	2280	3770	2.82	**3.42**	4
OS-38277	*Mulinia lateralis*	8.12	12.69	4550	40	3830	5410	4.47	**5.15**	5.89
OS-40239	*Nuculana concentrica*	9.47	14.04	6270	40	5960	7280	5.95	**6.61**	7.13
OS-40890	*Nuculana concentrica*	10.94	15.51	7520	130	7260	8560	7.44	**7.94**	8.4
OS-38278	*Mulinia lateralis*	12.6	17.17	7750	50	7520	8810	7.91	**8.43**	8.92
OS-38279	*Mulinia lateralis*	15.62	20.19	8750	40	8540	10100	9.03	**9.64**	10.21
OS-38280	*Brachidontes exustus*	17.01	21.58	9360	55	9300	10810	9.59	**10.22**	10.88

Simms et al. (2008) originally used a radiocarbon reservoir correction of 760 ^{14}C a based on one paired wood/barnacle date. This reservoir is much larger than other reservoirs found within estuaries in the region (Aten, 1983; Törnqvist et al., 2015). Rice (2015) revisited this reservoir by obtaining an additional paired wood/bivalve radiocarbon age from the upper reaches of the Corpus Christi Bay system and found a reservoir age of 365±40 ^{14}C a. Törnqvist et al. (2015) suggests that a reservoir correction of 500±300 ^{14}C a is the most realistic for estuarine carbonates in the Gulf of Mexico; this corresponds to a ΔR of 100±300 ^{14}C, which was used in this study.

2.3.2 Sampling and Palynological Processing

Sixty-eight samples were collected at 10 to 20 cm intervals (based on availability and selection of fine grain sediment) for analysis. Samples were chemically processed by Global GeoLab using standard laboratory procedures (Brown, 2008). Each dry sample was weighed before processing (~9 g each), and a known quantity of *Lycopodium* spores was added in order to

determine concentration values (cysts/gram). A minimum of 300 identifiable palynomorphs were tabulated for each sample when available to ensure accurate paleo-environmental representation.

2.4 Results

Simms et al. (2008) conducted a detailed study of the Holocene evolution of Corpus Christi Bay using an extensive grid of seismic data and sediment cores and a robust radiocarbon chronology consisting of 48 radiocarbon ages. Their results were later augmented with magnetic chronology (Simms et al., 2008; Simkins et al., 2012). Mustang Island was studied using 11 drill cores that penetrated the barrier and 15 radiocarbon ages (Simms et al., 2006).

Simms et al. (2008) identified four flooding surfaces (landward shifts in bay and back-barrier sedimentary facies) within Corpus Christi Bay (Fig. 3). The oldest of these surfaces (FS1) marks the initial flooding of the Nueces River valley at ~9.6 ka, which was followed by a period of relative stability that lasted until ~8.0 ka (FS2) when the Nueces bay-head delta shifted landward, coincident with a landward shift in proximal washover and tidal delta deposits in cores CCB02-03 and CCB02-04 (Fig. 3; Simms et al., 2008). Two additional flooding events (FS3 and FS4) occurred during the late Holocene, after the rate of sea-level rise had slowed to between 0.4 and 0.6 mm/yr (Fig. 1; Milliken, 2008). The present investigation aims at assessing the cause, magnitude and duration of these flooding events using fossil dinoflagellate cysts to measure salinity variations within the bay and our updated age model.

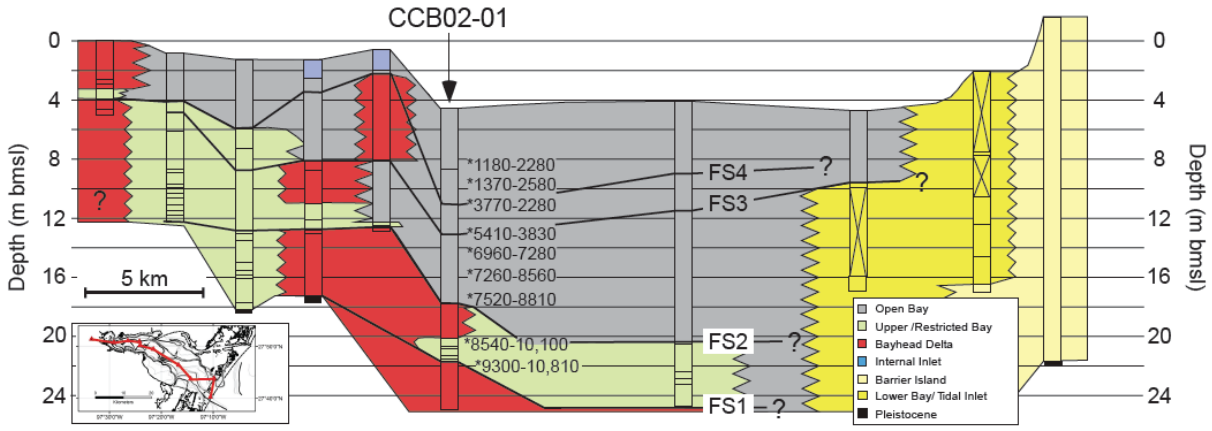

Figure 3. Generalized stratigraphic cross section through Mustang Island and Corpus Christi Bay based on sediment cores and high-resolution seismic data (modified from Simms et al., 2008). Core CCB02-01 and the MS2 flooding surface are highlighted. Inset map shows profile location. See Simms et al. (2008) for more detailed core descriptions and for radiocarbon ages from other drill sites used to correlate flooding surfaces between these sites.

Core CCB02-01 was selected for this study because of its location in central Corpus Christi Bay and its well-dated sedimentary record based on 9 radiocarbon ages (Simms et al., 2008). Furthermore, the events recorded in this core are tied to changes elsewhere within the bay using the detailed stratigraphic framework of Simms et al. (2008) and Simkins et al. (2012), (Fig. 3). Seven marine incursion events (ME) were identified in the studied 21 m section (Fig. 4). The first (ME1), which occurred at 10.15 ka, is the most subtle, and represents the initial marine incursion of the Nueces incised valley and birth of Corpus Christi Bay. The dinoflagellate assemblage includes the First Appearance Datum (FAD) of *Polysphaeridium zoharyi*, designating a near to full marine sea surface salinity (SSS) of 28.4 psu to 39.4 psu based on known SSS ranges (Zonneveld et al., 2013). Continuous presence of dinoflagellate cysts following this first marine event indicates that the bay has since been at least partially connected to the Gulf of Mexico, with ME1 roughly coincident with the oldest coastal sands in sediment cores from Mustang Island (Simms et al., 2006) and oldest marine flooding surface observed in seismic sections and cores from the southern portion of the bay (FS1) (Simms et al., 2008).

Subsequent marine events were identified as peaks in dinoflagellate concentrations that exceeded the core mean concentration (Fig. 4).

Overall dinoflagellate cyst relative abundance remained low from 10.15 ka until 8.86 ka (Fig. 4; Appendix Table A1). The presence of *Spiniferites* spp., *Operculodinium centrocarpum.* and *Lingulodinium machaerophorum* indicates a productive environment with euryhaline conditions (Zonneveld et al., 2013; Warny et al., 2003; Warny and Wrenn, 2002). *Polysphaeridium zoharyi*, which dominates the dinoflagellate record in the bay, is a common coastal/nearshore species and indicates constant warm surface water conditions (Warny and Wrenn, 2002; Warny et al., 2003; Zonneveld et al., 2013).

Dinoflagellate concentrations increased from 8.86 to 8.18 ka, with a maximum value at 8.38 ka (ME2, Fig. 4). *Polysphaeridium zoharyi* dominates this assemblage. Following ME2, dinoflagellate cysts declined below the core mean until ME3 at 6.89 ka. This was followed by four smaller events ending at 2.49 ka, after which dinoflagellate concentrations have remained below the core mean.

Four of our palynologically identified marine events occur within 120 cm of flooding surfaces previously identified using combined high-resolution seismic data and drill cores (Simms et al., 2008), (Fig. 3, 4). The revised ages of these surfaces were estimated by the Bchron model as 10.20, 8.86, 5.49 and 3.62 ka (FS1— 4), Table 2. Our dinoflagellate cyst data records additional flooding events that were not recognized using the coupled seismic-stratigraphy dataset.

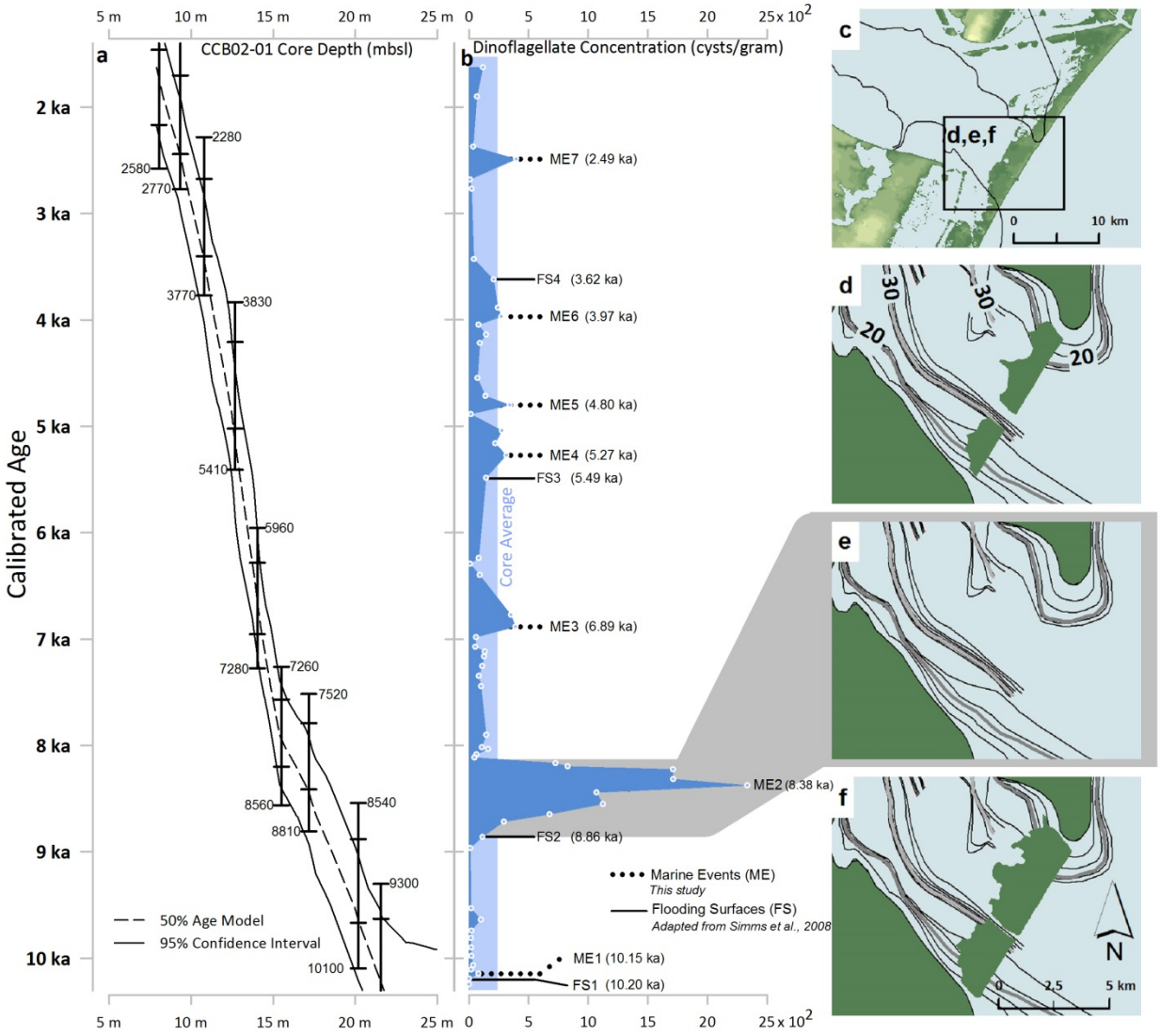

Figure 4. (a) Age-depth model for core CCB02-01. The model was produced based on an updated calibration of previously published radiocarbon dates (Simms et al., 2008), using a ΔR of 100±300 14C and Marine13 (Törnqvist et al., 2015; Reimer et al., 2013), and Bchron for R (Haslett and Parnell, 2008; Parnell et al., 2008). The 50% quantile age model is shown by the dashed line and is reported within the text; the 2.5% and 97.5% models are also shown as a 95% confidence interval. Error bars show radiocarbon ages at the 1σ and 2σ range. Full age model data is reported in Table 1. (b) Summary diagram showing distribution of dinoflagellate cysts against the 50% quantile age model. White circles indicate sample locations. Marine events (ME) were determined from dinoflagellate cyst results (CCB02-01, this study) and flooding surfaces (FS) were converted from CCB02-01 depths reported in Simms et al. (2008). The average dinoflagellate cyst concentration for core CCB02-01 (2.4 x 10^2 cysts/g) is shaded in blue. (c) Modern DEM of the Corpus Christi Bay (Holcombe, 2007). Black lines show 15 m paleobathymetric contour interpreted for Simms et al. (2006). (d) Interpretation of the potential extent of Mustang Island following the return of estuarine conditions after ME2. The interpreted surface area has been reduced to 50% of the assumed area shown in Fig. 2(f). Paleobathymetric contours (meters) are from (Simms et al., 2006), with 10 m intervals. (e) Collapse of Mustang Island at 8.38 ka, ME2. (f) Interpretation of the potential extent of Mustang Island immediately prior to ME2. The island is constrained laterally NE-SW by the 15 m paleobathymetric contour (Simms et al., 2006), while NW-SE widths are only representative, and have been derived from a modern DEM (Holcombe, 2007). Fig. 4(c) — (f) was prepared using ESRI ArcMap© 10.3 software (http://desktop.arcgis.com/en/arcmap/).

Table 2. Bchron quantile ages for marine events (ME1–7) found in this study and flooding surfaces (FS1–4) from Simms et al. (2008). Ages in text are reported from the 50% quantile age model.

	Bchron Quantile Ages (ka)		
Surface	2.50%	**50.00%**	97.50%
ME1	9.51	**10.15**	10.76
ME2	7.85	**8.38**	8.86
ME3	6.36	**6.89**	7.38
ME4	4.6	**5.27**	6.03
ME5	4.04	**4.8**	5.37
ME6	3.31	**3.97**	4.64
ME7	1.95	**2.49**	3.02
FS1	9.54	**10.2**	10.83
FS2	8.28	**8.86**	9.4
FS3	4.82	**5.49**	6.25
FS4	3.01	**3.62**	4.27

2.5 Discussion

The ME2 event is the most significant dinoflagellate cyst event, with a five-fold increase in dinoflagellate concentrations (Fig. 4). Lithologic evidence from drill cores in Corpus Christi Bay indicate that the Nueces bay-head delta experienced a landward shift of approximately 15 km during this event (Simms et al., 2008). Impact on the bay ecosystem is marked by widespread destruction of seismically imaged oyster reefs and by dramatic shifts in bay environments (Simms et al., 2006; Goff et al., 2015). These combined results indicate that the island was not an effective barrier to marine influence during the ME2 event. Since the ME2 event, dinoflagellate cyst concentrations in the bay have varied, but never reached levels greater than 1/6 of the ME2 event.

Our age model indicates that the ME2 event most likely resulted from the most rapid eustatic rise of the Holocene (Barber et al., 1999; Simms et al., 2008; Rodriguez et al., 2010; Törnqvist and Hijma, 2012; Simkins et al., 2012), which peaked at 8.18—8.31 ka. Coastal areas around the

world, including southwest Scotland (Lawrence et al., 2016), the Rhine-Meuse Delta (Törnqvist and Hijma, 2012), and several bay-head deltas of the Gulf of Mexico (Rodriguez et al., 2010; Törnqvist and Hijma, 2012;) show evidence of flooding at this time with differences among them due to local glacial-isostatic factors (Kendall et al., 2008). This event is attributed to late stage ice sheet disintegration, particularly in North America, by rapid draining of Lake-Agassiz-Ojibway (Kendall et al., 2008; Törnqvist and Hijma, 2012).

The magnitude of sea-level rise during the 8.2 ka event is estimated to have been between 0.2-0.56 m in the western Gulf of Mexico (Li et al., 2012) and occurred when the long-term average rate of sea-level rise was 4.2 mm/yr (Fig. 1; Milliken, 2008). The elevation of Mustang Island during this event is unknown, but a minimum elevation of 1.0 meters is assumed, based on the elevations of modern coastal barriers of Texas. Thus, the island was not simply drowned in place. This is consistent with results from field studies (e.g. Wallace and Anderson, 2013) and numerical modeling (e.g. Lorenzo-Trueba and Ashton, 2014) which indicate that barrier islands respond more actively to sea-level rise than by drowning in place. Rather, the rate and magnitude of change depends on a number of factors and their relative influence is still poorly understood (Moore et al., 2010; Lorenzo-Trueba and Ashton, 2014). This explains the highly variable response of the coastal barriers of the western Gulf Coast to past and current changes in the rate of sea-level rise (Anderson et al., 2014).

In all of the Texas bays that have been studied in detail, the associated FS2 flooding surface manifests itself in sediment cores most prominently as a sharp contact separating bay-head delta from overlying open-bay sediments (Anderson et al., 2008; Rodriguez et al., 2010; Troiani et al., 2011), implying rapid shifts in these environments. However, our dinoflagellate data and age model indicate that the bay experienced anomalous salinities for nearly five centuries,

culminating in open marine salinities (Fig. 4). This implies that removal of Mustang Island as an effective salinity barrier was a prolonged process. Likewise, it took between two and three centuries for the bay to return to its normal estuarine conditions (Fig. 4).

The current rate of relative sea-level rise in the western Gulf of Mexico has accelerated from a late Holocene average rate of 0.5 mm/yr to a modern rate that is on average an order of magnitude faster. The current rate approaches that of the early Holocene average rate of 4.2 mm/yr. This implies that the acceleration of sea-level rise in historical time has reached the point where Mustang Island and Corpus Christi Bay are again susceptible to change. However, we do not know how the current width and elevation of the island compare to its early Holocene state, or how other factors that control barrier stability have changed. What is known is that other narrow, low coastal barriers of the Texas coast, including west Galveston Island, Follets Island, Matagorda Peninsula and South Padre Island, are experiencing unprecedented change (Wallace and Anderson, 2013; Anderson et al., 2014; Odezulu et al., In Press). This suggests that these barriers are susceptible to dramatic change due to accelerated sea-level rise, which is consistent with current high rates of shoreline change in these areas (Paine et al., 2016). We emphasize the need for improved understanding of those variables that control coastal stability and improved numerical models that predict the response of coastal barriers to accelerated sea-level rise in light of the other factors that regulate their stability.

The ME3 through ME7 events occurred during the late Holocene when rates of sea-level rise were slowing and no known meltwater pulses occurred (Milliken et al., 2008; Livsey and Simms, 2013). Events ME4-7 overlap within error other flooding events within bays which have been studied in the western Gulf Coast (Anderson et al., 2010; 2014; Livsey and Simms, 2016). These events, as well as ME3, may have resulted from autogenic drivers such as changes in inlet

location and area, which may have been triggered by hurricanes, or climate-driven sediment supply changes (e.g. Livsey and Simms, 2016). While the ME3 through ME7 events were smaller in magnitude relative to the ME2 event, three of them (ME3, ME4, and ME6) lasted for centuries and collectively they provide a record of barrier-bay instability throughout the middle to late Holocene.

2.6 Conclusions

Although coastal barriers are generally believed to be quite resilient, our results show that an abrupt increase in the rate of sea-level rise between 8.86 and 8.17 ka led to the removal of Mustang Island as an effective salinity barrier. This event is recorded by a 5-fold increase of dinoflagellates within Corpus Christi Bay culminating at ~8.38 ka (ME2, Fig. 4). These results indicate that accelerated, decimeter-scale sea-level rise can lead to dramatic change in coastal barriers and their associated back-barrier bays. Based on our age model, this period of change lasted several centuries. During this time, the Nueces bay-head delta shifted landward approximately 15 kilometers and the bay experienced widespread destruction of oyster reefs (Simms et al., 2008; Goff et al., 2015). Five additional marine incursions occurred through the Holocene since the ME2 event, but they appear to be regionally confined and are interpreted as having resulted from changes in inlet size and location, likely caused by hurricanes, or regional climate changes such as droughts affecting freshwater input. These events also led to increases in estuarine salinity, three of which had measurable effects for centuries.

The current rate of relative sea-level rise in the western Gulf of Mexico is as much as an order of magnitude greater than the late Holocene rate and within the range of the overall rate of rise when the ME2 event occurred. There is also increasing concern for punctuated sea-level rise due

to ice stream collapse events by the end of this century exists (Church et al., 2013; Bamber and Aspinall, 2013; DeConto and Pollard, 2016). There is a need for improved understanding of coastal barrier response to accelerated sea-level rise and for numerical models for predicting future changes in coastal barrier-bay systems.

CHAPTER 3
HOLOCENE VEGETATION AND CLIMATE EVOLUTION OF CORPUS CHRISTI AND TRINITY BAYS: IMPLICATIONS ON COASTAL TEXAS SOURCE-TO-SINK DEPOSITION

3.1 Introduction

A major challenge in interpreting earth's history is understanding how climate has changed in the past. Understanding these changes is important for placing present and future climate change into context. Coastal regions are both densely populated and susceptible to the negative effects of these changes, particularly as they relate to sea-level rise and increasing strength of tropical cyclones (Emanuel, 2005; Knutson et al., 2010; Törnqvist and Hijma, 2012).

The extensive Texas coastline is characterized by a large precipitation gradient across the region, making it vulnerable to climate variability. Yet, relatively few studies have documented the climate and vegetative change of the region through the Holocene. This study aims to fill this gap; we examine the record of coastal marine and terrestrial palynoflora, create a record of coastal vegetative change through the Holocene, and finally examine whether the climate histories available for central and western Texas are also reflective of coastal Texas climate.

The modern mean annual precipitation gradient along the coast ranges from 50 to 150 cm/yr from north to south (Fig. 1), while temperatures vary little across the region. Given this strong precipitation gradient, the region is sensitive to climate change and associated changes in coastal ecosystems (Osland et al., 2014; Gabler et al., 2017). Holocene paleoclimate records for the region are sparse, but reveal shifts between cold-wet and warm-dry conditions over millennial time scales (Toomey et al., 1993; Humphrey and Ferring, 1994; Wilkins and Currey, 1999; Nordt et al., 2002) that are believed to be driven by large scale climate forcing mechanisms (e.g. North American Monsoon; Atlantic Multidecadal Oscillation, and El Nino-Southern Oscillation)

(Buzas-Stephens et al., 2014; Livsey et al., 2016). Records from central and south Texas suggest that the early Holocene was dominated by cool/wet conditions, followed by warm dry conditions of the mid-Holocene Climate Optimum, and a shift to higher-frequency changes during the late Holocene (Humphrey and Ferring, 1994; Nordt et al., 1994; Russ et al., 2000; Nordt et al., 2002; Buzas-Stephens et al., 2014). However, the actual duration and magnitude of these climate changes remains uncertain, especially for east Texas, so the potential climate forcing mechanisms remains uncertain. Thus, the value of the paleoclimate record for testing and refining climate models is limited.

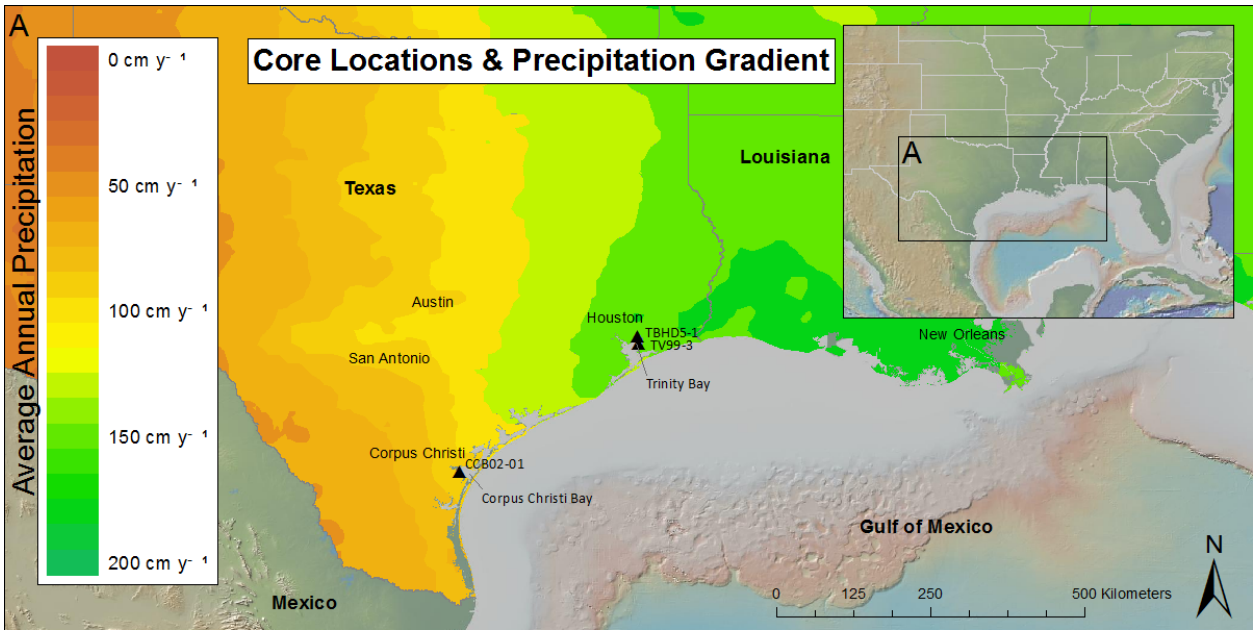

Figure 1. Location of Corpus Christi Bay and Trinity Bay, Texas. Corpus Christi Bay core CCB02-01 and Trinity Bay cores TBHD5-1 and TV99-3 were used for this investigation. Precipitation gradients were mapped in ArcGis (metadata source from https://www. sciencebase.gov/catalog/item/513e317ce4b07b9dc9e7e9fb)

This study uses subaqueous cores, which both eliminate the palynomorph preservation problems of coastal Texas and have the added benefit of containing both terrestrial (pollen) and marine (dinoflagellate) palynomorphs. Samples come from sedimentary records obtained from 3 cores collected from subaqueous bayhead deltas and associated upper bay deposits in Corpus

Christi Bay (central coast) and Trinity Bay (eastern coast). Both bays exhibit significant changes in paleo-environments throughout the Holocene, but the cause of these changes (sea-level, climate change or changes in valley geomorphology that influenced bay flooding history) have remained uncertain. We rely on results from detailed seismic and sedimentological analyses of these and other bays of the western Gulf Coast region (Galveston estuary complex, Matagorda Bay, Sabine Lake, Calcasieu Lake, Corpus Christi Bay, and Copano Bay; Anderson et al., 2008; Maddox et al., 2008; Milliken, 2008a; Simms et al., 2008; Troiani et al., 2011) to address the potential causes of environmental changes observed in these bays during the Holocene, and to investigate likely forcing mechanisms for climate change in the region.

3.2 Study Areas

3.2.1 Physical Attributes

Corpus Christi Bay is a moderate-sized bay located within Texas' central coast with a surface area of roughly 434 km^2 (Fig. 2A). The bay is a shallow estuary, with an average a depth of 3 to 4 m (Simms et al., 2008). Average subsidence rates for this region are less than 0.05 mm/yr (Paine, 1993; Simms et al., 2013). The bay is fed water and sediment by the Nueces River. It provided 6.3 x 10^8 m^3 yr^{-1} of freshwater (Henley and Rauschuber, 1981; Mannino and Montagna, 1996; Wermund, 1996) and 750,000 tons yr^{-1} of sediment before installation of Nueces basin dams (constructed in 1958 and 1982) (Shepard, 1953; Shepard, 1955; Montagna et al., 2002). The river is 500 km in length and has a drainage area of 43,502 km^2 (Hudson and Heitmuller, 2008). Mustang Island separates Corpus Christi Bay from Gulf of Mexico waters, and has been stable since ~7.5 ka (Morton and McGowen, 1980; Simms et al., 2006; Simms et al., 2008; Ferguson et al., in press). Corpus Christi Bay's proximity to both semiarid and subhumid

climatic zones makes it an ideal location for a palynological study (Fig. 1). Because this area serves as the boundary between these climate zones, even a small climatic change would cause a shift in vegetation, and in turn be preserved in the palynological record.

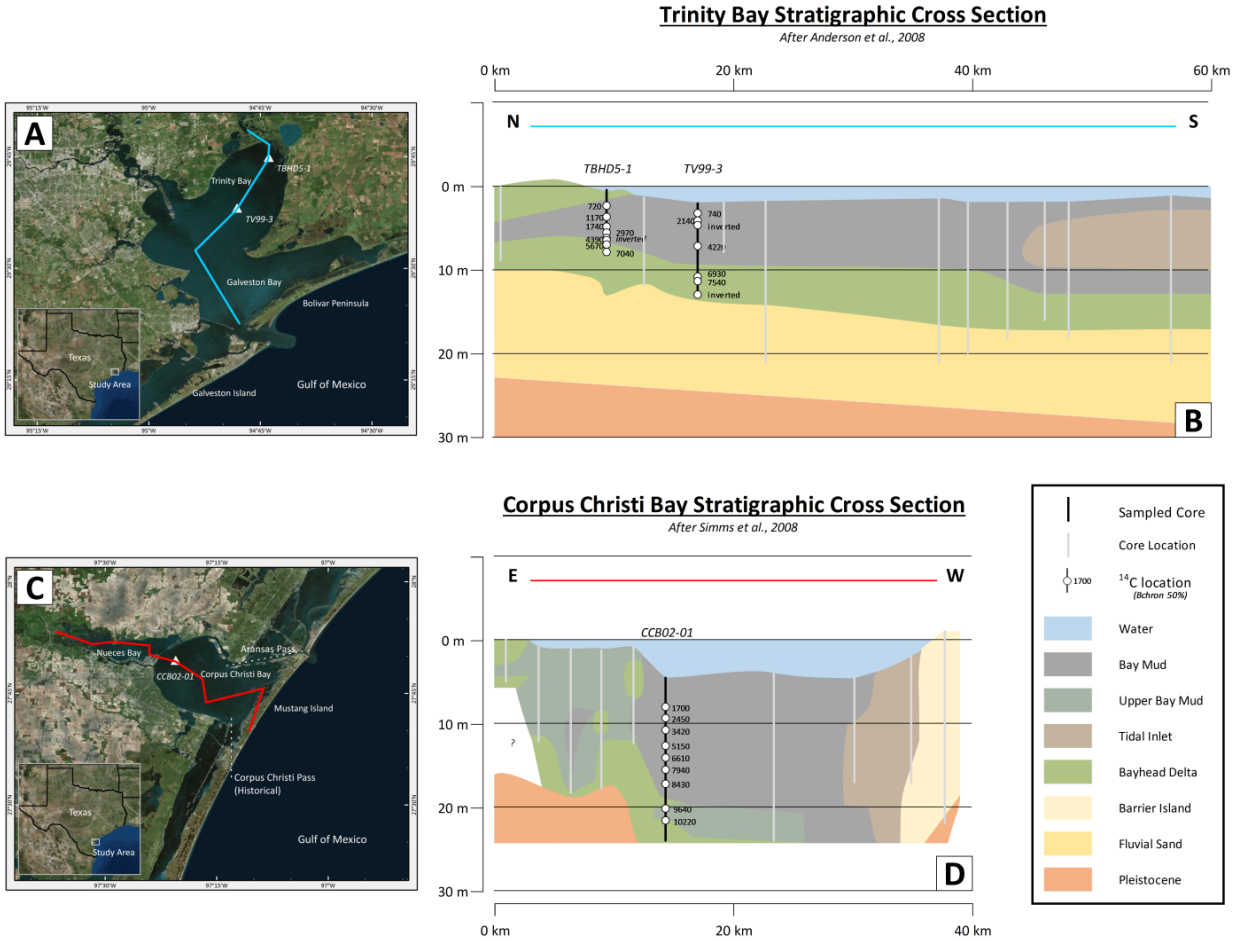

Figure 2. (A) Trinity Bay, TX core locations TBHD5-1 and TV99-3. (B) Generalized cross section of Trinity Bay, TX (from Anderson et al., 2008). Blue line shows section location. (C) Location of Corpus Christi Bay, TX core CCB02-01. (D) Generalized cross section of Corpus Christi Bay (from Simms et al., 2008). Red Line shows section location.

Trinity Bay is located along Texas' northern coastal plain and is one of the five bays that comprise the Galveston estuary complex (Fig. 2C). This complex averages 2– 3 m in depth (Anderson et al., 2008), and has more than twice the amount of subsidence seen in Corpus Christi Bay (0.13 mm/yr) (Paine, 1993; Simms et al., 2013). Trinity Bay is fed freshwater by the Trinity River with a mean daily discharge rate of 395 $m^3 s^{-1}$ and a combined upper and lower

watershed area of 84,500 km^2 (Lester et al., 2002; Wen et al., 2008). The Trinity River has been impounded upstream by the U.S. Army Corps of Engineers at Lake Livingston Dam since 1968 serving as major water source for Houston, TX (Traverse, 1990). Galveston Island and Bolivar Peninsula have separated the Galveston estuary complex from the Gulf of Mexico since 5.5 ka and 2.5 ka, respectively (Anderson et al., 2008; Rodriguez et al., 2004). Marine waters currently flow partially through the 3 km wide Bolivar Roads inlet, located between the barrier island and spit (Anderson et al., 2008; Rodriguez et al., 2004). Trinity Bay is on the border between subtropical Prairie Parkland Province and Southern Mixed Forest Province, making it also potentially sensitive to shifts in vegetation.

3.2.2 Holocene Flooding Events

Both bays occupy incised valleys formed during the fall in sea-level between 120 and 20 thousand years before present (ka) (Rodriguez et al., 2004; Simms et al., 2006; Anderson et al., 2008; Simkins et al., 2012). The evolution of the modern bays spans much of the Holocene, from ~ 9.5 ka to present (Anderson et al., 2008; Simms et al., 2008). Throughout the Holocene, the average rate of sea-level rise in the western Gulf of Mexico declined, from 4.2 mm/yr in the early Holocene to 1.4 mm/yr in the mid-Holocene and 0.4 mm/yr in the late Holocene (Milliken et al., 2008b). The evolution of the bays of the western Gulf was characterized by punctuated episodes of change when environments stepped landward (Rodriguez et al., 2005; Anderson et al., 2008; Simms et al., 2008). Some of these flooding events appear to have occurred contemporaneously across the region and were interpreted as having been caused by episodes of accelerated sea-level rise (Milliken, 2008b; Rodriguez et al., 2010; Anderson et al., 2014). Other flooding events were more localized, effecting only one or two bays, and were associated with

changes in the antecedent topography of the incised valleys occupied by the different bays that resulted in variable flooding histories (Rodriguez et al., 2005). More specifically, these flooding events were caused by accelerated flooding of broad fluvial terraces along valley margins (Rodriguez et al., 2005). The remaining flooding surfaces were attributed to reductions in sediment supply to the bays in response to climate change, in particular reduced precipitation and fluvial discharge (Anderson et al., 2008; Simms et al., 2008). However, direct evidence for these climate changes remains limited.

The earliest known Holocene flooding event and occupation of the modern bays occurred around 9.6 ka, and was followed by the larger 8.2 ka sea-level rise event caused by the drainage of glacial Lake Agassiz-Ojibway (Rodriguez et al., 2010; Simms et al., 2010; Ferguson et al., in press). Several other flooding events have occurred in these bays during the mid- to late Holocene. This includes a 7.7– 7.4 ka flooding event in Trinity Bay, which is tentatively interpreted as resulting from a decrease in sediment supply to the bay (Anderson et al., 2008). Corpus Christi Bay experienced more recent flooding events at 5.4 ka, and at 3.6 ka that are also believed to have been caused by a decrease in sediment supply (Simms et al., 2008; Troiani et al., 2011).

3.2.3 Modern Coastal Vegetation and Habitat

Southern to central Texas upland extant vegetation is dominated by a variety of grasses (Poaceae) as well as a variety of coastal scrub species indicative of arid coastal environments. Due to southern Texas' aridity, bottomland hardwood forests (*Carya aquatica*, *Carya texana*, *Ulmus crassifolia, Quercus laurifolia, Liqiudambar styraciflua*, *Nyssa sylvatica*), and swamp

forests (*Quercus nigra*, *Nyssa biflora*, *Taxodium distichum*, *Salix nigra*) are not common in this area and are restricted to river floodplains (Hupp and Osterkamp, 1996).

The Strand Plain/Chenier Plain of Texas' eastern shoreline is home to the coastal live oak population (*Quercus virginiana*) (Williams et al., 1999). This species is the most common on Texas' forested barrier islands (or strand environments), on topographic highs, as well as the eastern shoreline (Shaw et al., 1980; Williams et al., 1999). *Carya cordiformis*, *Juglans nigra*, and *Ulmus americana* are restricted to fluvial floodplains and terraces (Hupp and Osterkamp, 1996). Eastern Texas' upland vegetation consists of a variety of grasses (Poaceae) and coastal scrub species like the southern cattail (*Typha domingensis*), which are indicative of moist coastal environments (Williams et al., 1999).

3.2.4 Previous Palynological Studies

Although the Gulf of Mexico is one of the most well-studied basins in the world, most of the focus has been on oil exploration or on seismic and sedimentological facies models. Rarely has the intent of these studies been to characterize the Holocene climatic record of coastal Texas. Of those studies that discuss Holocene vegetation change, the majority focus on either the Mississippi River Delta (Törnqvist and Hijma, 2012), the Edwards Plateau (Cooke et al., 2003), or central Florida (Grimm et al., 2006; Huang et al., 2006; Donders, 2014), leaving an absence of insight to western Gulf of Mexico climate in the Texas region. The strong precipitation gradient along the northwestern Gulf Coast results in a diverse coastal vegetation assemblage (Longley, 1995; Williams et al., 1999). Differences in precipitation and evapotranspiration have traditionally defined four different climatic regions, ranging from humid near the Louisiana

border to semiarid along the coast and to the Mexican border (Thornthwaite, 1948; Williams et al., 1999) (Fig. 1).

Less than forty palynological studies of Quaternary Texas deposits have been published since the emergence of the discipline in the 1940s. Many of these studies are old in the context of modern analytical techniques (Potzger and Tharp, 1947; Potzger and Tharp, 1954), frequently omitting or broadly estimating age control and pre-dating the standardization of palynological processing. The first Texas palynological studies between the '40s and '50s pre-dated widespread conventional radiocarbon dating and focused on peat bog sediments within the interior of the state (Potzger and Tharp, 1943; Potzger and Tharp, 1947; Potzger and Tharp, 1954). The presence of boreal conifers (*Picea glauca* and *Abies balsamea*) in Patschze Bog, Texas provided early evidence for the southern limit of what are now Canadian conifers, and thus dramatically cooler climate (Potzger and Tharp, 1943). In a subsequent study, Potzger and Tharp (1947) proposed a four-stage climate sequence for central Texas following the last glacial maximum. According to the authors, the sequence begins with the presence of spruce and fir (cool-moist climate), giving way to a variety of grasses and oaks (warm-dry period), then an emergence of alder and chestnut (warm-moist climate), and lastly a hickory and oak vegetation (warm-dry climate) (Potzger and Tharp, 1954). However, the lack of a robust geochronology in this early work limits its usefulness, especially in a modern context.

Graham and Heimsch (1960) included a single radiocarbon date of 7,280 ± 350 yr for their central Texas study, and did not agree with the Potzger and Tharp (1954) climate sequence. Rather than four distinct stages, they interpreted a more simplistic climatic history of cooler and wetter conditions at around 12.5 ka, transitioning slowly to today's warm-dry climate in central Texas (Graham and Heimsch, 1960). A subsequent pollen analysis of nearby Hershop Bog,

Texas with better age control shows the same gradual warming and drying since the early Holocene with decreasing arboreal vegetation (excluding *Quercus*) and an increasing amount of Poaceae and later Asteraceae (Graham and Heimsch, 1960).

Hafsten (1961) examined playa lakes in western Texas (Rich Lake and Arch Lake), and placed several radiocarbon-based age constraints to Potzger and Tharp's (1947; 1954) proposed 4-stage climate sequence. According to Hafsten (1961), at about 30 ka grasslands were present in west Texas and were replaced between 22.5–14 ka by conifer forests as climate cooled. Between 14 and 10 ka, a transitional period occurred with conifer forests being replaced by grasslands and some small shrubs. During the final stage from 10 ka to today, grasslands once again dominate the landscape in the lower elevations of the western region.

Several other palynological studies were completed following these first works (Bryant and Shafer, 1977; Hall, 1985; Holloway et al., 1987; Bousman, 1998), all of which studied the various peat bogs, lakes, and archaeological sites in central and western Texas. Eastern Texas and its associated coastal plains have largely been ignored due to the scarcity of sites promoting palynological preservation. Palynomorph preservation is generally poor due to a combination of factors including high microbial activity in leaf litter on forest floors, sporopollenin damage caused by the constant drying and wetting of soil, and soil oxidation (Bryant and Holloway, 1985). However, several of these later studies (McAndrews and Larson, 1966; Bryant, 1977) commonly provide brief climatic records, as they primarily focus on specific anthropological questions, and are based on cave samples or other samples that produce a skewed vegetation record, such as human coprolites (Williams-Dean and Bryant, 1975) or rat middens (Van Devender and Riskind, 1979). Indeed, there are only a handful of studies with reasonable age constraints, and therefore relevant to Texas' Holocene climate history (Graham and Heimsch,

1960; Albert, 1981; Holloway and Bryant, 1984; Bousman, 1998), without a clear consensus shared among them.

Here we provide a new record of Holocene climate for eastern Texas, based upon three subaqueous bay floor cores containing well-preserved palynomorphs and supported by an extensive modern radiocarbon geochronology and tied to in-depth seismic and sedimentological analyses of the Texas coast (Anderson et al., 2008; Simms et al., 2008).

3.3 Materials and Methods

3.3.1 Sampling and Radiocarbon Age Model

Drill core CCB02-01 from Corpus Christi Bay was selected for palynological analysis because it contains fine-grained (silt) central-upper bay sediments where sedimentary facies have remained relatively unchanged since approximately 7,500 years BP (Fig. 2; Simms et al., 2008). The site was cored to a depth of 21 meters. Nine radiocarbon dates from Simms et al. (2008) provide our basis for age control. Sixty-eight samples were collected for palynological analysis with samples occurring at 10 to 20 cm intervals depending on sediment availability within the archived core.

Two drill cores (TBHD-5-1 and TV99-3) from Trinity Bay were selected for palynological analysis (Fig. 2). Six radiocarbon dates for core TBHD-5-1 and four radiocarbon dates for core TV99-3 provide age control (Fig. 3; Table 1). Two additional radiocarbon samples from core TBHD-5-1 and three from TV99-3 were sent to UC Irvine Keck Carbon Cycle AMS Facility to help further constrain the late Holocene ages (Table 1).

All radiocarbon ages were calibrated using Marine13 (Reimer et al., 2013) and a basin-wide reservoir correction of 300 years was applied as suggested in Törnqvist et al. (2015). An age

model was produced for each core using the Bchron package for R (Haslett and Parnell, 2008; Parnell et al., 2008). Dates within the text and figures are reported at the Bchron 50% quantile. Output of the Bchron model quantiles 2.5%, 50%, and 97.5% are provided in Table S1.

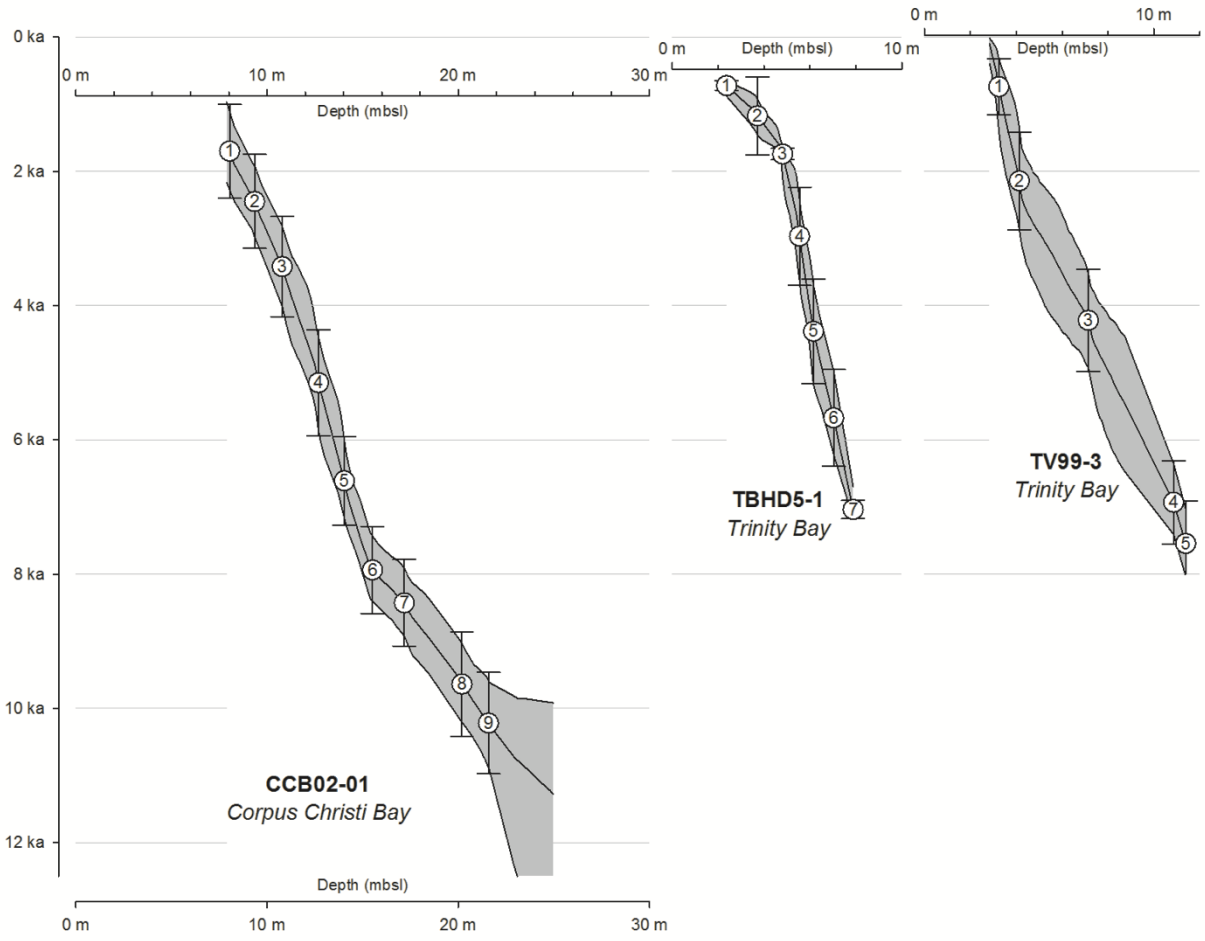

Figure 3. Complete Bchron Age Model and radiocarbon data for cores CCB02-01, TBHD5-1, TV99-3. See Table 1 for complete radiocarbon data.

Table 1. Radiocarbon dates used in this study.

		Lab Code	Species	Core Depth (m)	Depth (mbsl)	Uncalibrated Age (yr)	2σ Range[1] ΔR = 100 ± 300		Bchron 2.5% (ka)	**Bchron 50% (ka)**	Bchron 97.5% (ka)
CCB02-01	①	OS-38275	*Nuculana concentrica*	3.47	8.04	2310 ± 40	1180	2580	1.08	**1.7**	2.25
	②	OS-38276	*Abra ovalis*	4.78	9.35	2530 ± 45	1370	2770	1.92	**2.45**	2.98
	③	OS-40238	*Nuculana concentrica*	6.22	10.79	3290 ± 35	2280	3770	2.82	**3.42**	4
	④	OS-38277	*Mulinia lateralis*	8.12	12.69	4550 ± 40	3830	5410	4.47	**5.15**	5.89
	⑤	OS-40239	*Nuculana concentrica*	9.47	14.04	6270 ± 40	5960	7280	5.95	**6.61**	7.13
	⑥	OS-40890	*Nuculana concentrica*	10.94	15.51	7520 ± 130	7260	8560	7.44	**7.94**	8.4
	⑦	OS-38278	*Mulinia lateralis*	12.6	17.17	7750 ± 50	7520	8810	7.91	**8.43**	8.92
	⑧	OS-38279	*Mulinia lateralis*	15.62	20.19	8750 ± 40	8540	10100	9.03	**9.64**	10.21
	⑨	OS-38280	*Brachidontes exustus*	17.01	21.58	9360 ± 55	9300	10810	9.59	**10.22**	10.88
TBHD5-1	①	Beta-163927	Wood	1.76	2.37	810 ± 60	660	800	0.66	**0.72**	0.88
	②	Beta-163928	*Rangia cuneata*	3.11	3.72	1250 ± 70	140	1300	0.92	**1.17**	1.46
	③	AA39383	Wood	4.2	4.81	1730 ± 37	1550	1720	1.63	**1.74**	2.10
	④	144004	*Crassostrea virginica*	4.94	5.55	2790 ± 20	1670	3130	2.42	**2.97**	3.63
	⑤	Beta-163929	*Crassostrea virginica*	5.55	6.16	4180 ± 60	3350	4910	3.71	**4.39**	5.18
		144005	*Rangia cuneata*	5.85	6.46	6680 ± 20	6400	7630		inverted	
	⑥	AA38437	*Rangia cuneata*	6.42	7.03	5280 ± 75	4800	6240	4.97	**5.67**	6.22
	⑦	AA38439	Wood	7.27	7.88	6230 ± 55	7000	7270	6.70	**7.04**	7.18
TV99-3	①	144001	*Rangia cuneata*	0.5	3.24	860 ± 15	0	840	0.32	**0.74**	1.39
	②	144002	*Rangia cuneata*	1.4	4.14	2790 ± 15	1670	3130	1.36	**2.14**	2.87
		144003	*Rangia cuneata*	1.96	4.7	5370 ± 15	4880	6270		inverted	
	③	OS-34797	*Crassostrea virginica*	4.4	7.14	4130 ± 35	3310	4840	3.52	**4.22**	4.92
	④	OS-34796	*Rangia cuneata*	8.11	10.85	6530 ± 35	6270	7510	6.36	**6.93**	7.41
	⑤	Beta-135431	*Macoma Mitchelli*	8.64	11.38	6860 ± 60	6580	7850	7.03	**7.54**	8.04
		Beta-135429	Peat	10.19	12.93	8030 ± 150	8540	9320		inverted	

OS - Woods Hole Oceanographic Institute; Beta - Beta Analytic; AA - University of Arizona; 14 - University of California - Irvine

3.3.2 Palynological Analysis

Sediment samples were chemically processed by Global GeoLab Limited following standard palynological laboratory methods (Brown, 2008). Dry sample weights were recorded before processing, with an average of 10 grams used per sample. Lastly, a *Lycopodium* spores tablet with a known amount was added in order to determine palynomorph concentration values (palynomorph/gram). A minimum of 300 known in-situ palynomorphs (pollen, spores, and dinoflagellate cysts) were counted when available for each sample to ensure accurate paleo-environmental representation.

3.3.3 Statistical Analyses

Statistical analyses were used in combination with individual core age-models to determine the potential timing of shifts in paleo-environment or climate. Constrained cluster analysis using

Bray-Curtis similarity and correspondence analysis (CA), both based on raw abundance data, were used to examine changes in pollen and spore assemblages through time within each core. Similarity Percentage analysis (SIMPER) based on the Bray-Curtis similarity was achieved to determine which taxa were controlling the clustering. All statistical analyses were conducted using PAST v. 2.17c freeware (Hammer et al., 2001).

3.4 Results

3.4.1 Age Models

Corpus Christi Bay core CCB02-01 uses the same age model produced by an earlier study (Ferguson et al., in press). The age models for Trinity Bay's TBHD5-1 and TV-99-3 have been updated and revised from their previously published versions (Anderson et al., 2008), so that the three cores have similarly-derived age models and can be shown on the same age axis (Fig. 3). Ages in the text and figures always refer to the Bchron 50% quantile, and reported in thousands of years before present (ka). Core CCB02-01 covers the most time, from 11.5 ka to 1.6 ka. Our sampling of TBHD5-1 spans from 4.5–1.0 ka, and core TV99-3 includes a short yet detailed look into the most recent past from1.8 ka to 0.2 ka.

3.4.2 Palynological Results

Twenty-three unique taxa were observed within these cores (Appendix Table B1). Common to all samples were nonarboreal taxa including low and high spine Asteraceae (mainly *Ambrosia* and *Helianthus*), *Chenopodium*, Poaceae, and arboreal taxa such as *Carya*, *Pinus*, and *Quercus*. The abundance of these taxa varies between cores; however, the majority of taxa are shared by both bays. Absolute abundance of palynomorphs generally decreases down-core, likely due to oxidation after deposition. No clear first or last occurrence for any given taxa was found, but

rather a transition through time of dominance of one group versus another. Lack of reworked taxa and the high quality of observed palynomorphs imply that the studied cores are representative mostly of their immediately surrounding environment, and thus mostly represent their respective drainage basins only to a limited extent.

In general, these assemblage results from Trinity Bay and Corpus Christi Bay show a trend of herbaceous nonarboreal dominated assemblages in the early to mid-Holocene transitioning into arboreal dominated assemblages in the late Holocene (Fig. 4). The transition within Trinity Bay occurs much more rapidly. Two noteworthy peaks in *Carya* (hickory tree, pecan tree) are noted at 4.1 ka and 2.2 ka in Corpus Christi Bay. Overall, Corpus Christi Bay has much more nonarboreal then arboreal pollen throughout the studied interval (average relative abundance of nonarboreal is 72%) while Trinity Bay has been clearly more humid throughout the time interval studied with arboreal pollen dominating with average values of 70% (i.e., average relative abundance of nonarboreal of only 30%) (Fig. 5). Statistical results further explore this palynological trend and provide better constraint on the timing of observed changes.

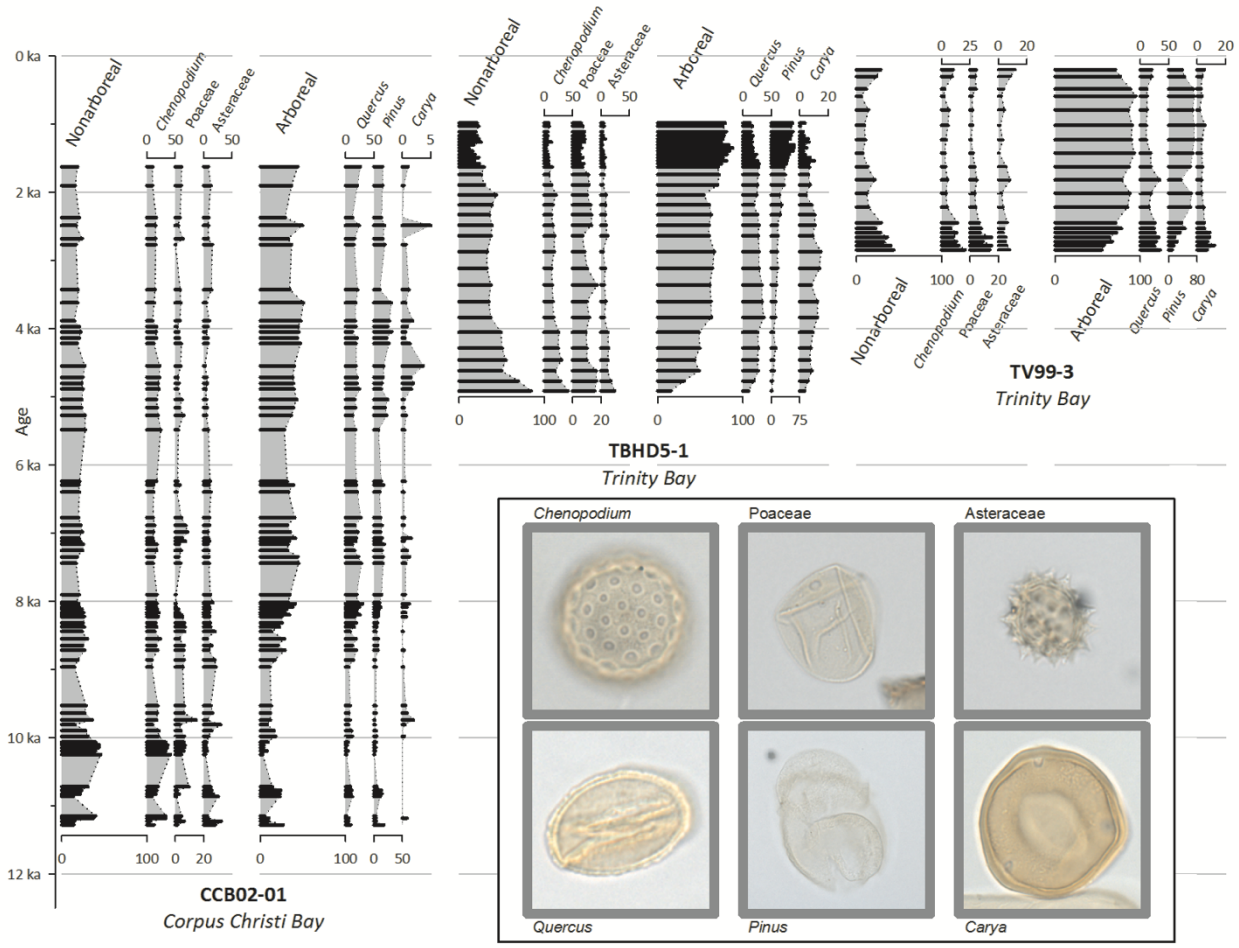

Figure 4. Summary pollen chart for Corpus Christi Bay and Trinity Bay with a common age axis. Inset plates show common species *Chenopodium*, *Quercus*, Poaceae, *Pinus*, Asteraceae, and *Carya*.

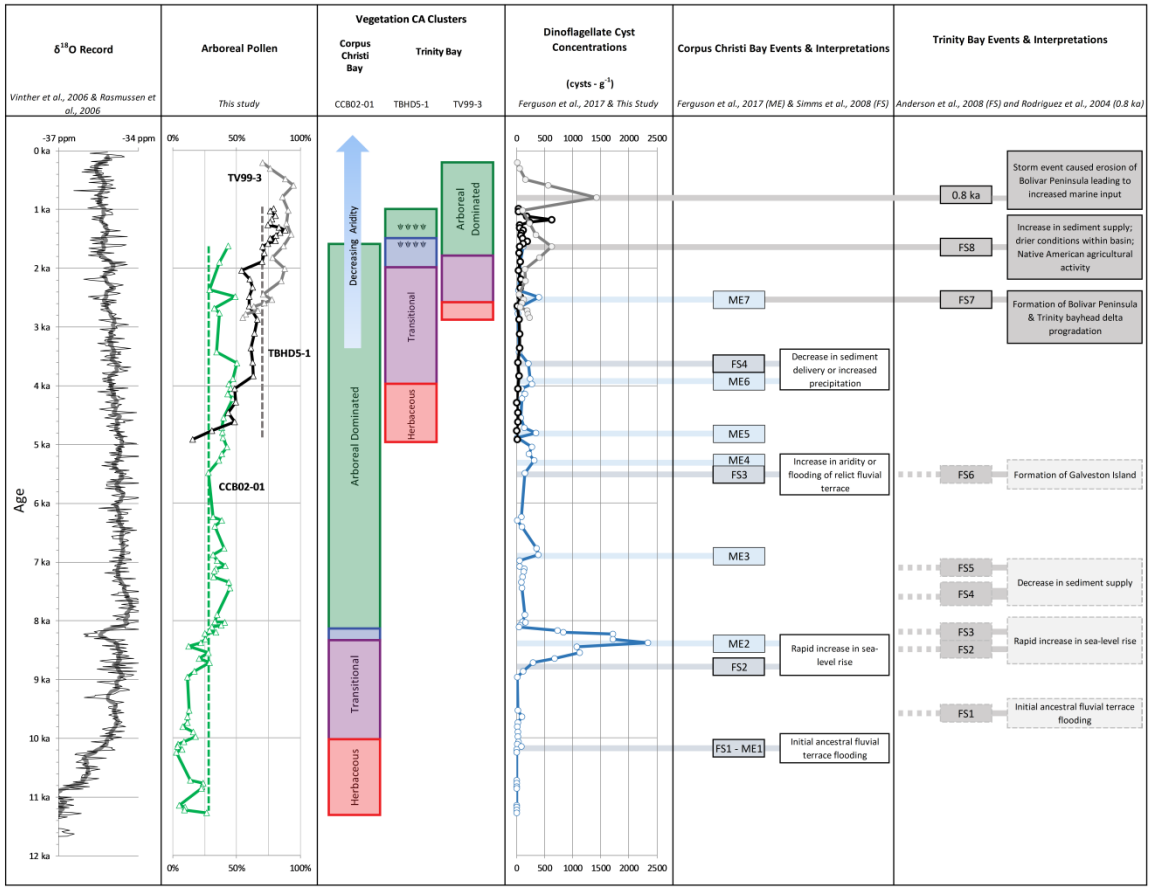

Figure 5. Summary plot of the arboreal pollen concentrations, alongside a gradually sloping δ18O record (Rasmussen et al., 2006; Vinther et al., 2006) Overlaps of core records show that each is a part of the same overall linear record of arboreal pollen increasing during the Holocene. Dinoflagellate cyst concentrations from this study are also shown, along with Corpus Christi Bay marine events (ME) from Ferguson et al. (in press), flooding surfaces (FS) from Simms et al. (2008) with revised ages reported from Ferguson et al. (in press). Trinity Bay flooding surfaces and geologic events from Anderson et al. (2008) shown with 1.6 ka (FS8) event matching with our TV99-3 dinoflagellate record. The Trinity Bay (TV99-3) 0.8 ka event corresponds to a major storm event recorded by erosion of beach ridges on Bolivar Peninsula (Rodriguez et al., 2004). The vertical dashed green line represents the average arboreal value for Corpus Christi (28%) while the dashed grey line represents the average arboreal value for Trinity Bay (70%).

3.4.3 Statistical Results

Cluster analysis (Appendix Figure B1; Appendix Table B2) followed by correspondence analysis were performed on complete pollen assemblages within each core (Fig. 6A–C), as well on just the 11 taxa common to each core. The all-taxon and 11-taxon analyses for each separate core produced essentially similar results, as the 11 common taxa together control more than 80% of among-cluster differences. These 11 major taxa are Asteraceae, *Chenopodium*, Poaceae, *Ilex*, Onagraceae, *Acer*, *Alnus*, *Carya*, *Juglans*, *Pinus*, and *Quercus*.

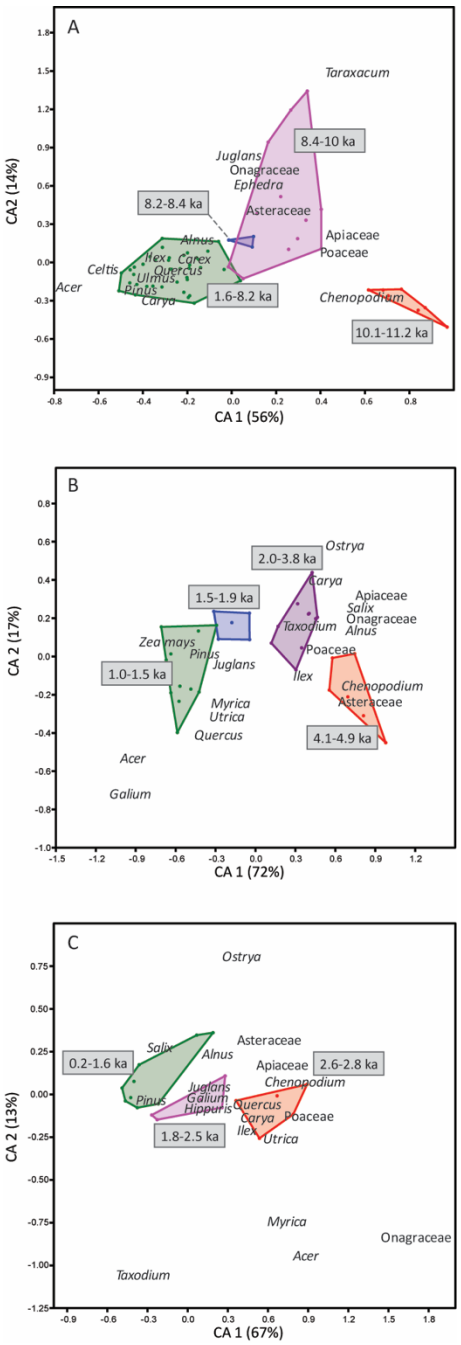

Figure 6. All-taxon correspondence analysis results for each studied core. Polygon grouping was derived from cluster analysis (Supplementary Figure 1¬–3). (A) Corpus Christi Bay, core CCB02-01. (B) Trinity Bay, core TBHD5-1. (C) Trinity Bay, core TV99-3.

Four distinct sample clusters (Fig. 6A, colored polygons) are present in both CCB02-01 and TBHD5-1; TV99-3 has the fewest samples, and only produced three clusters. The clusters correspond to different age ranges within each core, with no inversions or mixing. The same observational trend seen within the palynological results (Fig. 4) is also seen within these clusters: deeper samples are dominated by herbaceous and nonarboreal taxa, which transition to mostly arboreal taxa towards the top of the cores. In addition, the clusters provide important age control for each transitional

event. At Corpus Christi, the first cluster occurs from 11.2 to 10.1 ka, and is characterized by the strongest representation of herbaceous plants with mostly *Chenopodium*. A second cluster occurs from 10 to 8.4 ka; the samples included in this cluster are mainly composed of herbaceous plants (Poaceae, Asteraceae) but also a variety of angiosperms (*Juglans*, Onagraceae, and Apiaceae) and *Ephedra*. A unique 200 year-long cluster occurs from 8.4 until 8.2 ka. The vegetation is not extremely different in this horizon, however pollen abundance decreases tremendously, while dinoflagellate cyst peaks in abundance (Fig. 5). Finally, the fourth cluster represents a tree-dominated environment (*Alnus, Carex, Quercus, Ulmus, Pinus* and *Carya*) from 8.2 ka onwards.

Although the interval at Trinity Bay is shorter (the last 4.9 ka), a similar trend towards an increasingly tree-dominated environment is noted. Some minor changes allow the subdivisions of the period of tree dominance into four time intervals for core TBHD5-1 (Fig. 6B). These sub-intervals occur at the age intervals 4.9 to 4.1 ka, 3.8 to 2.0 ka, 1.9 to 1.5 ka, and 1.5 to 1.0 ka. It is interesting to note that one of the markers allowing for the separation of the fourth interval is the presence of *Zea mays*, or maize. Despite being wind-pollenated, *Zea mays* pollen grains are large in size and density causing the grains to sink from the air quickly near the crop itself allowing for a local signal (Traverse, 2007). The presence of maize occurs in core TBHD5-1 at 1.5 ka, 1.3 ka, and 1.2 ka (one grain per interval; Table S2).

Core TV99-3 has three distinct palynological clusters (Fig. 6C). Between 2.8 and 2.6 ka a majority of herbaceous genera (*Chenopodium*, Poaceae, *Utrica*, and *Ilex*) and two arboreal taxa (*Quercus*, and *Carya*). From 2.5 to 1.8 ka arboreal *Juglans*, *Galium*, and *Hippuris* control this transitional cluster. Lastly, between 1.6 ka and 0.2 ka *Pinus* (pine), *Salix* (willow), and *Alnus* (alder) characterize the most recent time period. This core has more taxa as outliers than the other cores because of the relatively low abundance of many of the taxa (Fig 6C).

The same analyses performed on a dataset including all three cores shows that samples from the three cores plot amongst one another, and not within separate, core-dependent groups (Fig. 7). Comparison of the first correspondence axis (CA1) resulting from the combined core analysis against the CA1 resulting from the separate correspondence analysis of core CCB02-01 yields an almost perfect linear relation (R^2 = 0.96) (Fig. 8A); comparison with both Trinity Bay cores yields an even higher R^2 of 0.99 (Fig. 8B). Such congruence of the first correspondence (CA1) axis between the three separate cores and the combined core analyses indicates that this axis within each separate core points toward the same environmental gradient controlled by the same taxa. This makes it possible for direct comparisons of the environmental changes seen within the three cores, and strongly suggests that these changes were driven by allogenic factors influencing both bays, rather than separate autogenic forcings.

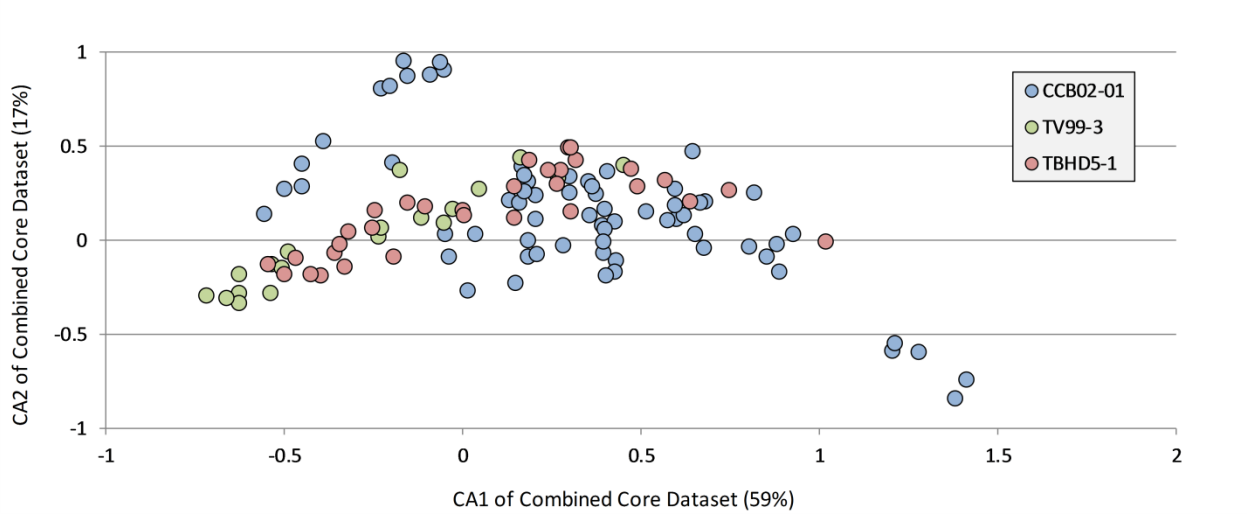

Figure 7. Correspondence analysis result based on the combined three-core 11-taxon dataset. Samples from different cores plot amongst one another instead of within separate, core-dependent groups.

Based on the sample groups resulting from the cluster analyses of each separate core, SIMPER analyses enable the identification of the taxa that most contribute to cluster's differentiation – i.e., the taxa that most strongly vary in abundance from one cluster to another

(Appendix Table B2). At Corpus Christi Bay, contrasting the two oldest samples groups D and C (Fig. 6A: red and purple clusters) shows that 78% of the overall average difference (OAD) between these two clusters is controlled by changes in abundances of *Chenopodium*, Asteraceae, *Quercus*, and Poaceae (in order of percent contribution; Table S3). Contrasting the second (C) and third (B) samples groups shows that 72% of their OAD is driven by Asteraceae, *Chenopodium*, *Quercus*, and Poaceae. Last, contrasting the most recent sample groups B and A shows 82% of their OAD is controlled by changes in abundances of *Pinus*, *Quercus*, *Chenopodium*, and Asteraceae. In Trinity Bay these same taxa are involved at similar percentages of contribution to between-group OAD, indicating similar changes in vegetational habitats from one cluster to another. Thus, the main difference between the bays is based not upon the individual clusters of vegetation, but rather the timing and appearance of these clusters (Fig. 6).

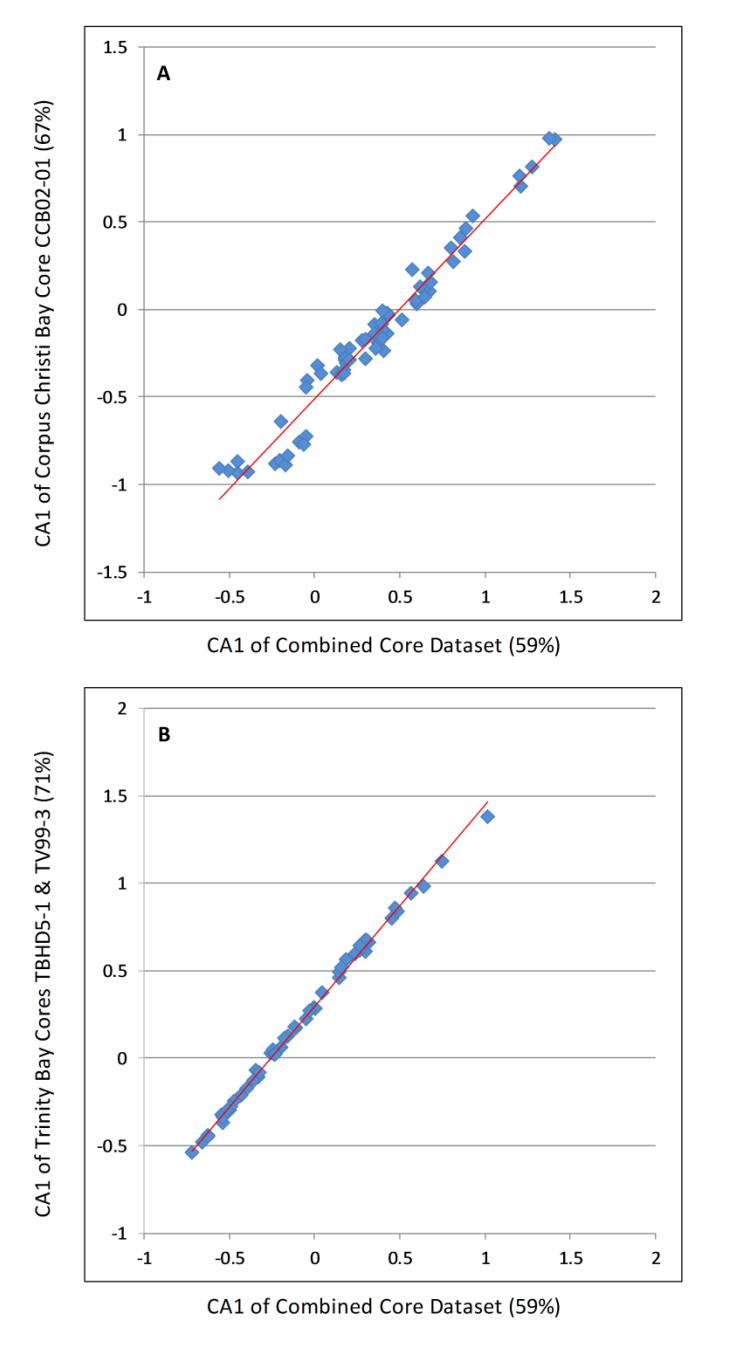

Figure 8. Comparison of the first correspondence axis (CA1) of the combined three-core dataset with the CA1 of datasets from the individual bays. (A) Comparison with CCB02-01 yields an R^2 of 0.96. (B) Comparison with both Trinity Bay cores yields an R^2 of 0.99.

3.5 Discussion

3.5.1 Vegetational Holocene Evolution

Factors such as soil type, water or soil pH, flooding frequency, light intensity, nutrients, and anthropogenic disturbances can produce different community structures composed of different plants or mixtures of plants with or without a climatic forcing (Wharton et al., 1982). This said, clear trends are observed and statistically validated in the studied cores. Cores from both bays show a vegetational trend from nonarboreal-dominated to arboreal-dominated vegetation through the Holocene, the change being more pronounced in Trinity Bay (Fig. 5). Assemblages determined from cluster, correspondence, and SIMPER analyses show little variation between the two bays despite their geographic separation. Overall, the higher relative abundance of trees at Trinity Bay confirms that this area was more humid than Corpus Christi Bay throughout the time interval covered by all three cores. An exception occurs at the base of the observed Trinity Bay record, where arboreal pollen is close to 15%; it is unclear if this suggests that mid-Holocene Trinity Bay was much drier than it is now, or if this is simply because the Trinity bayhead delta was further away from the cored locations at this point in time, which reduced input of arboreal pollen.

Out of the dominant taxa observed in this study, many are tolerant of infrequent flooding of varying duration. The most tolerant taxon is *Taxodium distichum* (common in shallow waters that experience frequent drying periods between floods), while *Carya* and *Juglans* are unable to survive more than a few days of flooding at a time. Thus, all most likely represent low-lying forest cover types with *Taxodium* in lower sections, and exclude full marsh or backswamp locales. Most *Quercus* species currently living along Texas' coast can only tolerate minimal to occasional flooding (*Quercus alba, Q. fusiformis, Q. macrocarpa*) (Moulton et al., 1997). Other

species (*Q. nigra, Q. phellos, Q. lyrata*) are slightly more tolerant of flooding and typically occur along river floodplains at higher elevations than *Taxodium distichum* (Moulton et al., 1997). However, *Quercus* pollen is difficult to reliably isolate to the species level with a light microscope and therefore it is important to use other genera to help understand a habitat's tolerance to flooding and typical amount of water saturation. *Carya* is commonly associated with *Juglans*, *Fraxinus*, *Celtis*, and *Ulmus* along shallow marginal swamps and floodplains of the Gulf Coast. *Carya* is particularly common inland and is part of the riparian vegetation of the Nueces River (Vaughn Bryant, pers. comm.). Thus, the peaks observed at 4.1 ka and 2.2 ka in Corpus Christi Bay could indicate an increase in river discharge; *Myrica* is normally an understory shrub within this community (Moulton et al., 1997). The prevalence of *Pinus* pollen found in samples is likely a product of regional pollen rain from the drainage basins' interfluvial wet pine flatlands (Moulton et al., 1997). While some *Pinus* pollen is considered to be autochthonous, the abundance of pollen *Pinus* produces, along with its morphological ability to travel large distances, should be kept in mind when determining its presence around the bays and basins they drain.

Herbaceous taxa are abundant, particularly in the lower sections of all the cores. Many of these species are confined to open coastal habitats due to their need for full sunlight. Herbaceous plants can also dominate drier environments and tundra plains, but some species of Chenopodiaceae, low-lying Asteraceae, Cyperaceae, and Poaceae (for instance *Spartina* marsh grasses) are also adapted to growing in continually wet fresh to brackish conditions, with many species able to tolerate the salinity of coastal soils in return for the freedom of little to no canopy cover. The occurrence, and at times dominance, of these species within some intervals indicates dominance of a marsh environment.

In summary, the environment at both study areas evolved from a marsh-dominated environment to an increasingly dense riparian canopy of trees along the rivers and bays. The trend occurs over a much shorter period in Trinity Bay, as Corpus Christi Bay was transitioning away from nonarboreal vegetation as much as 4 ka earlier. The shorter record from Trinity Bay makes direct comparison of these bay's coeval vegetation regimes impossible for much of the early Holocene, but correspondence analysis results confirm that the clusters occurring at both bays are identical. Thus, a longer record in Trinity Bay would likely only extend the base of the oldest nonarboreal-dominated cluster, and not affect the age of the transition between clusters.

3.5.2 Relationship Between Holocene Climate Evolution and Sedimentation of Coastal Texas

In Trinity Bay, *Chenopodium* and Asteraceae are the main vegetational component of the oldest samples from 4.91–4.05 ka (TBHD5-1; Fig. 6B). The vegetational landscape began experiencing more diversity around 3.83 ka, at which time a number of other nonarboreal elements such as Apiaceae, Onagraceae, Poaceae, and *Ilex* appear in core TBHD5-1. TV99-3's shorter record begins at 2.84 ka, and mirrors the assemblages found within TBHD5-1. *Alnus* and *Carya* are important arboreal components beginning at 2.04 ka, while *Pinus* and *Juglans* have the greatest influence from 1.89–1.53 ka (TBHD5-1 and TV99-3). Increased fluvial discharge, frequency of flooding, and associated increase in sediment delivery to Trinity Bay are thus indicated for the late Holocene. This corresponds to significant growth of the Trinity bayhead delta, as documented by Anderson et al. (2008), and is corroborated by the low dinoflagellate cyst concentrations seen within proximal TBHD5-1 during this time, interpreted as indicating increased freshwater discharge to the bay (Fig. 2; Fig. 5).

Dinoflagellate cyst concentrations at more distal TV99-3 were unaffected in the same way, with a peak in concentrations at that location at ~1.7 ka. This peak is smaller in magnitude than a peak occurring at 0.8 ka that we hypothesize is related to an established major storm (Rodriguez et al., 2004; Anderson et al., 2008). Rodriguez et al. (2004) suggest that the storm cut deeply into the Bolivar Peninsula and resulted in a reduction of the Galveston-Bolivar barrier complex as an effective salinity barrier. Thus, perhaps the 1.7 ka event is similarly storm-related.

Finally, a major shift to oak-pine woodland vegetation occurred around 1.49 ka based on our correspondence analysis. *Pinus* and *Quercus* are the major overall contributors to the pollen assemblage in this recent core section. This assemblage also includes *Zea mays*, which is an indication of early agriculture. Thus, this assemblage is likely either indicative of, or coincides with, anthropological influence rather than a climatic change. Native American activity in coastal Texas is known for that time period from other records (Ricklis, 2004), and is thought to have occurred as far back as 9.5 ka (Warny et al., 2012).

The Corpus Christi Bay palynological record generally shows a similar overall vegetational evolution as observed in Trinity Bay, but this evolution occurred much earlier. In general, Corpus Christi Bay has an overall lower arboreal component than Trinity Bay, but its transition to dominance of that component occurred up to 4 ka sooner. Similar to Trinity Bay core TBHD5-1, Corpus Christi Bay core CCB02-01 had enough within-core differences allowing for the subdivision of four vegetation assemblages through time. As stated previously, these assemblages are statistically identical to the assemblages seen later in Trinity Bay (TBHD5-1 and TV99-3). *Chenopodium* primarily controls variability in the earliest part of the Corpus Christi Bay record from 11.2–10.1 ka. More herbaceous elements (Asteraceae, Apiaceae, Onagraceae, and Poaceae) are added to the assemblage starting from 10–8.4 ka (Fig. 4a). From

8.4–8.2 ka (Fig. 4a, blue cluster), a brief period of time is isolated by cluster analysis (Appendix Figure B1), likely due to the low pollen yield recovered during this time. This interval is also marked by a flooding surface (FS2) expressed in seismic records and cores from the bay (Simms et al., 2008; Rodriguez et al., 2010). Ferguson et al. (in press) observed a marked increase in dinoflagellate cysts during that same interval of time with an assemblage dominated by *Polysphaeridium zoharyi*, a dinoflagellate species requiring marine salinity. They postulated that this prominent and sudden increase corresponds to the overtopping of Mustang Island during the ~8.2 ka northern hemisphere ice sheet mass wasting event and associated abrupt sea-level rise (the only major perturbation in the $\delta^{18}O$ curve for the Holocene, Fig. 5). That interval is not marked by notably different vegetation, so it is indeed likely that the sedimentation at that time was controlled by a punctuated sea-level rise event, rather than a regional climatic event. After this time, from 8.2–1.6 ka, the increasing abundance of trees is the main element controlling the clustering. This is coincident with the progradation of the delta after the major flooding of the delta during the 8.2 ka event. *Pinus*, *Quercus*, *Acer*, *Alnus*, *Carya*, *Ulmus*, and *Celtis* all contribute to the clustering at this time.

Simms et al. (2008) noted two other potential flooding events at 5.4 ka and 3.6 ka (revised ages of FS3 and FS4 from Ferguson et al., (in press) age model. At 5.4 ka, our palynological record indicates that this time interval marks the beginning of an increase in arboreal pollen, along with a marine event marked by an increase of dinoflagellate cysts (Fig. 5) (Ferguson et al., in press). Simms et al. (2008) believed that this horizon was either due to a climatic change towards warmer and drier conditions or the flooding of a relict Nueces fluvial terrace. We suggest that the coupled increase of dinoflagellates and arboreal pollen indicates that this event was a result of flooding of relict terraces.

At 3.6 ka, our records from Corpus Christi Bay show arboreal pollen accounts for 50% of the palynological assemblage, well above the core average (Fig. 5). Simms et al. (2008) hypothesized that this horizon might have been associated with a decrease in sediment delivery due to a climatic drying event. Based on the palynological data, the 3.6 ka event was marked by a climate shift but was likely a return to more mesic climatic conditions, which would have increased tree cover, stabilized the landscape, and a decreased fluvial output/sediment supply. This shift to more mesic condition around 3 ka is also shown as a decrease in more salt tolerant foraminifera within Baffin Bay (Buzas-Stephens et al., 2014).

3.6 Conclusions

Our results show that the Holocene coastal environments of central Texas began transitioning from herbaceous (nonarboreal) dominated vegetation to arboreal dominated vegetation as early as ~8.4 ka. This is indicative of a transition to less aridity as coastal rivers and bays evolved from a marsh-dominated environment to an increasingly dense riparian canopy of trees. Lack of reworked palynomorphs indicate that our samples are indicative of local vegetation, rather than regional or basin-scale vegetation changes.

In Corpus Christi Bay, pollen indicates potentially increased discharge from Nueces river at 4.1 ka and 2.2 ka. Marine flooding events are seen at 8.2 ka, 5.4 ka, and 3.6 ka. As suggested by Ferguson et al. (in press), the 8.2 ka event is associated with the rapid draining of Lake Agassiz-Ojibway. Simms et al. (2008, FS2) suggested that the 5.4 ka event was the flooding of relict fluvial terraces, which we support with an associated increase in dinoflagellate concentrations likely related to the areal increase in warm brackish surface waters. At about 3.6 ka there was an increase in mesic conditions, indicated by a large abundance of arboreal pollen. This was

coincident with a slight increase in dinoflagellate cysts indicating low freshwater input into the bay. This event corresponds to a flooding surface observed by Simms et al. (2008, FS4) which they interpret as the product of low sediment delivery to the bay.

Flooding events in Trinity Bay were observed at 1.7, 1.2, and 0.8 ka; the 0.8 ka event is likely related evidence of a major storm that Rodriguez et al. (2004) suggest cut through the Bolivar Peninsula at that time. The 1.7 and 1.2 ka events are smaller in magnitude, and may also be storm-related. Finally, the most recent vegetation assemblage includes *Zea mays*, indicative of native American activity around Trinity Bay starting at least 1.49 ka.

Our record from Corpus Christi Bay shows a gradual change during the middle Holocene Climate Optimum, which appears to have been a significant climate event based on other paleoclimate records (Toomey, 1993; Humphrey and Ferring, 1994; Nordt et al., 1994; Nordt et al., 2002). We see no evidence that the vegetation assemblage of coastal Texas changed in direct response to the Holocene Climate Optimum. There is subtle, but not statistically significant, evidence of the more variable climate oscillations for the late Holocene. But, our data indicates that Coastal Texas' climate operated independently from the central Texas regions previously studied. Both bays underwent a nonarboreal to arboreal environmental change, starting around 8.4 ka in Corpus Christi Bay, but not until ~5 ka in Trinity Bay. The late Holocene record for Trinity Bay shows a greater dominance of arboreal pollen than in Corpus Christi Bay for the same time interval, likely due to its greater precipitation and lower evapotranspiration rates.

CHAPTER 4
PALYNOLOGICAL RESPONSE TO EARLY- TO MID-HOLOCENE CHANGES IN EUSTASY AND CLIMATE IN BAFFIN BAY, TEXAS

4.1 Introduction

Worldwide, coastal and low-lying regions face the challenge of rising sea levels in the coming centuries. These areas are some of the most densely populated on Earth, and understanding how they will react is paramount to mitigating the high cost of increased coastal hazards. Studies of how these environments responded to sea level rise following the Last Glacial Maximum (LGM) can offer timely insight. These are much needed considering what we know of past Holocene sea level rise and what is expected for the next century. When controlling for variability from subsidence and potential glacial-isostatic adjustments across the region, the average late Holocene rate of sea level rise for the western Gulf of Mexico has been estimated to range between 0.4 and 0.6 mm/yr (Törnqvist et al., 2004a; Törnqvist et al., 2004b; Tornqvist et al., 2006; Simms et al., 2007; Milliken, 2008; Livsey and Simms, 2013). Modern rates of sea level rise are as much as an order of magnitude higher, and are expected to double by 2100 (Törnqvist and Hijma, 2012; Bamber and Aspinall, 2013; Church et al., 2013; Anderson et al., 2014). Retreat of the Antarctic Ice Sheet alone due to ocean and atmospheric warming is projected to cause >1 m of eustatic sea-level rise by 2100 and as much as 15 m over the next 500 years (DeConto and Pollard, 2016), likely in episodic pulses (Feldmann and Levermann, 2015). These pulses can have catastrophic effects on coastal infrastructure. For instance, Ferguson et al. (2017) recently showed that a coastal barrier island that partially protected Corpus Christi Bay, Texas, was breached in response to a sudden sea level rise at approximately 8.2 ka. This

occurred as a result of the melt and collapse of the Laurentide Ice Sheet during the early Holocene (Ullman et al., 2016). Similar style of punctuated eustatic sea-level rise is likely to occur with the accelerated melting of Antarctic Ice Sheets (Anderson et al., 2014), adding relevance to records of coastal change in response to these rapid eustatic changes. Here we present a new Holocene palynological record from neighboring Baffin Bay, an area of coastal Texas lacking a coastal barrier during the time interval studied.

4.2 Geologic Setting

Baffin Bay is located along the semi-arid south central coast of Texas, approximately 50 km south of Corpus Christi Bay, TX and perpendicular to the Gulf of Mexico coastline (Figure 1). The bay is one of many in the Gulf of Mexico formed by incision during the ~120 ka eustatic sea-level fall of last glacial maximum (26 to 20 ka) (Fisk and McClelland, 1959; Simms et al., 2010). Global sea-level was 90 to 120 m lower during the LGM, allowing the San Fernando, Petronilla, and Los Olmos Creeks to incise within Baffin Bay, its tributaries Cayo del Grullo and Alazan and its shoreward lagoon Laguna Salada.

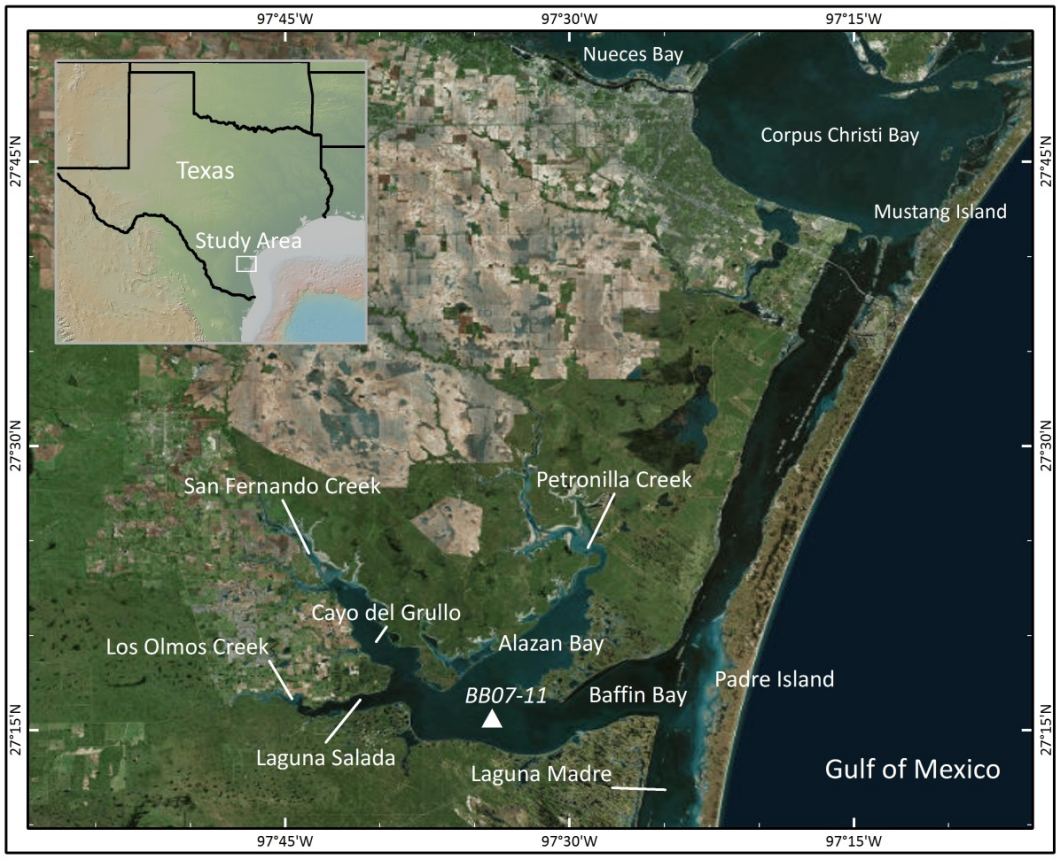

Figure 1. Location of Baffin Bay, Texas and surrounding area. Core BB07-11 (originally collected by Simms et al., 2010) location is shown with triangle symbol.

Modern Baffin Bay has a maximum depth of 3 m, and extensive rocky shoals at the mouth of Alazan Bay, and between Baffin Bay and Laguna Madre. These shoals inhibit both fresh and marine water exchange (Dalrymple, 1964). The climate is semi-arid; evapotranspiration rates here exceed precipitation by ~53 cm- y^{-1} (Thornthwaite, 1948), and the low precipitation leads to only an ephemeral freshwater input from the creeks. Salinity within the modern bay is usually hypersaline, ranging from 40 to 50‰ (Buzas-Stephens et al., 2014), with short-term variability of salinity controlled by extreme precipitation changes such as droughts and cloudbursts (Gunter, 1944; Behrens, 1966). Southern and coastal Texas have gradually become wetter through the

Holocene, likely due to the North American monsoon being weakened by southern migration of the inter-tropical convergence zone (ITCZ) (Poore et al., 2003; Buzas-Stephens et al., 2014).

The bay lies at the northern extent of the relatively small (<8500 km^2) Texas Coastal Sand Plain, bordered to the south and west by the Texas Savanna, and to the north by the Texas Coastal Prairie region (Fulbright et al., 1990). The semiarid Coastal Sand Plain is recognized as its own distinct region due to the unique geology and climate that have combined to create a mosaic of different habitats. Wind-worked Quaternary sand substrate forms active unvegetated dunes, more stable vegetated dune and swale terrain, and expansive tidal flats dotted with low-lying ephemeral ponds (Fulbright et al., 1990).

Baffin Bay has had no direct connection to the Gulf of Mexico since the formation of Padre Island barrier complex around 5.5 ka, currently the longest barrier island in the world (Simms et al., 2010). Following 5.5 ka, the semi-arid climate and marine isolation led to depositional environments and sedimentological deposits unique from all other northern Gulf of Mexico valleys (Buzas-Stephens et al., 2014). Carbonate muds, ooids, evaporites (gypsum), aeolian deposits, dolomite, and serpulid-worm tube reefs are all currently found here (Emery and Stevenson, 1957; Behrens, 1966; Judd et al., 1977; Simms et al., 2010). As none of these deposits existed prior to 5.5 ka, Simms et al. (2010) postulated that the formation of Padre Island occurred at about 5.5 ka. Prior to that, during the initial flooding of the incised valley, sediments deposited are characterized as open bay silts and fine sands (Simms et al., 2010).

4.3 Materials and Methods

4.3.1 Core Selection and Age Model

The core selected for palynological sampling in this study was collected for a sedimentological study conducted by Simms et al. (2010). The chosen core (BB07-11) was the longest (17.7 m) and oldest core recovered. The core has been dated by Simms et al. (2010). Their study provides 5 radiocarbon ages, 3 of which are relevant to the time period of interest for this study (Figure 2). Radiocarbon dates have been re-calibrated using the Marine13 curve (Reimer et al., 2013) and a western Gulf of Mexico reservoir correction (ΔR) of 100±300 ^{14}C (Törnqvist et al., 2015). The Bchron package (Haslett and Parnell, 2008; Parnell et al., 2008) for R was used to create the final age model. Bchron reports age estimates for each sample depth at five quantiles (2.5%, 10%, 50%, 90%, and 97.5%, Appendix Table C1), each of which refers to the likelihood that the age of a given sample depth is younger than the estimate. Dates within the text are reported at the 50% quantile, in thousands of years before present (BP).

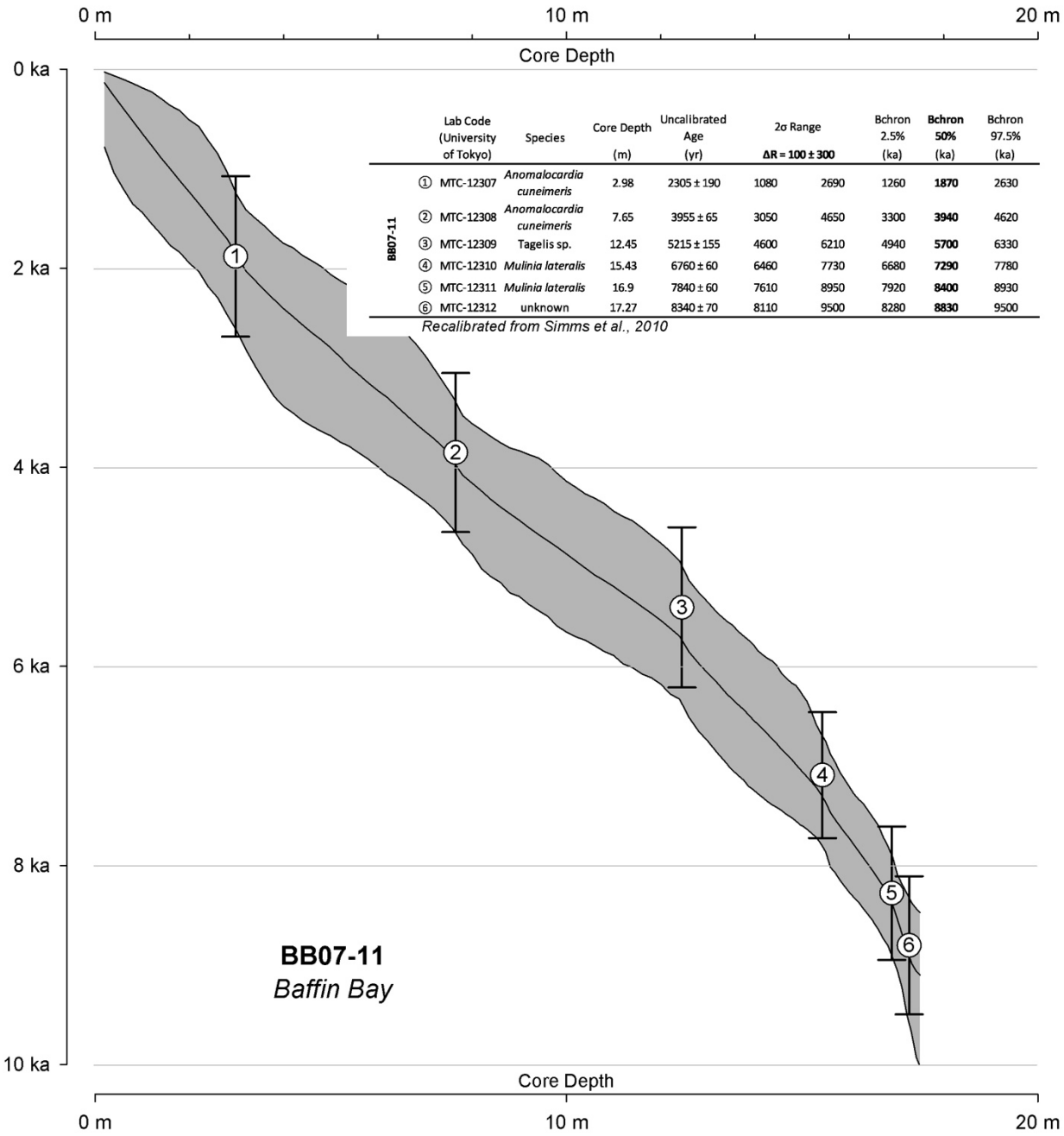

Figure 2. Bchron age model and radiocarbon dates for core BB07-11. All dates reported in text are from the 50% quantile.

4.3.2 Palynological Sample Selection, Processing, and Analyses

Core BB07-11 was also chosen based on its recovery of well-preserved open bay deposits dated to 9.5–5.7 ka. Thirty-two samples from this this time period of interest were chosen for palynological analysis, at 10 cm intervals (when sediment was available). Samples were processed by Global GeoLab Limited, Alberta, Canada using a laboratory chemical digestion technique, including use of hydrofluoric and hydrochloric acids to remove the mineral components (silicates and carbonates) (Brown, 2008). Approximately 4 grams of sediment per sample was processed, and a known quantity of *Lycopodium* spores was added to the sediment in order to determine concentration values (palynomorphs/gram). A minimum of 300 identifiable palynomorph specimens were counted per sample to ensure accurate paleo-environmental representation. Microscope analysis was completed at the CENEX Microscopy Center, Louisiana State University using a BX41 Olympus microscope mounted with 60x and 100x oil-immersion objectives. Specimens were photographically documented using a digital QCapture camera and software.

4.4 Results

4.4.1 Dinoflagellate Cyst Results

The assemblage of dinoflagellate cysts recovered is rich but low in diversity. Only six types of dinoflagellate cyst taxa are present in our observed section: *Spiniferites* spp., *Lingulodinium machaerophorum*, *Polysphaeridium zoharyi, Operculodinium centrocarpum*, *Nematosphaeropsis rigida* and *Tuberculodinium vancampoae* (Figure 3). Dinoflagellate cysts are present at 9.1 ka (the bottom of our record), and rise to a peak at 8.4 ka where they mark the

largest marine event seen in our record. By this time coastal species *Polysphaeridium zoharyi* dominates the assemblage with a concentration value of $6.6x10^3$ cysts – g^{-1} out of a total dinoflagellate concentration value of $7.8x10^3$ cysts – g^{-1} (Figure 4A; Appendix Table C2). Dinoflagellate cyst concentrations remain high following the 8.4 ka peak, only gradually decreasing until another prominent peak at 8.1 ka (Figure 4A). A third and final peak occurs at 7.6 ka, second in magnitude to the 8.4 ka event.

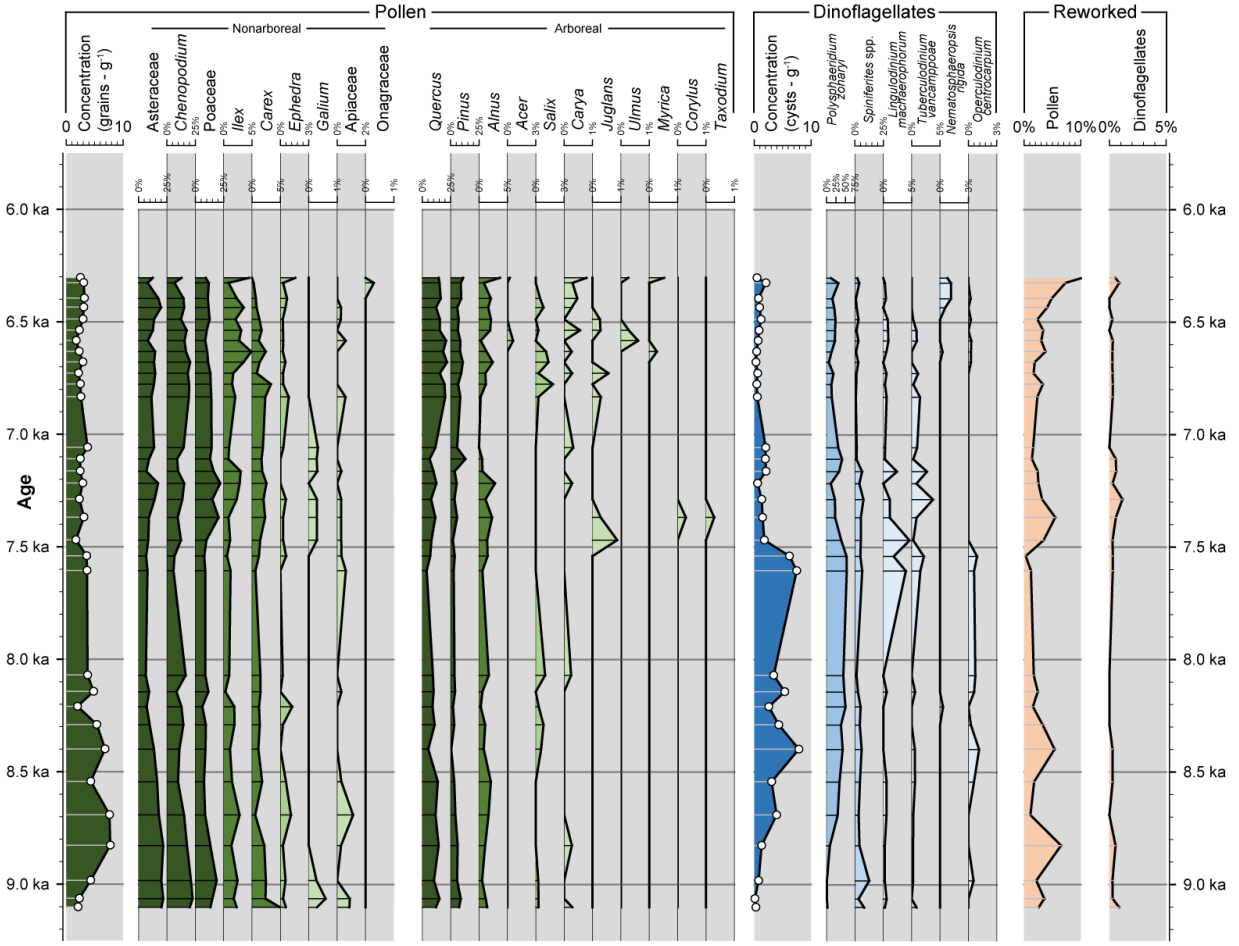

Figure 3. Complete palynological data. Overall concentration values shown for pollen and dinoflagellate cysts. Relative abundance reported for individual taxon.

4.4.2 Pollen Results

A total of 20 different pollen taxa were present in this study (Figure 3; Appendix Table C2). In order of decreasing abundance, nonarboreal (herbaceous) taxa include Asteraceae (Compositae), *Chenopodium* (goosefoot), Poaceae (grasses), *Ilex* (holly), *Carex* (sedge), *Ephedra*, *Galium*, Apiaceae (Umbeliferae), and Onagraceae (evening primrose family). Arboreal taxa include *Quercus* (oak), *Pinus* (pine), *Alnus* (alder), *Acer* (maple), *Carya* (hickory), *Juglans* (walnut), *Ulmus* (elm), *Myrica* (bayberry), *Corylus* (hazel), and *Taxodium* (likely bald cypress). Herbaceous pollen dominates the entire studied section (Figure 4B). The abundance of arboreal pollen increases in a fairly linear fashion through the studied interval (Figure 4B), but herbaceous pollen remains above 50% relative abundance for the entire study period (9.1 ka to 6.3 ka).

Reworked palynomorphs are low throughout the study with 11% of reworked palynomorphs at 6.3 ka (Figure 3). There are also notable peaks of abundance associated with increases in dinoflagellates at ~8.8 ka, 8.4 ka, and lastly at 7.6 ka occurring immediately after the last major increase of dinoflagellate cysts.

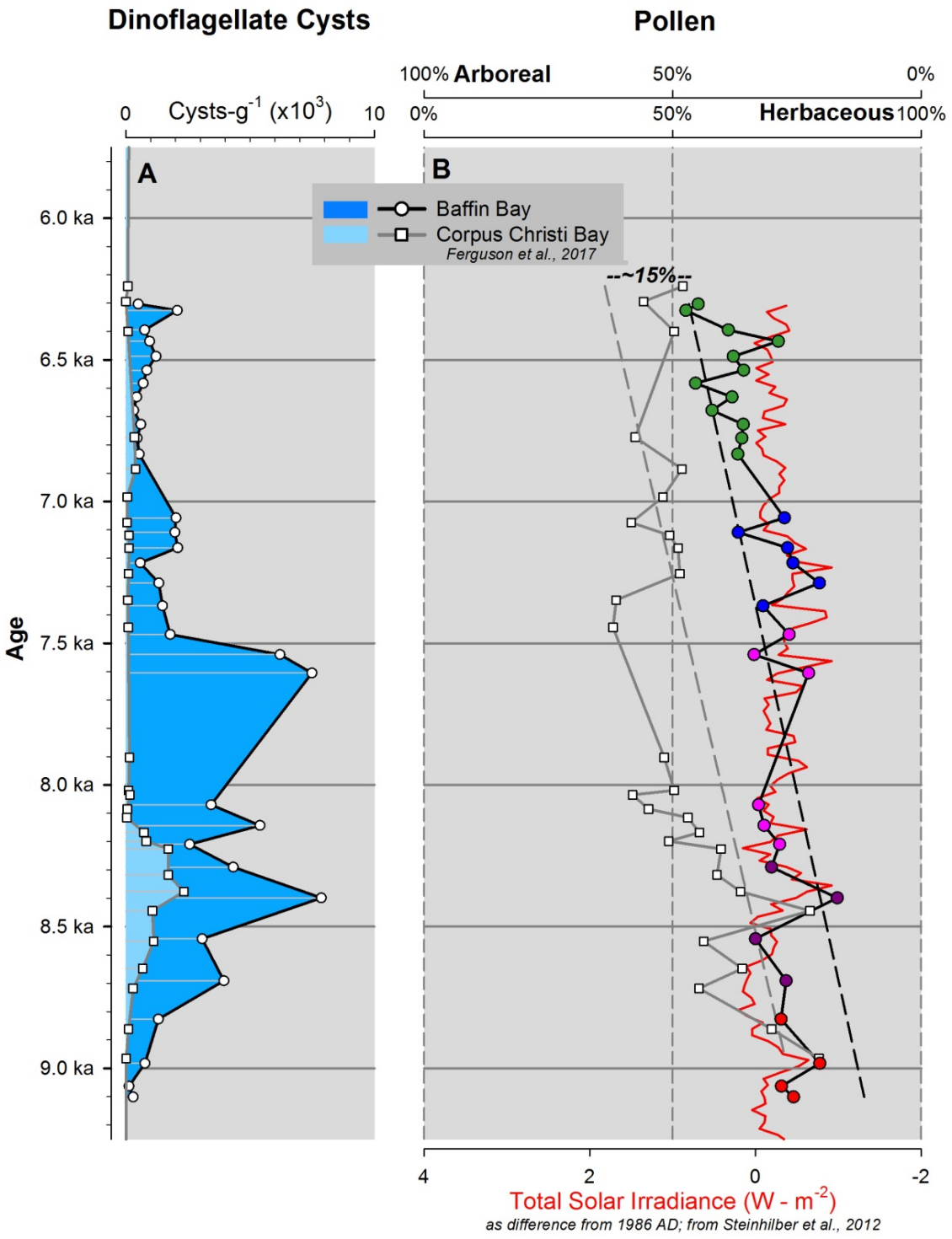

Figure 4. (A) Dinoflagellate cyst concentration comparison of Baffin Bay, TX (BB07-11) with Ferguson et al.'s (2017) data from Corpus Christi Bay, TX (CCB02-01). (B) Comparison of herbaceous vs arboreal pollen in BB07-11, and CCB02-01 (from Ferguson et al., 2017). Trend line shows an increase of arboreal pollen in both cores during this time with 15% difference between the bays. Cluster analysis results for BB07-11 shown in corresponding colors.

4.4.3 Statistical Results

Constrained Bray-Curtis cluster analysis for Baffin Bay shows five distinct clusters for Baffin Bay (Figure 5). Correspondence analysis (CA) of the clusters (Figure 6) show that these clusters are more similar to one another than the more separated clusters seen in Ferguson et al. (submitted). However, analysis of similarity between samples (ANOSIM) shows the 5 sample clusters from Baffin Bay are still significantly different from one another (Table 1). For convenience, the Baffin Bay clusters are shown as colored points in Figure 4B. Joint analysis of Baffin Bay with Corpus Christi Bay (from Ferguson et al., submitted) shows that our pollen data plots within the same CA space as Corpus Christi Bay pollen from the same time period (Figure 7). Corpus Christi Bay's assemblage at this time had more control from arboreal pollen than did Baffin Bay; this is also evident in the shifted plots of Figure 4B. The associated similarity percentage analysis (SIMPER) results indicate that Asteraceae, *Quercus*, *Chenopodium*, Poaceae, *Pinus* and *Ilex* together explain ~90% of the overall compositional differences of the five Baffin Bay clusters (Appendix Table C3).

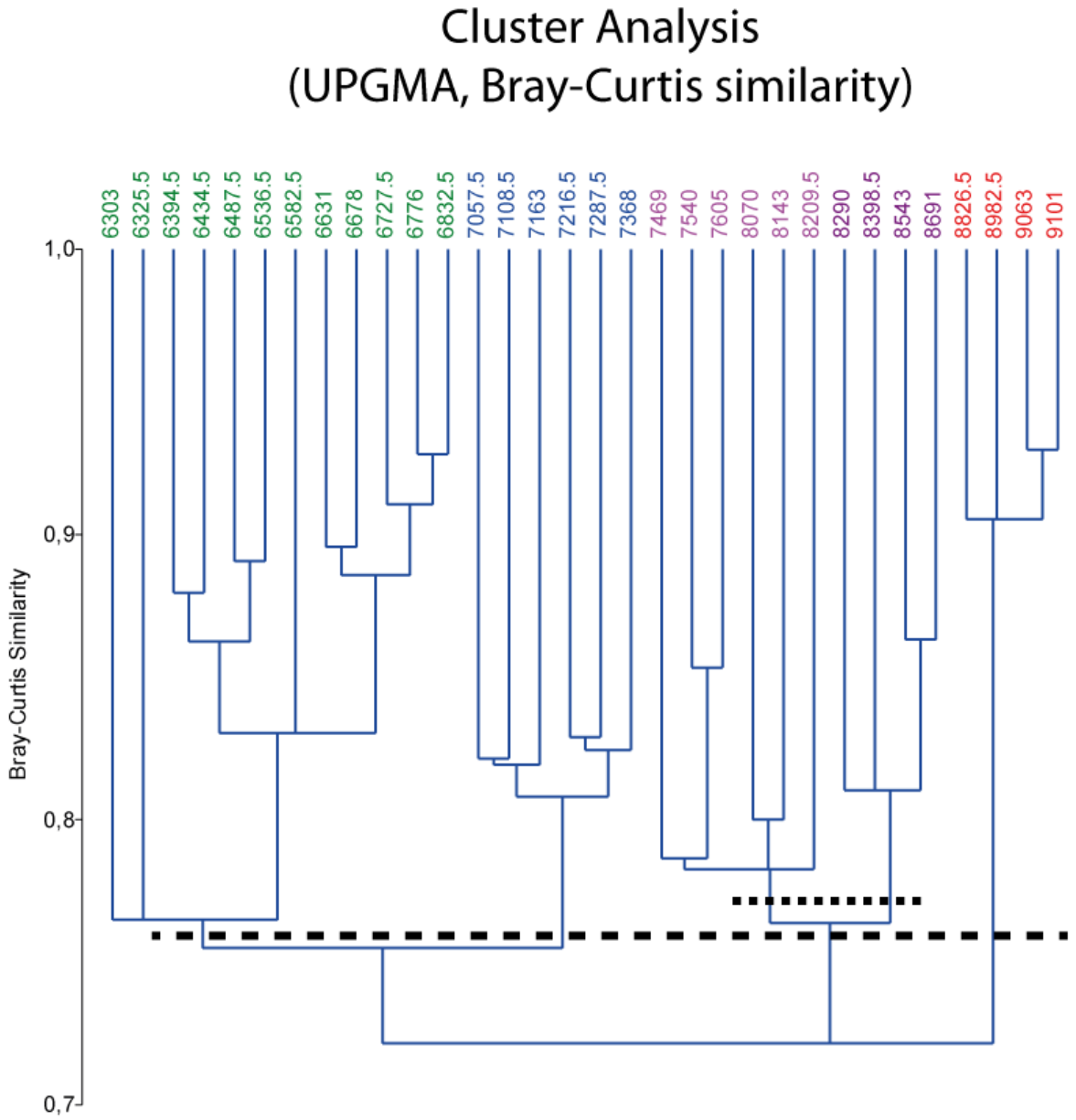

Figure 5. Cluster analysis (Bray-Curtis similarity) results for BB07-11 show five significant clusters for this study. Results created using PAST software (Hammer et al., 2001).

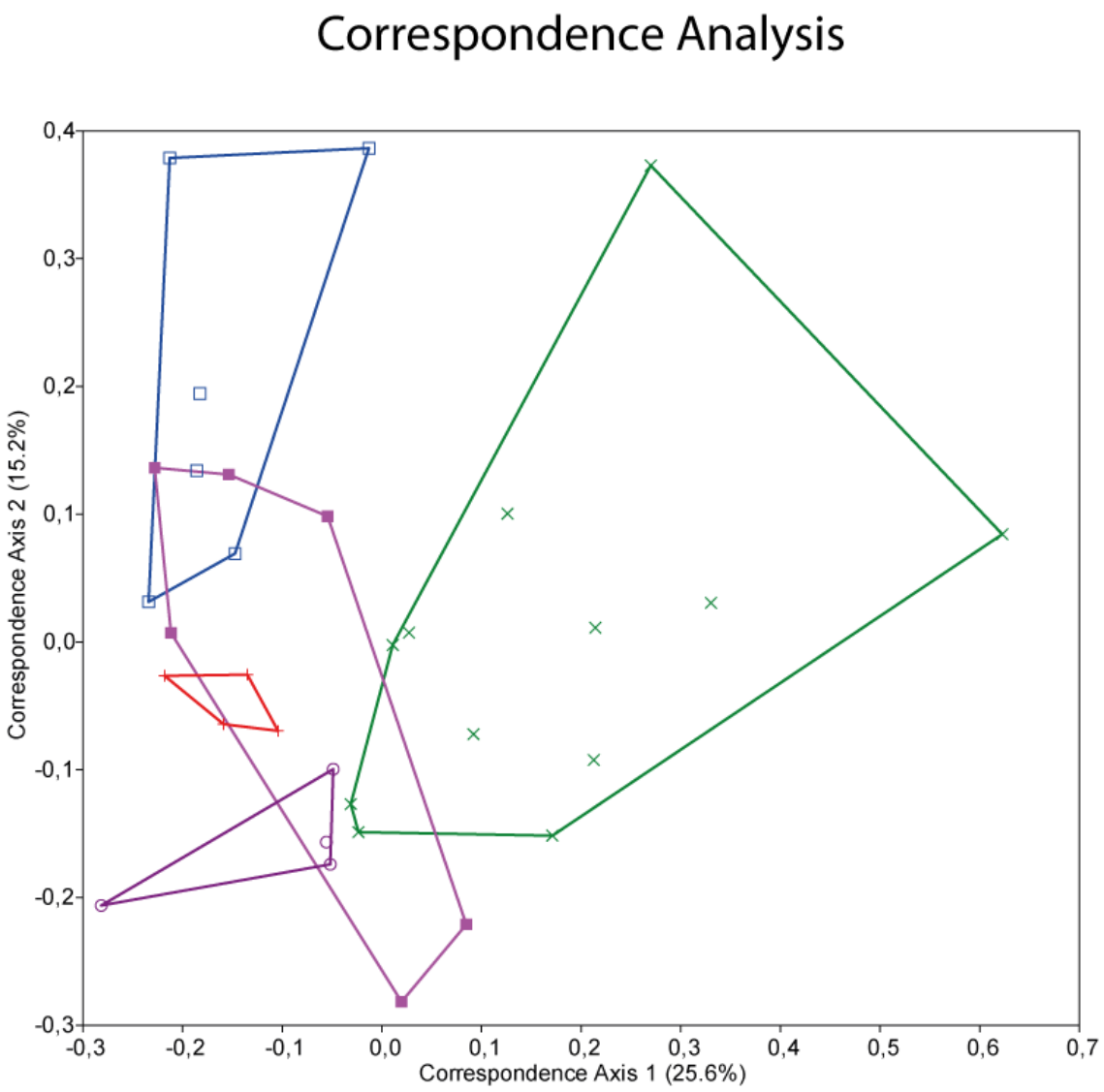

Figure 6. Correspondence analysis (CA) of Baffin Bay pollen. The red cluster includes the oldest part of the record, then dark purple, light purple, blue, and finally the green cluster being the youngest section. The plot was made using PAST software (Hammer et al., 2001).

Table 1. Analysis of Similarities (ANOSIM) shows the five clusters seen in Baffin Bay pollen are significantly different between one another.

Overal 5-group ANOSIM (99,999 permutations) :

R = 0.641 $p < 10^{-5}$

Pairwise ANOSIM (99,999 permutations) :

R \ p	**6303**	**7057.5**	**7469**	**8290**	**8826.5**
6303	---	**0.00017**	0.00014	0.00221	0.07247
7057.5	0.722	---	**0.00228**	0.01881	0.01939
7469	0.890	0.498	---	**0.024**	0.005
8290	0.668	0.441	0.387	---	**0.028**
8826.5	0.278	0.611	0.893	0.883	---

==> ***All successive groups significantly different***

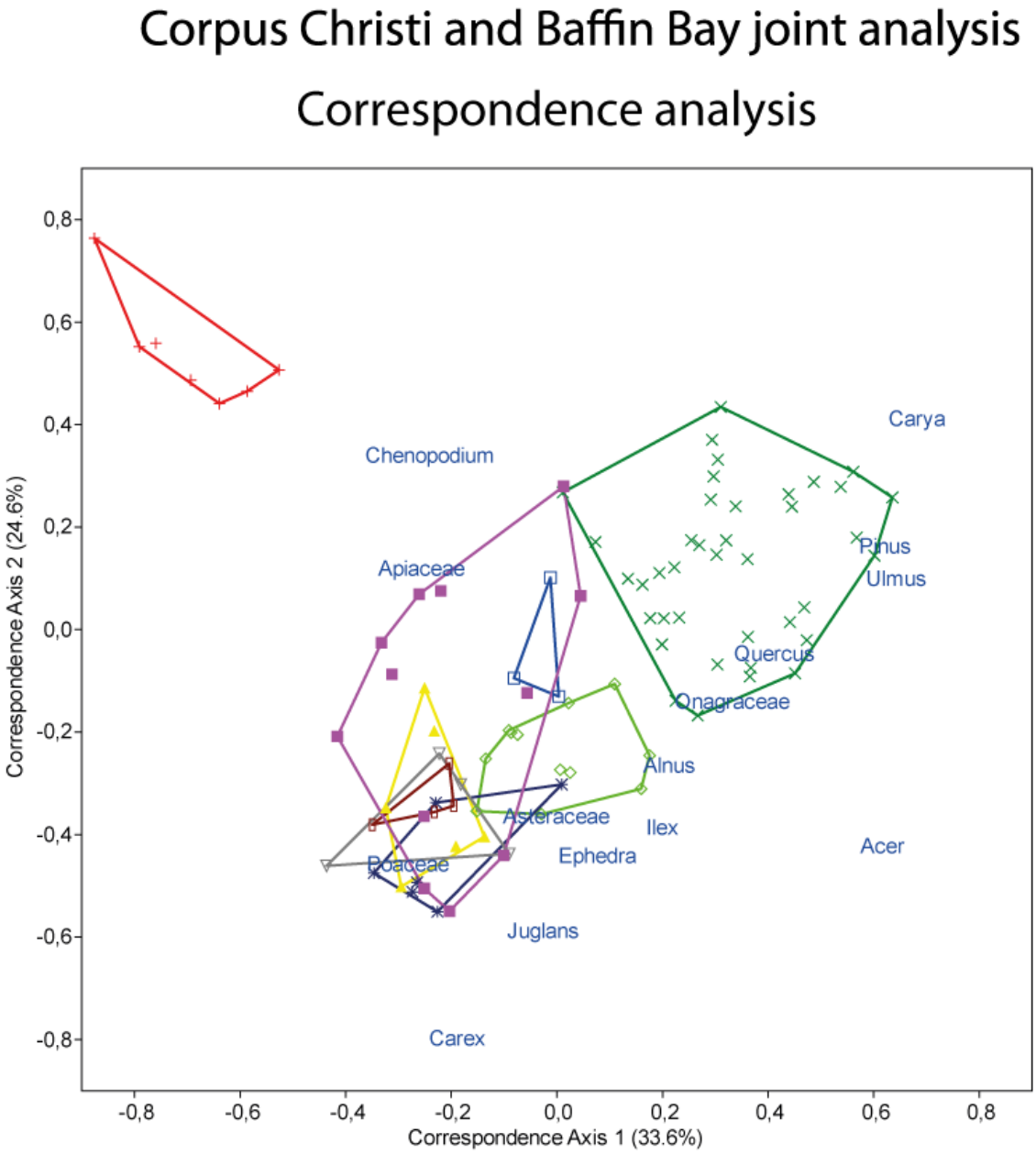

Figure 7. Correspondence analysis (CA) of Baffin Bay pollen data plotted along with Corpus Christi Bay pollen from (Ferguson et al., submitted). Pollen from Baffin Bay plots with the Corpus Christi Bay cluster (polygon) from the same time period. Plot made using PAST software (Hammer et al., 2001).

4.5 Discussion

4.5.1 Vegetation Profile

Windborne transport of pollen is generally low, with at least 95% of all airborne pollen settling out within a f local flora of Baffin Bay during our study period, and is also largely reflective of modern assemblages, albeit in different abundances. Ferguson et al. (submitted) concluded from their lack of reworked palnynomorphs that their bay-core records were of only local palynoflora as well, despite the large drainage basins feeding their study areas of Corpus Christi and Trinity Bay, Texas. Finally, minimal water and sediment input from the San Fernando, Petronilla, and Los Olmos Creeks eliminates the possibility of significant allochthonous pollen input. Our pollen assemblage indicates that the habitats that created our pollen record likely included tidal flats, salt marshes, prairies, and strands of oak forest. The tidal flats along the eastern coastal edge of the Sand Plain includes expansive forelands (Chenopodiaceae family), which commonly dominate from temperate to arid regions with a lack of moisture, poor drainage, and in this case high soil salinity largely prevent the dominance of trees (Fulbright et al., 1990; Leigh, 1994; Keith, 2004). A variety of grasses such as smooth cordgrass (*Spartina alterniflora*), marshhay cordgrass (*Spartina patens*), and saltgrass (*Distichlis spicata*), are found within and along the marshes (Fulbright et al., 1990). The open prairies to the northeast of this region contain a mixture of grasses with seacoast bluestem (*Schizachyrium scoparium* var. *littorale*), and dominating the wettest prairies, along with Camphor daisy (*Rayjacksonia phyllocephala*) in moderate to well-drained soils (Diamond and Fulbright, 1990; Fulbright et al., 1990). Along the northern portion, large live oak mottes (*Quercus virginiana*) form discontinuous oak belts along the Sand Plain, and thicker forests are able to form where mottes connect with one another, supporting a shrub understory (Fulbright et al., 1990).

Statistical analysis of our data shows that within the context of nearby Corpus Christi Bay, there is little change in vegetation assemblage through the studied period. Both before and after the post-LGM sea-level events seen in Baffin Bay, the pollen record is controlled by herbaceous Asteraceae and Poaceae with a few shrub taxa (*Ilex*, *Ephedra*) and trees (*Juglans*, *Alnus*). However, assemblages older than the 8.2 ka event are much closer to each other in CA space, and thus are much more homogeneous from a taxonomic composition and relative abundance point of view than the assemblages younger than the 8.2 ka event. This may suggest more variable environmental conditions after than before the 8.2 ka event. Overall, results from pollen indicate that the Baffin Bay region was continuously drier than nearby Corpus Christi Bay throughout the time interval studied.

4.5.2 Marine Profile

Dinoflagellate species and abundances are controlled by salinity, temperature and water depth (Zonneveld et al., 2013). Species that we observe in mid-early Holocene Baffin Bay are ubiquitous across Texas bays and the Gulf of Mexico (Limoges et al., 2013; Zonneveld et al., 2013; Ferguson et al., in prep; Ferguson et al., in press). *Polysphaeridium zoharyi* is the dominant cyst present, both here and throughout the Gulf, as is the case in modern assemblages (Marret and Zonneveld, 2003; Zonneveld et al., 2013). However, *Spiniferites* spp. is the most abundant of the first dinoflagellates that appear during the initial flooding of the incised valley at 9 ka. Its abundance decreases through the section, but together *Spiniferites* spp. and *Polysphaeridium zoharyi* are rarely less than 50% of the assemblage.

Modern Baffin Bay is a hypersaline environment, and likely has a much different assemblage of dinoflagellates adapted to those salinities. However, the earliest that transition occurred was

after the formation of Padre Island at about 5.5 ka (Simms et al., 2010), which is just outside our sampled section. The dinoflagellates we observed are all tolerant of similar salinities and temperatures, all indicative of normal marine salinities and fairly warm surface waters (likely SSS 28.4–39.4 °C autumn-autumn; SST 8.9–29.8 °C winter-summer) (Zonneveld et al., 2013).

One measurement that adds important value to the dinoflagellate record lies within observed changes in total concentration through time. Indeed, we know from the type of species present that Baffin Bay was a warm, open marine environment from 9 to 6 ka. But additional information can be gathered from the concentration plot as it reflects overall changes to sea level, salinity within the bay, or both. Peaks in dinoflagellate cyst concentrations are observed at 8.4 ka, 8.2 ka, and 7.6 ka, each of which we attribute to eustatic response to melting of the Laurentide Ice Sheet (Figure 4A).

4.5.3 Environmental Synthesis and Effects of Solar Activity

Our record for Baffin Bay becomes more powerful when paired with the similarly-derived record of Ferguson et al. (2017) derived from sediments sampled in nearby Corpus Christi Bay (Figure 4). Figure 4B clearly shows that both bays have the same pollen trend for this time; from herbaceous to arboreal. Even on a centennial timescale, the sample-to-sample shifts in arboreal-herbaceous abundances are often similar (best demonstrated from 9 ka to 8.4 ka). Figure 4B also shows the trend-lines for both bays are parallel. Corpus Christi Bay is just north of Baffin Bay and correspondingly less arid, which likely explains the overall shift towards arboreal in its plot (Figure 4B). The shift between the two lines corresponds to a difference in about 15% of more herbaceous taxa for Baffin Bay then Corpus Christi. The two bays are geographically close to one another, but geologically and climatically are quite different from one another. The

comparison of the trends in the two graphs (Figure 4B) shows that these climatic differences, especially the precipitation gradient, have been continuously present throughout the early to mid-Holocene, with Baffin Bay consistently drier than Corpus Christi Bay.

In addition to the climate variability between the two bays, a large difference consists in water-sediment input and connectivity of the bays to the Gulf of Mexico. Corpus Christi Bay receives constant freshwater input from the Nueces River, while Baffin Bay is fed ephemerally by three small creeks. The freshwater input from the Nueces River acts as a buffer to the salinity in Corpus Christi Bay, leading to the much lower dinoflagellate cyst concentrations seen there than within Baffin Bay (Figure 4A). On average, Baffin Bay has over an order of magnitude higher of dinoflagellate cysts compared to Corpus Christi Bay. We also know that Baffin Bay had an unobstructed connection to the Gulf of Mexico during our studied time period; Padre Island did not form until around 5.5 ka (Simms et al., 2010). Corpus Christi Bay, however, had varying levels of connectivity with the Gulf due to the formation, breakup, and re-formation of Mustang Island (Ferguson et al., 2017). The formation of Mustang Island also led to decreased dinoflagellate cyst concentrations in Corpus Christi Bay. Ferguson et al. (2017) suggest that the 8.2 ka eustatic event was rapid enough to destabilize the island, leading to increased bay salinities. However, they were unable to constrain the timing of the island's reformation, and only estimated that it was an ineffective barrier water exchange with the Gulf at least 200– 300 years. Our record in Baffin Bay can at least provide an estimate that re-formation occurred no later than 7.6 ka (Figure 4A). This is because the 8.2 ka event is attributed to a large meltwater pulse of the Laurentide Ice Sheet, which continued to deteriorate until the majority of ice had melted by 7.6 ka with ~4.5 m GMSL (global mean sea-level) during this time interval (Ullman et al., 2016); we see this full record in Baffin Bay, but there are no concentration increases in

Corpus Christi Bay after the initial 8.2 ka burst. This implies that Mustang Island had reformed enough by 7.6 ka to dampen that signal; Ferguson et al. (2017) could only assume that Mustang Island accounted for the absence of this signal, and we can show that as indeed the case. A shift towards herbaceous pollen at 7.6 ka in Baffin Bay is likely due to the meltwater events of the preceding century which likely led to increased flooding of former terraces, and an increased production from marsh grasses. This shift is supported by the increase in reworked pollen mixed with the penecontemporaneous assemblages. The provenance of that reworking can likely be found within the terraces themselves. This same shift is not observed in Corpus Christi Bay; this could be due to buffered shifts in vegetation communities due to the presence of Mustang Island. At 6.89 ka, there is a marked increase in dinoflagellates within Corpus Christi Bay but not within Baffin Bay; Ferguson et al. (2017) was unable to attribute anything specific to this signal, but our records together suggest that it represents the flooding of a former terrace of the Nueces River.

Finally, we have convincing evidence that the centennial-scale shifts in herbaceous-arboreal pollen assemblages that match between Corpus Christi and Baffin Bays are probably controlled by the effects of solar irradiance (Figure 4B). Steinhilber et al. (2012) created a proxy record of total solar irradiance (TSI) for much of the Holocene based off of records of cosmogenic radionuclides ^{10}Be and ^{14}C. They synthesized data from the European Project for Ice Coring in Antarctica-Dronning Maid Land (EPICA-DML) in Antarctica, the European Greenland Ice Core Project (GRIP), and global ^{14}C from tree rings as reported in the Intcal09 radiocarbon curve (Reimer et al., 2009) in order to de-convolute individual system effects within each record (i.e., Solanki et al., 2013), and produce a global record of solar irradiance. Even without considering the different age-models and that no "wiggle-matching" was applied between the Steinhilber et al. (2012) curve and our herbaceous-arboreal curve, the similarity between them is striking

(Figure 4B). Solanki et al. (2013) summarize that solar irradiance has direct effect on global mean surface temperatures, and that changes in irradiance can cause shifts in atmospheric and oceanic circulation. Livsey and Simms (2016) summarized proxies for Baffin Bay climate over the late Holocene (<6 ka), each of which could be affected by changes in TSI. Our direct evidence of vegetation change induced by changing climate and eustasy combines with their observations to create some interesting interpretations for the perturbations in our linear trend of herbaceous-arboreal vegetation change. Potentially, minor peaks towards increasing herbaceous pollen in Figure 4B indicate a more negative phase of the North Atlantic Oscillation (NAO) (Solanki et al., 2013), a more positive phase of Atlantic Meridional Overturning (AMO) (Livsey et al, 2016; McCabe et al., 2004), and increased sea surface temperatures (SST) in the north Atlantic and Gulf of Mexico (McCabe et al., 2004; Montero-Serrano et al., 2010; Livsey et al., 2016).

4.6 Conclusions

The present study presents a record of palynological changes within Baffin Bay, Texas over the relatively brief period following initial flooding of the incised valley at ~9 ka through the changes in eustasy due to melting of the LGM-era Laurentide Ice Sheet. This record contains evidence of three punctuated episodes of increased marine palynoflora at 8.4 ka, 8.2 ka and 7.6 ka, each of which we attribute to relatively rapid increases in eustatic sea-level. Coupling our record with Ferguson et al. (2017) record for the nearby Corpus Christi Bay constrains estimates on the time of reformation of Mustang Island to <600 a (8.2 ka to 7.6 ka), as we record a eustatic event in Baffin Bay at 7.6 ka not seen in Corpus Christi Bay. Our record provides compelling

evidence that sea-level rise occurred on relatively rapid (centennial) timescales in early-mid Holocene in support of evidence from sea-level data.

We also confirm that the vegetation surrounding Baffin Bay was very similar to nearby Corpus Christi Bay at this time, but with less arboreal influence indicative of an overall drier climate consistently throughout the time interval study. This agrees with Ferguson et al. (submitted), who concluded that the Texas coast has a northward gradient of increasing arboreal control, related to decreasing aridity. The 15% difference in arboreal/herbaceous ratio between the two sites indicates that the precipitation gradient has been constant over the time range of this study between the two bays, and has evolved in a linear way through the Holocene. Finally, small shifts in the herbaceous-arboreal curve seen over-printed on the linear increasingly-arboreal trend are likely due to the climate effects of changing solar irradiance and shifts in atmospheric and oceanic circulation.

CHAPTER 5
SUMMARY & CONCLUSIONS

This dissertation consisted of three principle projects (Chapters 2, 3, & 4) that studied climatic and marine events along coastal Texas. Chapter 2 focused on the marine record from dinoflagellates in Corpus Christi Bay, Texas, and found convincing evidence that the bay's coastal barrier island was compromised for several hundred years due to a rapid pulse of sea-level rise. Chapter 3 combined the marine (dinoflagellate) and terrestrial (pollen and spores) records from Trinity Bay, Texas and Corpus Christi Bay, Texas and used statistics to explore trends through time. Both bays had similar assemblages and transitioned through time from herbaceous-dominated assemblages to arboreal-dominated, as early as 8.4 ka within Corpus Christi Bay, and 3.8 ka within Trinity Bay. Chapter 4 focused exclusively on Baffin Bay, Texas, which is <60 km south of Corpus Christi Bay and Mustang Island. Baffin Bay experienced a similar vegetative shift as seen in Chapter 2, and we also found that sample-to-sample shifts in arboreal-herbaceous abundances are likely correlated with the climatic effects of changing solar irradiance. Major conclusions and descriptions of each chapter follow.

5.1 Breakdown of Ancestral Mustang Island-Corpus Christi Bay Complex in Response to the 8.2 Ka Sea-Level Event: Implications for Future Coastal Change

Results from an investigation of the coupled Mustang Island-Corpus Christi Bay complex shows that the island was eliminated as an effective salinity barrier between 8.86 and 8.17 ka. This event is recorded by a 5-fold increase of dinoflagellates within Corpus Christi Bay. During this time the bay-head delta shifted 15 km landward and oyster reefs within the bay died off. Our age model indicates that this event most likely resulted from the most rapid eustatic rise of the Holocene, which peaked at 8.18–8.31 ka. This event is attributed to late stage ice sheet

disintegration, particularly in North America, punctuated by rapid draining of Lake-Agassiz-Ojibway. Local glacial-isostatic factors resulted in a sea-level rise of only 0.2–0.56 m in the western Gulf of Mexico, which was less than needed to submerge the barrier. Rather, it was the punctuated nature of this sea-level rise that led to the virtual destruction of Mustang Island as an effective salinity barrier. These results provide an analogue for predicting coastal morphodynamic response to accelerated sea-level rise and emphasize the need for better understanding of barrier response to sea-level rise and improved numerical models for predicting future changes to coastal barrier shorelines.

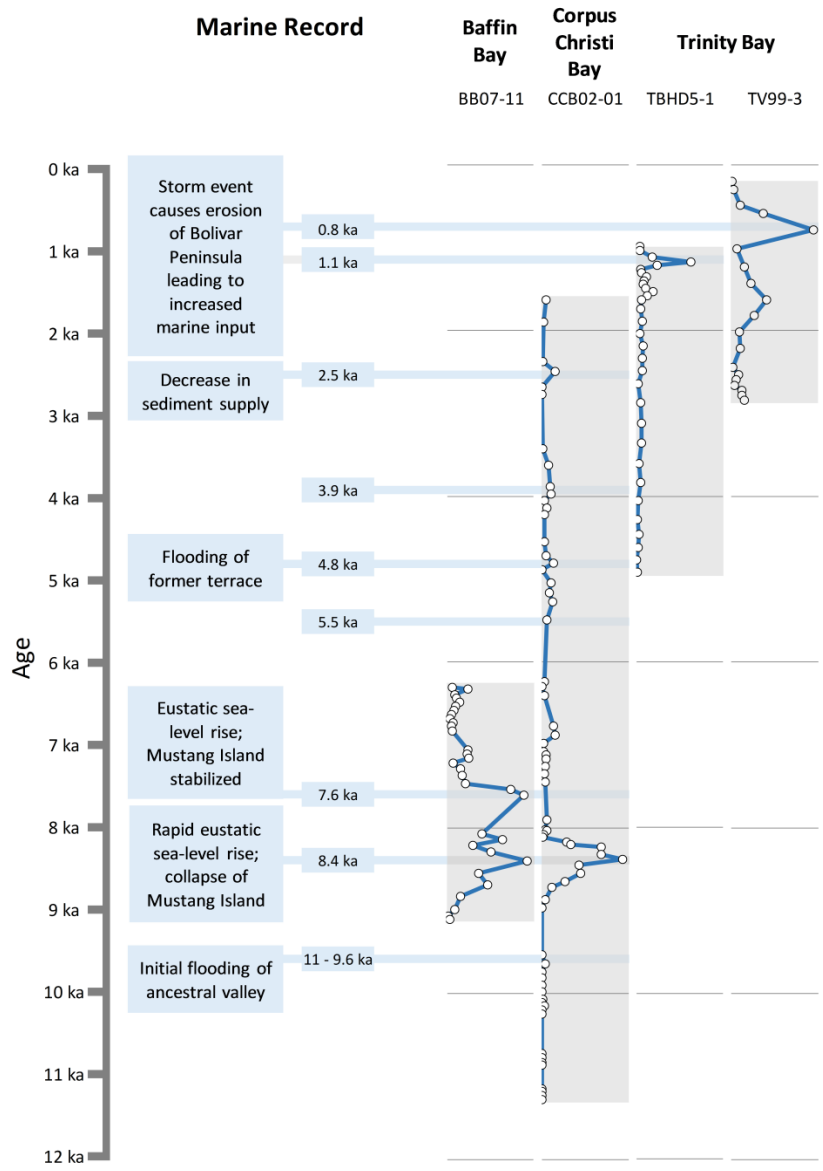

Figure 1. Summary figure of dinoflagellate cyst records for Baffin Bay, Corpus Christi Bay, and Trinity Bay, TX with the main marine events noted.

5.2 Holocene Vegetation and Climate Evolution of Corpus Christi and Trinity Bays: Implications on Source-to-Sink Deposition on the Texas Coast

The Texas coastline stretches 595 km across almost 4° of latitude and is home to diverse coastal vegetation assemblages, yet there are very few studies of climate and vegetative change of this region through the Holocene. We provide a detailed palynological record of Holocene

climate for southeast and coastal Texas, based upon three subaqueous sediment cores from Corpus Christ Bay, TX and Trinity Bay, TX. Cluster analysis and correspondence analysis were used to investigate changes in palynological assemblages through time within each core. Common to both bays are nonarboreal taxa including Asteraceae (mainly *Ambrosia*, and *Helianthus*), *Chenopodium*, Poaceae, and arboreal taxa such as *Carya*, *Pinus*, and *Quercus*. Our record shows that the coastal environments of central Texas began a transition from herbaceous (nonarboreal) dominated vegetation to arboreal vegetation as early as 8.4 ka within Corpus Christi Bay, and 3.8 ka within Trinity Bay. We note flooding events at 8.2 ka, 5.4 ka, and 3.6 ka in Corpus Christi Bay, and at 1.7 ka, 1.2 ka, and 0.8 ka in Trinity Bay. These events are caused by storms, changes to sea level including flooding of relict river terraces, and changes in sediment delivery to the bays. There is also evidence for changes in fluvial discharge to Corpus Christi Bay at 4.1 ka and 2.2 ka, and at 1.8 ka in Trinity Bay. We also see *Zea mays* in Trinity Bay at 1.5 ka, an indication of local Native American agriculture. We observe no significant changes during the middle Holocene Climatic Optimum, and subtle, but not statistically significant evidence of the more variable climate oscillations other records from more interior Texas show for the late Holocene. This indicates that coastal Texas' climate has operated semi-independently from central Texas regions, and is primarily driven by a coast-wise gradient of precipitation and evapotranspiration.

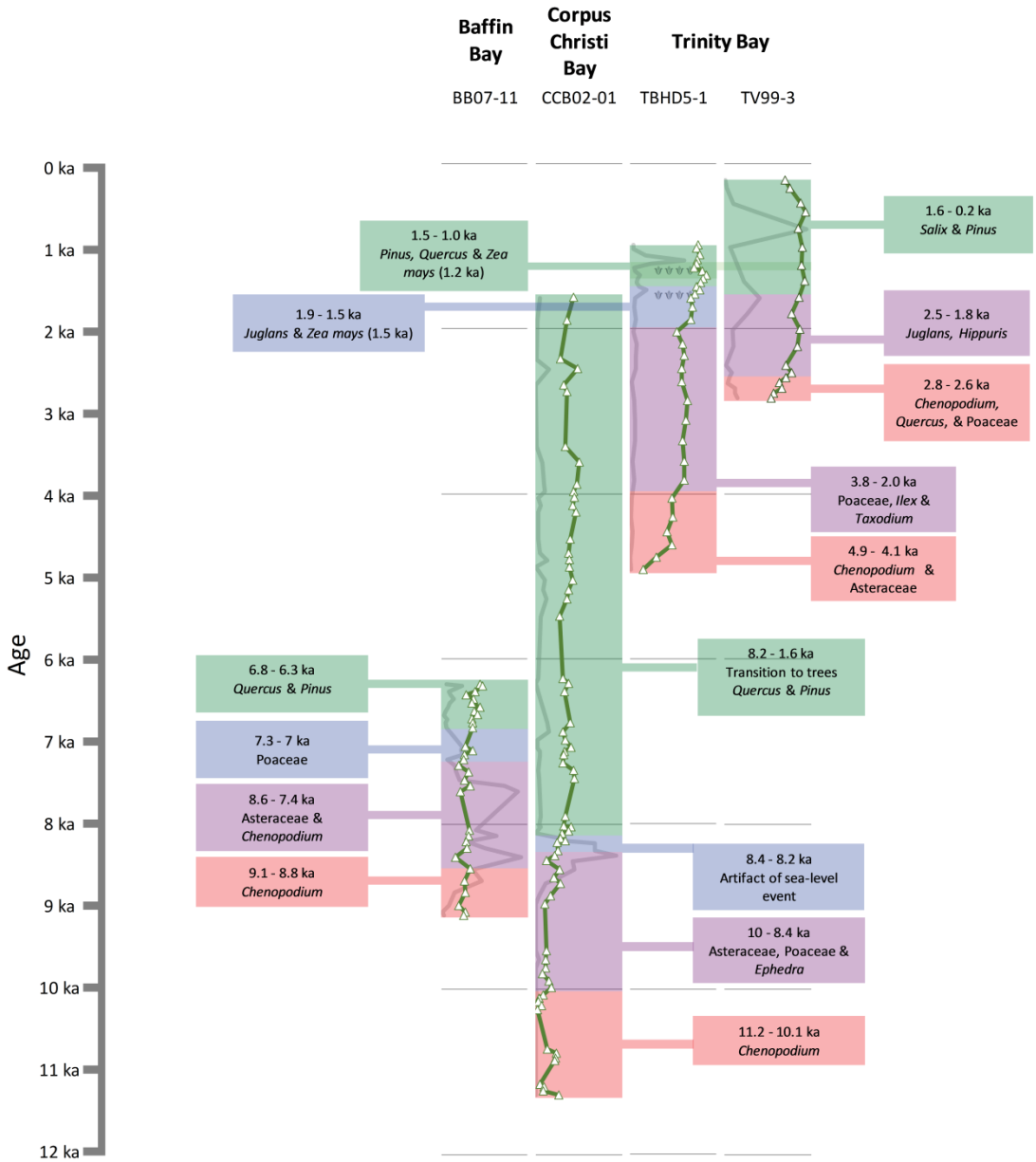

Figure 2. Summary figure of pollen records for Baffin Bay, Corpus Christi Bay, and Trinity Bay, TX showing the vegetational shifts for all three bays. Dinoflagellate cyst record shown in background.

5.3 Palynological Response to Early- to Mid-Holocene Changes in Eustasy and Climate in Baffin Bay, Texas

We present a record of changes in palynoflora within and around Baffin Bay, Texas through the early-mid Holocene. This record contains evidence of three punctuated episodes of increased marine dinoflagellate cyst concentrations at 8.4 ka, 8.2 ka and 7.6 ka, each of which

we attribute to relatively rapid increases in eustatic sea-level due to melting of the LGM-era Laurentide Ice Sheet. Coastal dinoflagellate *Polysphaeridium zoharyi* dominates the marine assemblage. The continuous presence of this species indicates that the bay had normal salinities and thus, that it was an open marine environment. The terrestrial signal is dominated by herbaceous taxon throughout, with a gradual roughly linear increase in arboreal taxon. This record is similar to recently published work on nearby Corpus Christi Bay; the slope of the herbaceous-arboreal transitions are parallel, and sample-to-sample shifts in arboreal-herbaceous abundances are often similar. Baffin Bay was an open bay at this time, while Corpus Christi Bay was protected by a coastal barrier, Mustang Island. Leveraging similarities in the vegetation profiles of the bays against differences in the marine assemblage allowed for direct assessment of the ability of this coastal barrier island to buffer the effects of episodic sea-level rise. These rises led to minor yet observable shifts in coastal vegetation away from larger arboreal species, and towards smaller shrubs and grasses likely more resilient in the face of increased coastal hazards and saltwater intrusion associated with sea-level rise. We also show that these herbaceous-arboreal shifts are likely correlated with the climatic effects of changing total solar irradiance.

REFERENCES

Abdulah, K.C., Anderson, J.B., Snow, J.N. and Holdford-Jack, L., 2004. The late Quaternary Brazos and Colorado deltas, offshore Texas, USA—their evolution and the factors that controlled their deposition. SEPM Special Publication, 79: 237–269.

Albert, L.E., 1981. Ferndale bog and natural lake: five thousand years of environmental change in southeastern Oklahoma.

Anderson, J.B., Rodriguez, A.B., Milliken, K.T. and Taviani, M., 2008. The Holocene evolution of the Galveston estuary complex, Texas: Evidence for rapid change in estuarine environments. Geol. Soc. Spec. Pap., 443: 89–104.

Anderson, J.B., Wallace, D.J., Simms, A.R., Rodriguez, A.B. and Milliken, K.T., 2014. Variable response of coastal environments of the northwestern Gulf of Mexico to sea-level rise and climate change: Implications for future change. Mar. Geol., 352: 348–366.

Aten, L.E., 1983. Indians of the upper Texas coast. Academic Press.

Bamber, J.L. and Aspinall, W.P., 2013. An expert judgement assessment of future sea level rise from the ice sheets. Nat. Clim. Change, 3(4): 424–427.

Barber, D.C., Dyke, A., Hillaire-Marcel, C., Jennings, A.E., Andrews, J.T., Kerwin, M.W., Bilodeau, G., McNeely, R., Southon, J., Morehead, M.D. and Gagnon, J.M., 1999. Forcing of the cold event of 8,200 years ago by catastrophic drainage of Laurentide lakes. Nature, 400(6742): 344–348.

Behrens, E.W., 1966. Surface salinities for Baffin Bay and Laguna Madre, Texas, April 1964-March 1966. Publications of the Institute of Marine Science, University of Texas, 11: 168–179.

Bousman, C.B., 1998. Paleoenvironmental change in central Texas: the palynological evidence. The Plains Anthropologist: 201–219.

Brown, C.A., 2008. Palynological techniques. American Association of Stratigraphic Palynologists Foundation.

Bryant Jr, V.M., 1977. A 16,000 year pollen record of vegetational change in central Texas. Palynology: 143–156.

Bryant, V.M. and Shafer, H.J., 1977. Late Quaternary Paleoenvironment of Texas: A Model for Archeologist. Bulletin of the Texas Archaeological Society, 48: 1–25.

Bryant, V.M. and Holloway, R.G., 1985. A late-Quaternary paleoenvironmental record of Texas: an overview of the pollen evidence. Pollen record of late Quaternary North

American sediments: Calgary, Canada, American Association of Stratigraphic Palynologists: 39–70.

Buzas-Stephens, P., Livsey, D.N., Simms, A.R. and Buzas, M.A., 2014. Estuarine foraminifera record Holocene stratigraphic changes and Holocene climate changes in ENSO and the North American monsoon: Baffin Bay, Texas. Palaeogeography, Palaeoclimatology, Palaeoecology, 404: 44–56.

Church, J.A., Clark, P.U., Cazenave, A., Gregory, J.M., Jevrejeva, S., Levermann, A., Merrifield, M.A., Milne, G.A., Nerem, R.S. and Nunn, P.D., 2013. Sea level change, PM Cambridge University Press.

Cooke, M.J., Stern, L.A., Banner, J.L., Mack, L.E., Stafford, T.W. and Toomey, R.S., 2003. Precise timing and rate of massive late Quaternary soil denudation. Geology, 31(10): 853–856.

Dalrymple, D.W., 1964. Recent sedimentary facies of Baffin Bay, Texas (Doctoral dissertation, Rice University).

DeConto, R.M. and Pollard, D., 2016. Contribution of Antarctica to past and future sea-level rise. Nature, 531(7596): 591–597.

Diamond, D.D. and Fulbright, T.E., 1990. Contemporary plant communities of upland grasslands of the Coastal Sand Plain, Texas. The Southwestern Naturalist: 385–392.

Donders, T.H., 2014. Middle Holocene humidity increase in Florida: Climate or sea-level? Quaternary Science Reviews, 103: 170–174.

Emery, K.O. and Stevenson, R.E., 1957. Estuaries and Lagoons I. Physical and Chemical Characteristics. Geological Society of America Memoirs, 67: 673–750.

Feldmann, J. and Levermann, A., 2015. Collapse of the West Antarctic Ice Sheet after local destabilization of the Amundsen Basin. Proceedings of the National Academy of Sciences, 112(46): 14191–14196.

Ferguson, S., Warny, S., Anderson, J., Simms, A.R. and White, C.M., 2017. Breakdown of ancestral Mustang Island-Corpus Christi Bay complex in response to the punctuated 8.2 ka sea-level event: implications for future coastal change. The Holocene: in press.

Ferguson, S., Warny, S., Simms, A.R., Anderson, J.B. and Escarguel, G., submitted. Holocene vegetation and climate evolution of Corpus Christi and Trinity bays: implications on source-to-sink deposition on the Texas coast. Geobios: submitted.

Fisk, H.N. and McClelland, B., 1959. Geology of continental shelf off Louisiana: Its influence on offshore foundation design. Geological Society of America Bulletin, 70(10): 1369–1394.

Fulbright, T.E., Diamond, D.D., Rappole, J. and Norwine, J., 1990. The coastal sand plain of southern Texas. Rangelands: 337–340.

Gabler, C.A., Osland, M.J., Grace, J.B., Stagg, C.L., Day, R.H., Hartley, S.B., Enwright, N.M., From, A.S., McCoy, M.L. and McLeod, J.L., 2017. Macroclimatic change expected to transform coastal wetland ecosystems this century. Nature Climate Change, 7(2): 142–147.

Goff, J.A., Lugrin, L., Gulick, S.P., Thirumalai, K. and Okumura, Y., 2015. Oyster reef die-offs in stratigraphic record of Corpus Christi Bay, Texas, possibly caused by drought-driven extreme salinity changes. Holocene, 26(4): 511–519.

Graham, A. and Heimsch, C., 1960. Pollen studies of some Texas peat deposits. Ecology, 41(4): 751–763.

Grimm, E.C., Watts, W.A., Jacobson, G.L., Hansen, B.C.S., Almquist, H.R. and Dieffenbacher-Krall, A.C., 2006. Evidence for warm wet Heinrich events in Florida. Quaternary Science Reviews, 25(17): 2197–2211.

Gunter, G.P., 1944. Studies on marine fishes of Texas: relative abundance and cyclic behavior related to salinity and temperature: 13–16.

Hafsten, U., 1961. Pleistocene development of vegetation and climate in the southern High Plains as evidenced by pollen analysis. Paleoecology of the Llano Estacado: 59–91.

Hall, S.A., 1985. Quaternary pollen analysis and vegetational history of the Southwest. Pollen records of late-Quaternary North American sediments: 95–123.

Hammer, Ø., Harper, D. and Ryan, P., 2001. PAST: Paleontological Statistics Software Package for Education and Data Analysis Palaeontol. Electronica 4: 1–9.

Haslett, J. and Parnell, A., 2008. A simple monotone process with application to radiocarbon-dated depth chronologies. Journal of the Royal Statistical Society: Series C (Applied Statistics), 57(4): 399–418.

Henley, D.E. and Rauschuber, D.G., 1981. Freshwater Needs of Fish and Wildlife Resources in the Nueces–Corpus Christi Bay Area, Texas: A Literature Synthesis: Washington, D.C., U.S. Fish and Wildlife Service, Office of Biological Services Report FWS/OBS-80/10.

Heusser, L., 1978, Spores and Pollen in the Marine Realm: Introduction to Marine Micropaleontology: 327–339.

Holcombe, T.L., Holcombe, L. H., and Bryant, W. R., 2007. Bathymetry TX Coast v0.1. Texas Parks and Wildlife Department.

Holloway, R., Raab, L.M. and Stuckenrath, R., 1987. Pollen analysis of Late-Holocene sediments from a central Texas bog. The Texas journal of science (USA), 39(1): 71–79.

Holloway, R.G. and Bryant, V.M., 1984. *Picea glauca* pollen from Late Glacial deposits in central Texas. Palynology, 8(1): 21–32.

Huang, Y., Shuman, B., Wang, Y., Webb, T., Grimm, E.C. and Jacobson, G.L., 2006. Climatic and environmental controls on the variation of C 3 and C 4 plant abundances in central Florida for the past 62,000 years. Palaeogeography, Palaeoclimatology, Palaeoecology, 237(2): 428–435.

Hudson, P.F. and Heitmuller, F.T., 2008. Rivers and landscapes of the Texas Gulf Coastal Plain. Southwestern Geogr, 12: 90–123.

Humphrey, J.D. and Ferring, C.R., 1994. Stable isotopic evidence for latest Pleistocene and Holocene climatic change in north-central Texas. Quaternary Research, 41(2): 200-213.

Judd, F.W., Lonard, R.I. and Sides, S.L., 1977. The vegetation of South Padre Island, Texas in relation to topography. The Southwestern Naturalist: 31–48.

Keith, D.A., 2004. Ocean shores to desert dunes: the native vegetation of NSW and the ACT (Selected Extracts). Department of Environment and Conservation (NSW).

Kendall, R.A., Mitrovica, J.X., Milne, G.A., Törnqvist, T.E. and Li, Y., 2008. The sea-level fingerprint of the 8.2 ka climate event. Geology, 36(5): 423–426.

Kolker, A.S., Allison, M.A. and Hameed, S., 2011. An evaluation of subsidence rates and sea-level variability in the northern Gulf of Mexico. Geophysical Research Letters, 38(21).

Leigh, J.H., 1994. Chenopod shrublands. RH Groves, Australian flora: 345–367.

Lester, J., Gonzalez, L.A., Sage, T. and Gallaway, A., 2002. The state of the bay: A characterization of the Galveston Bay ecosystem, Galveston Bay Estuary Program.

Li, Y.-X., Törnqvist, T.E., Nevitt, J.M. and Kohl, B., 2012. Synchronizing a sea-level jump, final Lake Agassiz drainage, and abrupt cooling 8200 years ago. Earth Planet. Sci. Lett., 315–316: 41–50.

Limoges, A., Londeix, L. and de Vernal, A., 2013. Organic-walled dinoflagellate cyst distribution in the Gulf of Mexico. Marine Micropaleontology, 102: 51–68.

Livsey, D. and Simms, A.R., 2013. Holocene sea-level change derived from microbial mats. Geology, 41(9): 971–974.

Livsey, D. and Simms, A.R., 2016. Episodic flooding of estuarine environments in response to drying climate over the last 6000 years in Baffin Bay, Texas. Marine Geology, 381: 142–162.

Livsey, D., Simms, A.R., Hangsterfer, A., Nisbet, R.A. and DeWitt, R., 2016. Drought modulated by North Atlantic sea surface temperatures for the last 3,000 years along the northwestern Gulf of Mexico. Quaternary Science Reviews, 135: 54–64.

Longley, W.L., 1995. Estuaries. In: G.R. North, J. Schmandt and J. Clarkson (Editors), The impact of global warming on Texas: a report to the Task Force on Climate Change in Texas. University of Texas, Austin, Texas, USA, pp. 88–118.

Lorenzo-Trueba, J. and Ashton, A.D., 2014. Rollover, drowning, and discontinuous retreat: Distinct modes of barrier response to sea-level rise arising from a simple morphodynamic model. J. Geophys. Res. Earth Surf., 119(4): 779–801.

Maddox, J., Anderson, J.B., Milliken, K.T., Rodriguez, A.B., Dellapenna, T.M. and Giosan, L., 2008. The Holocene evolution of the Matagorda and Lavaca estuary complex, Texas, USA. Geological Society of America Special Papers, 443: 105–119.

Mannino, A.N. and Montagna, P.A., 1996. Fine-scale spatial variation of sediment composition and salinity in Nueces Bay of South Texas. Texas Journal of Science, 48(1): 87–96.

Marret, F. and Zonneveld, K.A.F., 2003. Atlas of modern organic-walled dinoflagellate cyst distribution. Review of Palaeobotany and Palynology, 125(1): 1–200.

McAndrews, J. and Larson, D., 1966. Pollen analysis of Eagle Cave. A preliminary study of the paleoecology of the Amistad Reservoir Area: 178–184.

McCabe, G.J., Palecki, M.A. and Betancourt, J.L., 2004. Pacific and Atlantic Ocean influences on multidecadal drought frequency in the United States. Proceedings of the National Academy of Sciences, 101(12): 4136–4141.

Milliken, K.L.T., 2008a. Holocene sea-level history and the evolution of Sabine Lake and Calcasieu Lake; east Texas and west Louisiana, USA and the glacial retreat history of Maxwell Bay, South Shetland Islands, Antarctica: Implications for ice cap thickness, retreat, and climate change (Doctoral dissertation, Rice University).

Milliken, K.T., Anderson, J.B., Rodriguez, A.B., 2008b. A new composite Holocene sea-level curve for the northern Gulf of Mexico. Geol. Soc. Spec. Pap., 443: 1–11.

Milliken, K.T., Anderson, J.B. and Rodriguez, A.B., 2008c. Tracking the Holocene evolution of Sabine Lake through the interplay of eustasy, antecedent topography, and sediment supply variations, Texas and Louisiana, USA. Geological Society of America Special Papers, 443: 65–88.

Montagna, P.A., Kalke, R.D. and Ritter, C., 2002. Effect of restored freshwater inflow on macrofauna and meiofauna in upper Rincon Bayou, Texas, USA. Estuaries, 25(6): 1436–1447.

Montero-Serrano, J.C., Bout-Roumazeilles, V., Sionneau, T., Tribovillard, N., Bory, A., Flower, B.P., Riboulleau, A., Martinez, P. and Billy, I., 2010. Changes in precipitation regimes over North America during the Holocene as recorded by mineralogy and geochemistry of Gulf of Mexico sediments. Global and Planetary Change, 74(3): 132–143.

Moore, L.J., List, J.H., Williams, S.J. and Stolper, D., 2010. Complexities in barrier island response to sea level rise: Insights from numerical model experiments, North Carolina Outer Banks. J. Geophys. Res. Earth Surf., 115(F3): 1–27.

Morton, R.A. and McGowen, J., 1980. Modern depositional environments of the Texas coast. University of Texas at Austin, Bureau of Economic Geology.

Moulton, D.W., Dahl, T.E. and Dall, D., 1997. Texas coastal wetlands: Status and trends, mid-1950's to early 1990's. US Fish and Wildlife Service, Southwestern Region.

NOAA, 2012. Chart 11309. NOAA.

Nordt, L.C., Boutton, T.W., Hallmark, C.T. and Waters, M.R., 1994. Late Quaternary vegetation and climate changes in central Texas based on the isotopic composition of organic carbon. Quaternary Research, 41(1): 109–120.

Nordt, L.C., Boutton, T.W., Jacob, J.S. and Mandel, R.D., 2002. C4 plant productivity and climate-CO2 variations in south-central Texas during the late Quaternary. Quaternary Research, 58(2): 182–188.

Odezulu, C.I., Lorenzo-Trueba, J., Wallace, D.J., and Anderson, J.B., In Press. Follets Island: a case of unprecedented change and transition from rollover to subaqueous shoals.

Osland, M.J., Day, R.H., Larriviere, J.C. and From, A.S., 2014. Aboveground allometric models for freeze-affected black mangroves (Avicennia germinans): equations for a climate sensitive mangrove-marsh ecotone. PloS one, 9(6): e99604.

Paine, J.G., 1993. Subsidence of the Texas coast: inferences from historical and late Pleistocene sea levels. Tectonophysics, 222(3–4): 445–458.

Paine, J.G., Caudle, T.L. and Andrews, J.R., 2016. Shoreline and Sand Storage Dynamics from Annual Airborne LIDAR Surveys, Texas Gulf Coast. Journal of Coastal Research, 0(0): null.

Parnell, A.C., Haslett, J., Allen, J.R.M., Buck, C.E. and Huntley, B., 2008. A flexible approach to assessing synchroneity of past events using Bayesian reconstructions of sedimentation history. Quaternary Science Reviews, 27(19–20): 1872–1885.

Poore, R.Z., Dowsett, H.J., Verardo, S. and Quinn, T.M., 2003. Millennial- to century- scale variability in Gulf of Mexico Holocene climate records. Paleoceanography, 18(2).

Potzger, J. and Tharp, B., 1943. Pollen record of Canadian spruce and fir from Texas bog. Science, 98(2557): 584–584.

Potzger, J.E. and Tharp, B.C., 1947. Pollen profile from a Texas bog. Ecology, 28(3): 274–280.

Potzger, J.E. and Tharp, B.C., 1954. Pollen study of two bogs in Texas. Ecology, 35(4): 462–466.

Reimer, P.J., Bard, E., Bayliss, A., Beck, J.W., Blackwell, P.G., Bronk Ramsey, C., Buck, C.E., Cheng, H., Edwards, R.L., Friedrich, M., Grootes, P.M., Guilderson, T.P., Haflidason, H., Hajdas, I., Hatté, C., Heaton, T.J., Hoffmann, D.L., Hogg, A.G., Hughen, K.A., Kaiser, K.F., Kromer, B., Manning, S.W., Niu, M., Reimer, R.W., Richards, D.A., Scott, E.M., Southon, J.R., Staff, R.A., Turney, C.S.M. and van der Plicht, J., 2013. IntCal13 and Marine13 Radiocarbon Age Calibration Curves 0–50,000 Years cal BP, 55(4): 1869–1887.

Rice, J., 2015. The Holocene History and Facies Architecture of the Nueces Bayhead Delta of the Northwestern Gulf of Mexico, University of California, Santa Barbara: 63.

Ricklis, R.A., 2004. The archeology of the Native American occupation of southeast Texas. The prehistory of Texas: 181–202.

Rodriguez, A.B., Anderson, J.B., Siringan, F.P. and Taviani, M., 2004. Holocene Evolution of the East Texas Coast and Inner Continental Shelf: Along-Strike Variability in Coastal Retreat Rates. Journal of Sedimentary Research, 74(3): 405–421.

Rodriguez, A.B., Greene, D.L., Anderson, J.B. and Simms, A.R., 2008. Response of Mobile Bay and eastern Mississippi Sound, Alabama, to changes in sediment accommodation and accumulation, Special Paper 443: Response of Upper Gulf Coast Estuaries to Holocene Climate Change and Sea-Level Rise. Geological Society of America: 13–29.

Rodriguez, A.B., Anderson, J.B. and Simms, A.R., 2005. Terrace inundation as an autocyclic mechanism for parasequence formation: Galveston Estuary, Texas, USA. Journal of Sedimentary Research, 75(4): 608–620.

Rodriguez, A.B., Simms, A.R. and Anderson, J.B., 2010. Bay-head deltas across the northern Gulf of Mexico back step in response to the 8.2 ka cooling event. Quat. Sci. Rev., 29(27–28): 3983–3993.

Russ, J., Loyd, D.H. and Boutton, T.W., 2000. A paleoclimate reconstruction for southwestern Texas using oxalate residue from lichen as a paleoclimate proxy. Quaternary International, 67(1): 29–36.

Shaw, R.B., Volman, K.C. and Smeins, F.E., 1980. Modern pollen rain and vegetation on the edwards plateau, texas. Palynology, 4(1): 205–213.

Shepard, F.P., 1953. Sedimentation rates in Texas estuaries and lagoons. AAPG Bulletin, 37(8): 1919–1934.

Shepard, F.P., 1955. Delta-front valleys bordering the Mississippi distributaries. Geological Society of America Bulletin, 66(12): 1489–1498.

Shideler, G.L., 1986. Stratigraphic studies of a late Quaternary barrier-type coastal complex, Mustang Island-Corpus Christi Bay area, South Texas Gulf Coast: 1328.

Simkins, L.M., Simms, A.R., Cruse, A.M., Troiani, T., Atekwana, E.A., Puckette, J. and Yokoyama, Y., 2012. Correlation of early and mid-Holocene events using magnetic susceptibility in estuarine cores from bays along the northwestern Gulf of Mexico. Palaeogeogr. Palaeoclimatol. Palaeoecol., 346–347: 95–107.

Simms, A.R., Anderson, J.B. and Blum, M., 2006. Barrier-island aggradation via inlet migration: Mustang Island, Texas. Sedimentary Geol., 187(1–2): 105–125.

Simms, A.R., Lambeck, K., Purcell, A., Anderson, J.B. and Rodriguez, A.B., 2007. Sea-level history of the Gulf of Mexico since the Last Glacial Maximum with implications for the melting history of the Laurentide Ice Sheet. Quaternary Science Reviews, 26(7–8): 920–940.

Simms, A.R., Anderson, J.B., Rodriguez, A.B. and Taviani, M., 2008. Mechanisms controlling environmental change within an estuary: Corpus Christi Bay, Texas, USA. Geol. Soc. Spec. Pap., 443: 121–146.

Simms, A.R., Aryal, N., Miller, L. and Yokoyama, Y., 2010. The incised valley of Baffin Bay, Texas: a tale of two climates. Sedimentology, 57(2): 642–669.

Solanki, S.K., Krivova, N.A. and Haigh, J.D., 2013. Solar irradiance variability and climate. Annual Review of Astronomy and Astrophysics, 51: 311–351.

Steinhilber, F., Abreu, J.A., Beer, J., Brunner, I., Christl, M., Fischer, H., Heikkilä, U., Kubik, P.W., Mann, M. and McCracken, K.G., 2012. 9,400 years of cosmic radiation and solar activity from ice cores and tree rings. Proceedings of the National Academy of Sciences, 109(16): 5967–5971.

Thomas, M.A. and Anderson, J.B., 1994. Sea-Level Controls on the Facies Architecture of the Trinity/Sabine Incised-Valley System, Texas Continental Shelf, Incised-Valley Systems. SEPM Society for Sedimentary Geology: 63–82.

Thornthwaite, C.W., 1948. An approach toward a rational classification of climate. Geographical review, 38(1): 55–94.

Toomey, R.S., 1993. Late Pleistocene and Holocene faunal and environmental changes at Hall's Cave, Kerr County, Texas (Doctoral dissertation).

Toomey, R.S., Blum, M.D. and Valastro, S., 1993. Late Quaternary climates and environments of the Edwards Plateau, Texas. Global and planetary change, 7(4): 299–320.

Törnqvist, T.E., Bick, S.J., González, J.L., van der Borg, K. and de Jong, A.F.M., 2004a. Tracking the sea-level signature of the 8.2 ka cooling event: New constraints from the Mississippi Delta. Geophysical Research Letters, 31(23).

Törnqvist, T.E., González, J.L., Newsom, L.A., van der Borg, K., de Jong, A.F.M. and Kurnik, C.W., 2004b. Deciphering Holocene sea-level history on the U.S. Gulf Coast: A high-resolution record from the Mississippi Delta. Geological Society of America Bulletin, 116(7–8): 1026–1039.

Törnqvist, T.E., Bick, S.J., van der Borg, K. and de Jong, A.F.M., 2006. How stable is the Mississippi Delta? Geology, 34(8): 697–700.

Törnqvist, T.E. and Hijma, M.P., 2012. Links between early Holocene ice-sheet decay, sea-level rise and abrupt climate change. Nature Geoscience, 5(9): 601–606.

Törnqvist, T.E., Rosenheim, B.E., Hu, P. and Fernandez, A.B., 2015. Radiocarbon dating and calibration, Handbook of Sea-Level Research. John Wiley & Sons, Ltd: 347–360.

Traverse, A., 1988, Paleopalynology: Springer, 28(2):1–27.

Traverse, A., 1990. Studies of pollen and spores in rivers and other bodies of water, in terms of source-vegetation and sedimentation, with special reference to Trinity River and Bay, Texas. Review of Palaeobotany and Palynology, 64(1–4): 297–303.

Traverse, A., 2007. Production, dispersal, sedimentation and taphonomy of spores/pollen in relation to the interpretation of palynofloras. Paleopalynology: 497–542.

Troiani, B., Simms, A., Dellapenna, T., Piper, E. and Yokoyama, Y., 2011. The importance of sea-level and climate change, including changing wind energy, on the evolution of a coastal estuary: Copano Bay, Texas. Marine Geology, 280(1): 1–19.

Ullman, D.J., Carlson, A.E., Hostetler, S.W., Clark, P.U., Cuzzone, J., Milne, G.A., Winsor, K. and Caffee, M., 2016. Final Laurentide ice-sheet deglaciation and Holocene climate-sea level change. Quaternary Science Reviews, 152: 49–59.

Van Devender, T.R. and Riskind, D.H., 1979. Late Pleistocene and early Holocene plant remains from Hueco Tanks State Historical Park: the development of a refugium. The Southwestern Naturalist: 127–140.

Wallace, D.J. and Anderson, J.B., 2013. Unprecedented erosion of the upper Texas coast: Response to accelerated sea-level rise and hurricane impacts. Geological Society of America Bulletin, 125(5–6): 728–740.

Warny, S.A. and Wrenn, J.H., 2002. Upper Neogene dinoflagellate cyst ecostratigraphy of the Atlantic coast of Morocco. Micropaleontology, 48(3): 257–272.

Warny, S.A., Bart, P.J. and Suc, J.-P., 2003. Timing and progression of climatic, tectonic and glacioeustatic influences on the Messinian Salinity Crisis. Palaeogeogr. Palaeoclimatol. Palaeoecol., 202(1): 59–66.

Warny, S., Jarzen, D.M., Evans, A., Hesp, P. and Bart, P., 2012. Environmental significance of abundant and diverse hornwort spores in a potential submerged Paleoindian site in the Gulf of Mexico. Palynology, 36(2): 234–253.

Wen, L.-S., Warnken, K.W. and Santschi, P.H., 2008. The role of organic carbon, iron, and aluminium oxyhydroxides as trace metal carriers: Comparison between the Trinity River and the Trinity River Estuary (Galveston Bay, Texas). Marine Chemistry, 112(1): 20–37.

Wermund, E.G., 1996. River Basin Map of Texas, Bureau of Economic Geology, The University of Texas at Austin.

Wharton, C.H., Kitchens, W.M., Pendleton, E.C. and Sipe, T.W., 1982. Ecology of bottomland hardwood swamps of the southeast: a community profile, Georgia Univ., Athens (USA). Inst. of Ecology; Fish and Wildlife Service, Slidell, LA (USA). National Coastal Ecosystems Team; Wabash Coll., Crawfordsville, IN (USA). Dept. of Biology.

Wilkins, D.E. and Currey, D.R., 1999. Radiocarbon chronology andδ13C analysis of mid-to late-Holocene aeolian environments, Guadalupe Mountains National Park, Texas, USA. The Holocene, 9(3): 363–371.

Williams, K., Ewel, K.C., Stumpf, R.P., Putz, F.E. and Workman, T.W., 1999. Sea-Level Rise and Coastal Forest Retreat on the West Coast of Florida, USA. Ecology, 80(6): 2045.

Williams-Dean, G. and Bryant, V.M., 1975. Pollen analysis of human coprolites from Antelope House. Kiva, 41(1): 97–111.

Zonneveld, K.A.F., Marret, F., Versteegh, G.J.M., Bogus, K., Bonnet, S., Bouimetarhan, I., Crouch, E., de Vernal, A., Elshanawany, R. and Edwards, L., 2013. Atlas of modern dinoflagellate cyst distribution based on 2405 data points. Review of Palaeobotany and Palynology, 191: 1–197.

APPENDIX A
CHAPTER 2 SUPPLEMENTARY TABLE

Supplementary Table A1. Palynological counts for Corpus Christi Bay core CCB02-01.

Corpus Christi Core CCB02-01			Bchron Age Estimates (YBP)					Dinoflagellates									Pollen		Spores				
Sample ID	Depth (ftbsl)	Depth (mbsl)	2.50%	10%	50%	90%	97.50%	*Lingulodinium machaerophorum*	*Nemaosphaeropsis labyrinthus*	*Operculodinium centrocarpum*	*Operculodinium floridium*	*Polysphaeridium zohari*	*Spiniferites* spp.	*Tuberculodinium vancampoae*	Total Identified Dinoflagellates	Reworked Dinoflagellates	Arboreal	Nonarboreal		*Lycopodium* Counted	*Lycopodium* per Tablet	Dry Sample Weight (g)	Dinoflagellate Concentration
(10') Seg 1 10cm	25.918636	7.9	973	1252	1627	1982	2177	0	3	0	0	0	13	0	16	0	180	108	0	448	20848	6.3	118
(10') Seg 1 60cm	27.230972	8.3	1344	1547	1902	2247	2451	1	0	0	0	0	19	0	20	0	155	124	0	979	20848	6.3	68
(15') Seg 2 17.78cm	30.183728	9.2	1856	2016	2372	2674	2859	0	0	0	0	0	10	0	10	0	140	148	0	1994	20848	3	35
(15') Seg 2 33.5cm	30.839896	9.4	1948	2128	2489	2798	3016	1	1	0	0	6	40	0	48	0	218	112	3	1144	20848	2.2	398
(15') Seg. 2 57.9cm	31.660106	9.65	2157	2331	2681	3005	3186	0	0	0	0	0	7	0	7	0	146	150	0	2105	20848	7.8	9
(15') Seg. 2 73cm	32.152232	9.8	2254	2427	2769	3089	3287	0	1	0	0	4	0	0	5	9	170	148	0	2592	20848	5	23
(20') Seg 3 17cm	35.433072	10.8	2831	3053	3430	3806	4022	0	0	0	0	10	0	0	10	1	60	57	0	1178	20848	4.7	41
(20') Seg 3 37cm	36.08924	11	3010	3254	3622	4034	4271	0	1	0	2	37	13	0	53	11	167	82	0	1057	20848	6.1	207
(20') Seg 3 50cm	37.073492	11.3	3272	3505	3887	4283	4587	0	2	0	3	49	11	0	65	5	156	87	0	799	20848	7.5	244
(20') Seg 3 60cm	37.401576	11.4	3311	3584	3971	4352	4642	0	0	0	3	46	30	0	79	1	152	97	0	932	20848	6.6	271
(20') Seg 3 70cm	37.72966	11.5	3368	3644	4047	4433	4710	0	0	0	2	6	19	0	27	0	166	101	0	996	20848	7	81
(20') Seg 3 80cm	38.057744	11.6	3409	3718	4139	4503	4780	0	0	0	4	10	33	0	47	7	196	129	0	1477	20848	5.3	144
(20') Seg 3 90cm	38.385828	11.7	3474	3786	4220	4583	4822	0	0	0	0	4	25	0	29	2	179	100	2	1050	20848	6.7	92
(25') Seg 4 5cm	39.698164	12.1	3718	4068	4547	4910	5108	1	0	0	0	8	14	0	23	0	206	156	1	577	20848	11.5	72
(25') Seg 4 15cm	40.354332	12.3	3901	4211	4716	5095	5271	2	3	0	0	20	21	0	46	2	150	121	0	1170	20848	6.2	138
(25') Seg 4 25cm	40.682416	12.4	4038	4301	4802	5177	5365	0	3	0	6	16	69	0	94	1	121	94	2	995	20848	5.8	343
(25') Seg 4 35cm	41.0105	12.5	4212	4422	4888	5305	5487	0	0	0	0	4	4	0	8	2	202	151	8	1123	20848	11.4	16
(25') Seg 4 45cm	41.338584	12.6	4350	4594	5042	5471	5658	2	2	0	8	4	74	0	90	15	156	105	0	518	20848	15.3	276
(25') Seg 4 55cm	41.666668	12.7	4488	4728	5161	5607	5894	1	0	0	8	5	61	0	75	17	137	109	0	1072	20848	8.1	221
(25') Seg 4 70cm	41.994752	12.8	4599	4860	5273	5699	6027	0	0	0	11	14	67	0	92	7	107	94	0	699	20848	9.4	314
(25') Seg 4 83cm	42.65092	13	4825	5072	5486	5934	6247	9	1	0	3	7	43	0	63	3	152	194	0	963	20848	10	143
(30') Seg 5 0cm	44.947508	13.7	5415	5784	6240	6586	6778	3	0	0	3	6	22	0	34	1	127	138	1	901	20848	9.9	82
(30') Seg 5 5cm	45.11155	13.75	5476	5850	6294	6630	6822	0	0	0	0	1	1	1	3	1	172	136	1	819	20848	10.3	10
(30') Seg. 5 15cm	45.439634	13.85	5609	5986	6400	6745	6943	8	1	0	4	12	25	1	51	2	147	149	0	1227	20848	9.9	91
(30') Seg 5 25cm	47.57218	14.15	6229	6440	6773	7134	7286	5	2	0	0	30	67	0	104	11	115	85	1	642	20848	10.6	352

Corpus Christi Core CCB02-01

Sample ID	Depth (ftbsl)	Depth (mbsl)	Bchron Age Estimates (YBP)					Dinoflagellates									Pollen		Spores				
			2.50%	10%	50%	90%	97.50%	*Lingulodinium machaerophorum*	*Nemaosphaeropsis labyrinthus*	*Operculodinium centrocarpum*	*Operculodinium floridium*	*Polysphaeridium zohari*	*Spiniferites* spp.	*Tuberculodinium vancampoae*	Total Identified Dinoflagellates	Reworked Dinoflagellates	Arboreal	Nonarboreal		*Lycopodium* Counted	*Lycopodium* per Tablet	Dry Sample Weight (g)	Dinoflagellate Concentration
(30') Seg 5 35cm	46.423886	14.25	6357	6552	6885	7248	7377	2	1	0	4	35	33	0	75	8	103	111	0	520	20848	8.5	391
(30') Seg 5 45cm	46.75197	14.35	6476	6652	6984	7313	7454	0	0	0	1	14	10	0	25	2	149	138	0	1048	20848	9	60
(30') Seg 5 55cm	47.080054	14.45	6586	6753	7074	7389	7535	3	1	0	4	12	17	0	37	2	158	113	0	1684	20848	9	54
(30') Seg 5 65cm	47.408138	14.5	6637	6797	7119	7429	7562	1	1	0	3	26	18	0	49	3	127	124	0	646	20848	12.6	133
(30') Seg 5 75cm	47.736222	14.55	6686	6849	7165	7466	7605	0	0	2	3	23	26	0	54	0	133	139	0	984	20848	9.1	126
(30') Seg 5 85cm	48.064306	14.65	6745	6939	7255	7540	7674	0	3	1	1	24	38	0	67	1	115	122	1	1477	20848	8.6	112
(30') Seg 5 95cm	48.39239	14.75	6814	7027	7348	7629	7766	2	1	0	1	8	16	8	36	0	176	111	3	680	20848	13.3	83
(30') Seg 5 105cm	48.720474	14.85	6878	7102	7444	7715	7856	1	2	0	6	13	21	9	52	0	155	95	0	1376	20848	7.8	101
(35') Seg 6 0cm	50.524936	15.4	7388	7570	7903	8216	8369	0	0	9	13	12	5	2	41	1	138	129	1	877	20848	6.9	145
(35') Seg 6 35cm	51.67323	15.75	7528	7687	8019	8317	8472	0	0	4	14	10	11	1	40	0	155	157	1	1120	20848	6.8	109
(35') Seg 6 40cm	51.837272	15.8	7546	7712	8035	8332	8484	0	7	1	16	44	0	4	72	6	166	120	0	1461	20848	6.9	161
(35') Seg 6 57cm	52.49344	16	7607	7774	8085	8391	8542	0	0	1	0	15	19	0	35	1	198	163	0	1022	20848	11.5	64
(35') Seg 6 65cm	52.821524	16.1	7634	7802	8115	8420	8568	0	0	1	0	6	6	0	13	0	137	155	0	824	20848	7.2	46
(35') Seg 6 85cm	53.477692	16.3	7685	7850	8168	8476	8625	4	5	0	4	106	137	2	258	4	140	174	0	1090	20848	6.9	726
(35') Seg 6 95cm	53.805776	16.4	7714	7874	8199	8510	8656	3	3	1	3	120	133	4	267	4	102	99	0	853	20848	8	828
(35') Seg 6 110cm	54.13386	16.5	7739	7907	8226	8542	8671	9	4	1	6	151	98	0	269	5	35	52	0	309	20848	10.8	1712
(40') Seg 7 10cm	55.118112	16.8	7791	7985	8318	8644	8795	9	6	0	6	161	71	0	253	47	71	102	0	619	20848	5.9	1713
(40') Seg7 30cm	55.77428	17	7847	8028	8377	8714	8858	6	6	0	3	148	57	0	220	62	45	79	0	311	20848	8.1	2334
(40') Seg. 7 50cm	56.430448	17.2	7927	8099	8444	8803	8936	2	0	5	3	211	72	1	294	8	100	347	2	1201	20848	4.9	1070
(40') Seg. 7 70cm	57.086616	17.4	8049	8208	8552	8914	9073	1	1	0	0	129	22	0	153	0	84	108	1	692	20848	4.1	1124
(40') Seg 7 90cm	57.742784	17.6	8131	8303	8648	9007	9207	13	0	0	0	51	96	0	160	1	77	137	5	679	20848	7.3	677
(40') Seg 7 110cm	58.398952	17.8	8178	8376	8718	9070	9270	9	0	2	12	68	51	0	142	1	88	109	0	985	20848	10.3	294
(45-55') Seg 8 10cm	59.711288	18.2	8279	8516	8862	9197	9398	2	0	2	4	23	21	0	52	1	74	172	0	696	20848	14	113
(45-55') Seg 8 30cm	60.69554	18.5	8377	8610	8966	9300	9499	0	0	0	3	5	5	0	13	0	61	236	0	4802	20848	4.7	12
(50') Seg 9 20cm	65.6168	20	8950	9166	9531	9922	10129	0	0	5	0	1	7	0	13	0	72	240	0	1804	20848	7.8	19
(50') Seg 9 40cm	66.272968	20.2	9037	9266	9640	10017	10212	0	0	0	0	4	10	1	15	0	59	223	0	740	20848	4.2	101

Corpus Christi Core CCB02-01

Sample ID	Depth (ftbsl)	Depth (mbsl)	Bchron Age Estimates (YBP)					Dinoflagellates									Pollen		Spores				
			2.50%	10%	50%	90%	97.50%	*Lingulodinium machaerophorum*	*Nemaosphaeropsis labyrinthus*	*Operculodinium centrocarpum*	*Operculodinium floridium*	*Polysphaeridium zohari*	*Spiniferites* spp.	*Tuberculodinium vancampoae*	Total Identified Dinoflagellates	Reworked Dinoflagellates	Arboreal	Nonarboreal		*Lycopodium* Counted	*Lycopodium* per Tablet	Dry Sample Weight (g)	Dinoflagellate Concentration
(50') Seg 9 63cm	67.0275612	20.43	9166	9379	9742	10100	10294	0	0	0	0	0	7	0	7	0	54	205	0	775	20848	9.2	20
(50') Seg 9 80cm	67.585304	20.6	9245	9439	9812	10166	10365	0	0	1	0	0	6	0	7	2	34	201	0	1512	20848	7.3	17
(50') Seg 9 100cm	68.241472	20.8	9344	9504	9899	10261	10450	0	0	0	0	0	6	0	6	0	97	256	0	667	20848	9.9	19
(50') Seg 9 120cm	68.89764	21	9397	9573	9980	10346	10547	0	1	0	0	0	7	0	8	0	111	252	2	988	20848	8.2	21
(45-55') Seg 10 15cm	69.553808	21.2	9453	9636	10067	10430	10644	0	0	0	0	1	6	0	7	0	53	284	0	362	20848	11.4	35
(45-55') Seg 10 25cm	69.881892	21.3	9480	9663	10109	10480	10710	0	0	0	0	0	3	0	3	0	27	329	0	508	20848	7.1	17
(45-55') Seg 10 35cm	70.209976	21.4	9508	9697	10147	10540	10757	1	1	1	0	1	10	0	14	0	28	365	0	463	20848	7.8	81
(45-55') Seg 10 45cm	70.53806	21.5	9536	9747	10194	10591	10831	0	0	0	0	0	0	0	0	0	54	331	0	405	20848	9.9	0
(45-55') Seg 10 57cm	70.9645692	21.63	9615	9820	10248	10670	10919	0	0	0	0	0	0	0	0	0	21	390	0	265	20848	10.4	0
(60-65') Seg11 1cm	75.131236	22.9	9817	10167	10720	11648	12335	0	0	0	0	0	0	0	0	0	38	118	1	2870	20848	9.3	0
(60-65') Seg 11 20cm	75.787404	23.1	9852	10188	10775	11761	12514	0	0	0	0	0	0	0	0	0	70	110	2	1721	20848	10.2	0
(60-65') Seg 11 40cm	76.443572	23.3	9853	10202	10826	11894	12666	0	0	0	0	0	0	0	0	0	40	67	1	1664	20848	13.7	0
(60-65') Seg 11 54cm	76.935698	23.45	9854	10206	10864	11993	12769	0	0	0	0	0	0	0	0	0	29	50	0	943	20848	13	0
(60-65') Seg 12 3cm	80.38058	24.5	9899	10283	11150	12651	13450	0	0	0	0	0	0	0	0	0	32	303	0	543	20848	9.9	0
(60-65') Seg 12 17cm	80.8070892	24.63	9905	10291	11181	12729	13527	0	1	0	0	0	1	0	2	0	72	335	0	1029	20848	13.3	3
(60-65') Seg 12 35cm	81.364832	24.8	9914	10298	11226	12796	13604	0	0	0	0	0	0	0	0	0	9	44	0	3186	20848	11.7	0
(60-65') Seg 12 52cm	81.9225748	24.97	9918	10309	11281	12909	13785	0	0	0	0	0	0	0	0	1	17	22	3	1199	20848	15.6	1

APPENDIX B
CHAPTER 3 SUPPLEMENTARY FIGURES AND TABLES

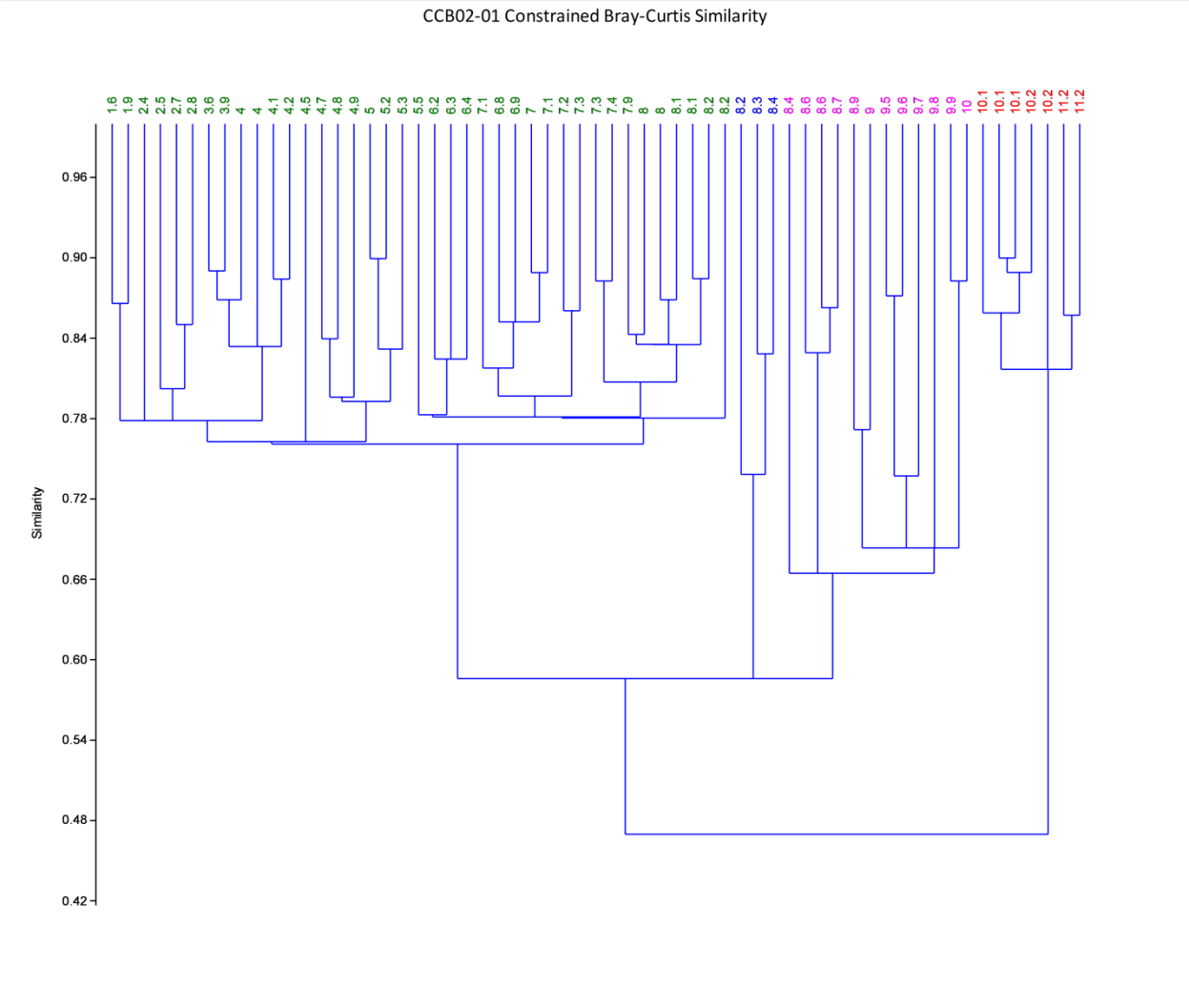

Supplementary Figure B1. Cluster analysis for core CCB02-01.

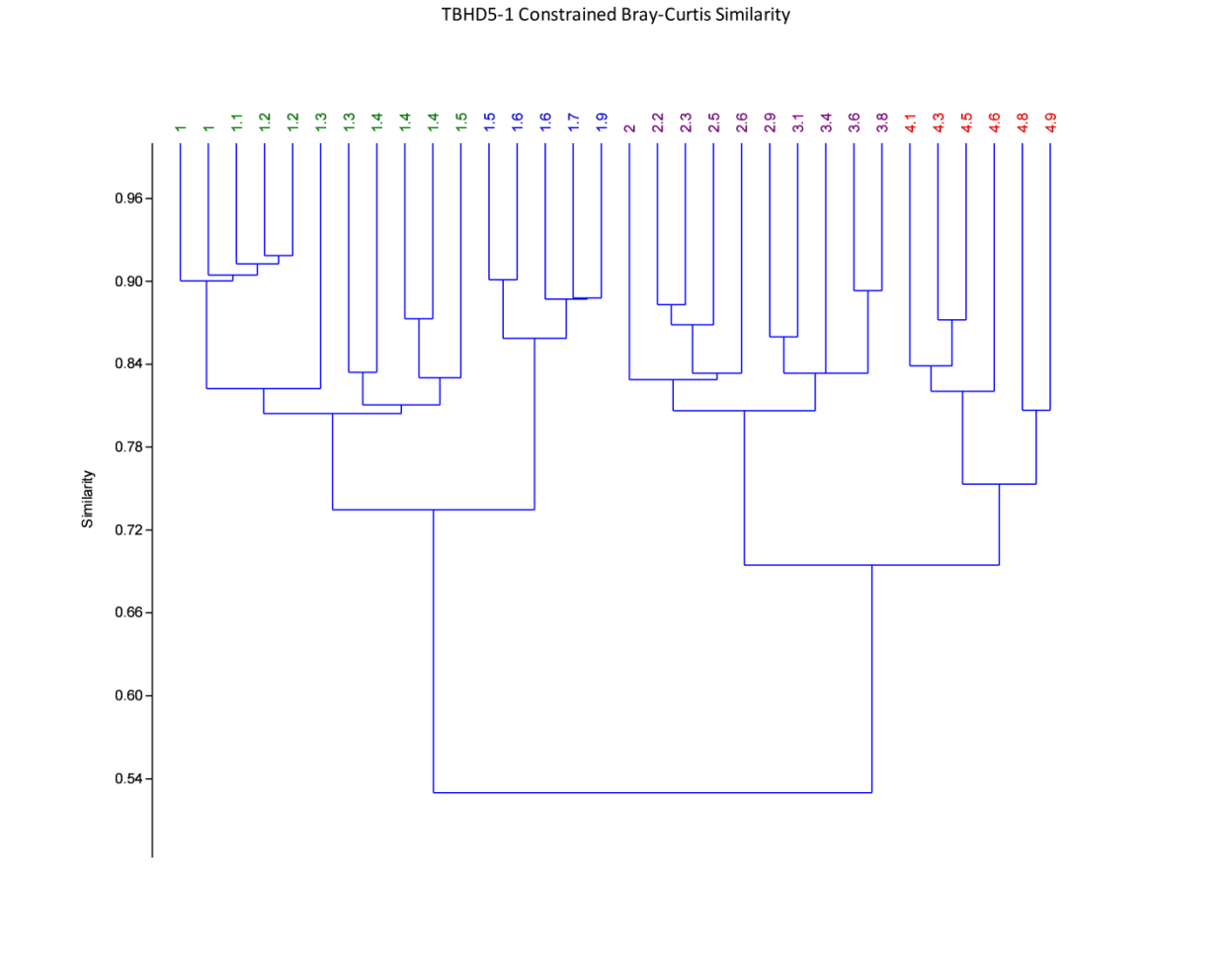

Supplementary Figure B2. Cluster analysis for Trinity Bay core TBHD5-1.

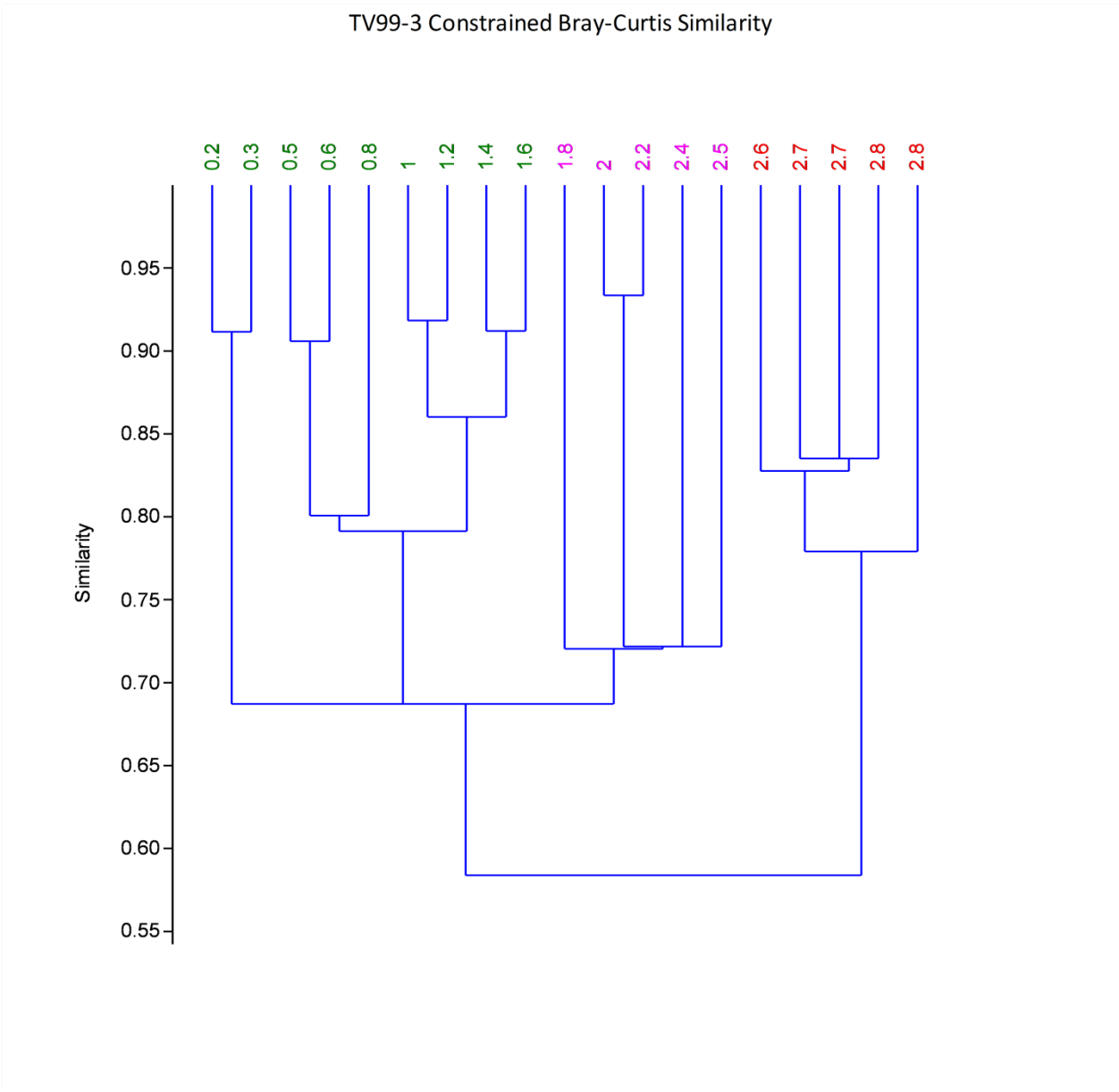

Supplementary Figure B3. Cluster analysis for Trinity Bay core TV99-3.

Supplementary Table B1. Complete record of observed pollen and dinoflagellate cysts.

				Nonarboreal (Herbs/sedges/shrubs)											
Core (Simms et al., 2008)	Sample ID Depth	Sample Depth (mbsl)	Age (50% quantile; Ferguson et al., 2017)	Asteraceae	*Chenopodium*	*Galium*	Poaceae	*Ilex*	*Myrica*	Apiaceae	Onagraceae	*Utrica*	*Hippuris*	*Zea mays*	*Acer*
CCB02-01	(10') Seg 1 10cm	7.9	1627	33	40	0	18	15	0	0	0	0	0	0	0
CCB02-01	(10') Seg 1 60cm	8.3	1902	42	40	0	17	6	0	0	0	0	0	0	0
CCB02-01	(15') Seg 2 17.78cm	9.2	2372	31	71	0	15	2	0	0	2	0	0	0	0
CCB02-01	(15') Seg 2 33.5cm	9.4	2489	35	66	0	9	0	0	0	0	0	0	0	0
CCB02-01	(15') Seg. 2 57.9cm	9.65	2681	34	68	0	24	4	0	0	0	0	0	0	0
CCB02-01	(15') Seg. 2 73cm	9.8	2769	68	72	0	1	2	0	0	0	0	0	0	0
CCB02-01	(20') Seg 3 17cm	10.8	3430	24	25	0	6	1	0	0	0	0	0	0	0
CCB02-01	(20') Seg 3 37cm	11	3622	13	43	0	13	5	0	0	0	0	0	0	0
CCB02-01	(20') Seg 3 50cm	11.3	3887	31	34	0	11	3	0	0	0	0	0	0	0
CCB02-01	(20') Seg 3 60cm	11.4	3971	21	59	0	4	4	0	0	0	0	0	0	0
CCB02-01	(20') Seg 3 70cm	11.5	4047	14	60	0	9	6	0	0	0	0	0	0	0
CCB02-01	(20') Seg 3 80cm	11.6	4139	35	75	0	12	3	0	0	1	0	0	0	0
CCB02-01	(20') Seg 3 90cm	11.7	4220	29	47	0	16	4	0	0	0	0	0	0	0
CCB02-01	(25') Seg 4 5cm	12.1	4547	12	117	0	20	0	0	0	0	0	0	0	0
CCB02-01	(25') Seg 4 15cm	12.3	4716	22	86	0	7	3	0	0	0	0	0	0	0
CCB02-01	(25') Seg 4 25cm	12.4	4802	19	61	0	8	2	0	0	2	0	0	0	0
CCB02-01	(25') Seg 4 35cm	12.5	4888	19	109	0	9	7	0	0	2	0	0	0	0
CCB02-01	(25') Seg 4 45cm	12.6	5042	18	62	0	17	1	0	0	6	0	0	0	0
CCB02-01	(25') Seg 4 55cm	12.7	5161	21	64	0	11	4	0	0	0	0	0	0	0
CCB02-01	(25') Seg 4 70cm	12.8	5273	12	58	0	17	3	0	0	0	0	0	0	0
CCB02-01	(25') Seg 4 83cm	13	5486	43	131	0	11	3	0	0	0	0	0	0	0
CCB02-01	(30') Seg 5 0cm	13.7	6240	45	70	0	7	7	0	0	0	0	0	0	0
CCB02-01	(30') Seg 5 5cm	13.75	6294	39	52	0	15	10	0	0	0	0	0	0	0
CCB02-01	(30') Seg. 5 15cm	13.85	6400	56	54	0	5	23	0	0	3	0	0	0	0
CCB02-01	(30') Seg 5 25cm	13.95	6773	28	31	0	12	9	0	0	0	0	0	0	0
CCB02-01	(30') Seg 5 35cm	14.15	6885	30	44	0	24	4	0	0	0	0	0	0	0
CCB02-01	(30') Seg 5 45cm	14.25	6984	29	50	0	37	7	0	0	1	0	0	0	0
CCB02-01	(30') Seg 5 55cm	14.35	7074	32	41	0	19	14	0	0	0	0	0	0	9
CCB02-01	(30') Seg 5 65cm	14.45	7119	37	43	0	27	6	0	0	1	0	0	0	8
CCB02-01	(30') Seg 5 75cm	14.55	7165	29	73	0	11	8	0	0	1	0	0	0	4
CCB02-01	(30') Seg 5 85cm	14.65	7255	30	62	0	15	3	0	0	0	0	0	0	2
CCB02-01	(30') Seg 5 95cm	14.75	7348	36	52	0	10	6	0	0	0	0	0	0	7
CCB02-01	(30') Seg 5 105cm	14.85	7444	32	39	0	13	1	0	0	0	0	0	0	0
CCB02-01	(35') Seg 6 0cm	15.4	7903	45	70	0	2	5	0	0	2	0	0	0	0
CCB02-01	(35') Seg 6 35cm	15.75	8019	74	75	0	1	0	0	0	0	0	0	0	0
CCB02-01	(35') Seg 6 40cm	15.8	8035	33	72	0	2	5	0	0	0	0	0	0	0
CCB02-01	(35') Seg 6 57cm	16	8085	54	85	0	4	8	0	0	0	0	0	0	0
CCB02-01	(35') Seg 6 65cm	16.1	8115	34	82	0	10	4	0	0	1	0	0	0	0
CCB02-01	(35') Seg 6 85cm	16.3	8168	42	102	0	14	9	0	0	0	0	0	0	0
CCB02-01	(35') Seg 6 95cm	16.4	8199	27	49	0	13	4	0	0	0	0	0	0	0
CCB02-01	(35') Seg 6 110cm	16.5	8226	11	28	0	7	1	0	0	0	0	0	0	0
CCB02-01	(40') Seg 7 10cm	16.8	8318	26	43	0	18	3	0	0	0	0	0	0	0
CCB02-01	(40') Seg7 30cm	17	8377	20	35	0	14	4	0	0	0	0	0	0	0
CCB02-01	(40') Seg. 7 50cm	17.2	8444	142	109	0	52	5	0	0	0	0	0	0	0
CCB02-01	(40') Seg. 7 70cm	17.4	8552	16	70	0	8	5	0	0	0	0	0	0	0
CCB02-01	(40') Seg 7 90cm	17.6	8648	35	55	0	22	7	0	0	0	0	0	0	0
CCB02-01	(40') Seg 7 110cm	17.8	8718	24	58	0	18	6	0	0	0	0	0	0	0
CCB02-01	(45-55') Seg 8 10cm	18.2	8862	51	38	0	26	2	0	0	4	0	0	0	0
CCB02-01	(45-55') Seg 8 30cm	18.5	8966	66	45	0	28	2	0	0	1	0	0	0	0
CCB02-01	(50') Seg 9 20cm	20	9531	46	106	0	35	1	0	0	1	0	0	0	0
CCB02-01	(50') Seg 9 40cm	20.2	9640	69	91	0	31	3	0	0	0	0	0	0	0
CCB02-01	(50') Seg 9 63cm	20.43	9742	26	80	0	68	3	0	0	2	0	0	0	0
CCB02-01	(50') Seg 9 80cm	20.6	9812	84	43	0	13	2	0	0	4	0	0	0	0
CCB02-01	(50') Seg 9 100cm	20.8	9899	73	129	0	24	2	0	0	2	0	0	0	0
CCB02-01	(50') Seg 9 120cm	21	9980	45	125	0	39	2	0	0	3	0	0	0	0
CCB02-01	(45-55') Seg 10 15cm	21.2	10067	23	206	0	38	3	0	0	0	0	0	0	0
CCB02-01	(45-55') Seg 10 25cm	21.3	10109	21	251	0	47	2	0	0	0	0	0	0	0
CCB02-01	(45-55') Seg 10 35cm	21.4	10147	35	273	0	49	5	0	0	0	0	0	0	0
CCB02-01	(45-55') Seg 10 45cm	21.5	10194	45	238	0	44	0	0	0	0	0	0	0	0
CCB02-01	(45-55') Seg 10 57cm	21.63	10248	23	331	0	35	0	0	0	0	0	0	0	0
CCB02-01	(60-65') Seg11 1cm	22.9	10720	34	54	0	26	2	0	0	2	0	0	0	0
CCB02-01	(60-65') Seg 11 20cm	23.1	10775	35	51	0	4	10	0	0	0	0	0	0	0
CCB02-01	(60-65') Seg 11 40cm	23.3	10826	26	27	0	5	4	0	0	0	0	0	0	0
CCB02-01	(60-65') Seg 11 54cm	23.45	10864	24	11	0	1	1	0	0	0	0	0	0	0
CCB02-01	(60-65') Seg 12 3cm	24.5	11150	40	211	0	28	0	0	0	0	0	0	0	0
CCB02-01	(60-65') Seg 12 17cm	24.63	11181	52	247	0	24	0	0	0	0	0	0	0	1
CCB02-01	(60-65') Seg 12 35cm	24.8	11226	13	6	0	6	2	0	0	0	0	0	0	0
CCB02-01	(60-65') Seg 12 52cm	24.97	11281	12	8	0	1	0	0	0	0	0	0	0	0

				Arboreal (Trees)											
Core (Simms et al., 2008)	Sample ID Depth	Sample Depth (mbsl)	Age (50% quantile; Ferguson et al., 2017)	*Alnus*	*Carya*	*Juglans*	*Pinus*	*Quercus*	*Salix*	*Ostrya virginiana*	*Taxodium*	*Celtis*	*Ulmus*	*Ephedra*	*Carex*
CCB02-01	(10') Seg 1 10cm	7.9	1627	6	4	0	59	80	0	0	0	1	0	0	0
CCB02-01	(10') Seg 1 60cm	8.3	1902	1	1	0	61	62	0	0	9	1	0	0	0
CCB02-01	(15') Seg 2 17.78cm	9.2	2372	7	0	0	57	34	0	0	6	5	5	0	0
CCB02-01	(15') Seg 2 33.5cm	9.4	2489	6	22	0	81	106	0	0	2	3	0	0	0
CCB02-01	(15') Seg. 2 57.9cm	9.65	2681	4	0	0	70	58	0	0	2	0	2	4	6
CCB02-01	(15') Seg. 2 73cm	9.8	2769	10	3	0	88	69	0	0	2	0	0	3	0
CCB02-01	(20') Seg 3 17cm	10.8	3430	3	2	0	18	37	0	0	0	0	0	1	0
CCB02-01	(20') Seg 3 37cm	11	3622	1	2	0	101	27	0	0	2	1	2	0	0
CCB02-01	(20') Seg 3 50cm	11.3	3887	3	6	0	89	24	0	0	2	1	0	0	0
CCB02-01	(20') Seg 3 60cm	11.4	3971	2	3	0	84	45	0	0	4	0	0	0	3
CCB02-01	(20') Seg 3 70cm	11.5	4047	6	2	0	115	38	0	0	1	0	0	5	2
CCB02-01	(20') Seg 3 80cm	11.6	4139	2	2	0	99	74	0	0	0	1	0	1	1
CCB02-01	(20') Seg 3 90cm	11.7	4220	4	5	0	100	56	0	0	0	0	0	2	0
CCB02-01	(25') Seg 4 5cm	12.1	4547	4	19	0	88	77	0	0	2	0	0	2	1
CCB02-01	(25') Seg 4 15cm	12.3	4716	2	6	0	63	72	0	0	0	0	0	0	0
CCB02-01	(25') Seg 4 25cm	12.4	4802	7	6	2	43	39	0	0	1	0	0	0	0
CCB02-01	(25') Seg 4 35cm	12.5	4888	3	8	1	66	100	0	0	1	0	0	1	0
CCB02-01	(25') Seg 4 45cm	12.6	5042	7	1	0	88	42	0	0	0	0	0	0	0
CCB02-01	(25') Seg 4 55cm	12.7	5161	5	1	0	69	54	0	0	2	0	0	1	0
CCB02-01	(25') Seg 4 70cm	12.8	5273	1	2	1	66	37	0	0	1	0	0	1	1
CCB02-01	(25') Seg 4 83cm	13	5486	11	2	0	44	86	0	0	2	0	0	1	2
CCB02-01	(30') Seg 5 0cm	13.7	6240	0	2	0	51	74	0	0	1	0	0	1	0
CCB02-01	(30') Seg 5 5cm	13.75	6294	13	0	0	75	73	0	0	4	0	0	1	5
CCB02-01	(30') Seg. 5 15cm	13.85	6400	7	1	1	46	87	0	0	1	0	0	2	0
CCB02-01	(30') Seg 5 25cm	13.95	6773	4	1	1	33	74	0	0	1	0	0	1	2
CCB02-01	(30') Seg 5 35cm	14.15	6885	3	1	0	45	46	0	0	3	0	0	0	0
CCB02-01	(30') Seg 5 45cm	14.25	6984	7	0	0	49	42	0	0	4	0	0	2	5
CCB02-01	(30') Seg 5 55cm	14.35	7074	9	6	0	55	23	0	0	1	0	5	1	3
CCB02-01	(30') Seg 5 65cm	14.45	7119	5	1	0	45	37	0	0	1	0	1	3	3
CCB02-01	(30') Seg 5 75cm	14.55	7165	6	0	0	74	33	0	0	2	0	1	2	3
CCB02-01	(30') Seg 5 85cm	14.65	7255	5	3	0	49	47	0	0	3	0	0	2	2
CCB02-01	(30') Seg 5 95cm	14.75	7348	7	5	0	65	90	0	0	1	0	2	1	4
CCB02-01	(30') Seg 5 105cm	14.85	7444	3	2	0	55	89	0	0	1	0	0	1	3
CCB02-01	(35') Seg 6 0cm	15.4	7903	6	2	0	52	72	0	0	2	0	0	1	0
CCB02-01	(35') Seg 6 35cm	15.75	8019	8	0	0	46	97	0	0	1	0	0	1	4
CCB02-01	(35') Seg 6 40cm	15.8	8035	3	5	0	37	121	0	0	6	0	0	1	0
CCB02-01	(35') Seg 6 57cm	16	8085	6	4	0	62	126	0	0	2	0	0	2	0
CCB02-01	(35') Seg 6 65cm	16.1	8115	6	0	0	42	89	0	0	15	0	0	5	1
CCB02-01	(35') Seg 6 85cm	16.3	8168	4	3	0	38	94	0	0	6	0	0	0	0
CCB02-01	(35') Seg 6 95cm	16.4	8199	3	0	0	23	72	0	0	1	0	0	4	0
CCB02-01	(35') Seg 6 110cm	16.5	8226	1	1	0	10	23	0	0	4	0	0	1	0
CCB02-01	(40') Seg 7 10cm	16.8	8318	4	0	0	16	51	0	0	6	0	0	3	3
CCB02-01	(40') Seg7 30cm	17	8377	4	0	0	10	31	0	0	5	0	0	1	0
CCB02-01	(40') Seg. 7 50cm	17.2	8444	10	1	1	26	62	0	0	17	0	0	14	8
CCB02-01	(40') Seg. 7 70cm	17.4	8552	4	0	0	22	55	0	0	2	0	3	1	0
CCB02-01	(40') Seg 7 90cm	17.6	8648	7	0	0	24	43	0	0	16	0	0	1	0
CCB02-01	(40') Seg 7 110cm	17.8	8718	6	1	0	22	57	0	0	2	0	0	0	0
CCB02-01	(45-55') Seg 8 10cm	18.2	8862	4	0	0	9	55	0	0	31	0	0	5	0
CCB02-01	(45-55') Seg 8 30cm	18.5	8966	8	1	2	19	30	0	0	49	0	0	2	0
CCB02-01	(50') Seg 9 20cm	20	9531	3	3	0	18	41	0	0	24	1	0	3	0
CCB02-01	(50') Seg 9 40cm	20.2	9640	2	4	1	21	30	0	0	11	0	0	4	0
CCB02-01	(50') Seg 9 63cm	20.43	9742	1	9	0	6	38	0	0	3	0	0	3	6
CCB02-01	(50') Seg 9 80cm	20.6	9812	2	2	0	8	22	0	0	46	0	0	4	0
CCB02-01	(50') Seg 9 100cm	20.8	9899	9	0	0	22	62	0	0	10	0	2	1	1
CCB02-01	(50') Seg 9 120cm	21	9980	6	2	0	28	73	0	0	9	0	1	4	1
CCB02-01	(45-55') Seg 10 15cm	21.2	10067	2	0	0	23	27	0	0	10	0	0	0	0
CCB02-01	(45-55') Seg 10 25cm	21.3	10109	1	0	0	9	17	0	0	4	0	0	1	0
CCB02-01	(45-55') Seg 10 35cm	21.4	10147	0	0	0	23	5	0	0	1	0	0	0	0
CCB02-01	(45-55') Seg 10 45cm	21.5	10194	4	0	0	16	34	0	0	2	0	0	0	0
CCB02-01	(45-55') Seg 10 57cm	21.63	10248	2	0	0	5	14	0	0	0	0	0	0	0
CCB02-01	(60-65') Seg11 1cm	22.9	10720	0	0	0	14	24	0	0	0	0	0	0	0
CCB02-01	(60-65') Seg 11 20cm	23.1	10775	0	0	0	39	31	0	0	7	0	0	1	0
CCB02-01	(60-65') Seg 11 40cm	23.3	10826	0	0	0	24	16	0	0	3	0	0	0	0
CCB02-01	(60-65') Seg 11 54cm	23.45	10864	0	0	0	14	15	0	0	9	0	0	0	0
CCB02-01	(60-65') Seg 12 3cm	24.5	11150	3	0	0	19	10	0	0	3	0	0	0	2
CCB02-01	(60-65') Seg 12 17cm	24.63	11181	0	6	0	21	39	0	0	7	0	0	0	1
CCB02-01	(60-65') Seg 12 35cm	24.8	11226	0	0	0	4	5	0	0	17	0	0	0	0
CCB02-01	(60-65') Seg 12 52cm	24.97	11281	0	0	0	11	6	0	0	1	0	0	0	0

				Reworked				Unidentifiable			
Core (Simms et al., 2008)	Sample ID Depth	Sample Depth (mbsl)	Age (50% quantile; Ferguson et al., 2017)	eworked Pollen	ked Dinoflage	eworked Spore	RW per sam	unknown 6	Triporate 2	unknown 26	unknown 25
CCB02-01	(10') Seg 1 10cm	7.9	1627	8	1	0	9	0	0	2	7
CCB02-01	(10') Seg 1 60cm	8.3	1902	21	0	1	22	0	0	10	8
CCB02-01	(15') Seg 2 17.78cm	9.2	2372	11	0	1	12	0	0	20	14
CCB02-01	(15') Seg 2 33.5cm	9.4	2489	0	0	0	0	0	0	0	0
CCB02-01	(15') Seg. 2 57.9cm	9.65	2681	5	0	0	5	0	0	8	0
CCB02-01	(15') Seg. 2 73cm	9.8	2769	0	9	0	9	0	0	0	0
CCB02-01	(20') Seg 3 17cm	10.8	3430	0	1	0	1	0	0	0	0
CCB02-01	(20') Seg 3 37cm	11	3622	9	11	0	20	0	0	5	0
CCB02-01	(20') Seg 3 50cm	11.3	3887	16	5	0	21	0	0	5	0
CCB02-01	(20') Seg 3 60cm	11.4	3971	10	1	0	11	0	0	1	0
CCB02-01	(20') Seg 3 70cm	11.5	4047	18	1	0	19	0	0	4	0
CCB02-01	(20') Seg 3 80cm	11.6	4139	25	7	0	32	0	0	1	0
CCB02-01	(20') Seg 3 90cm	11.7	4220	6	2	0	8	0	0	2	0
CCB02-01	(25') Seg 4 5cm	12.1	4547	15	0	1	16	0	0	1	0
CCB02-01	(25') Seg 4 15cm	12.3	4716	17	2	0	19	0	0	2	0
CCB02-01	(25') Seg 4 25cm	12.4	4802	7	1	0	8	0	0	1	0
CCB02-01	(25') Seg 4 35cm	12.5	4888	12	2	0	14	0	0	3	0
CCB02-01	(25') Seg 4 45cm	12.6	5042	49	16	0	65	0	0	1	0
CCB02-01	(25') Seg 4 55cm	12.7	5161	37	17	0	54	0	0	4	0
CCB02-01	(25') Seg 4 70cm	12.8	5273	74	7	0	81	0	0	0	0
CCB02-01	(25') Seg 4 83cm	13	5486	0	3	0	3	0	0	0	0
CCB02-01	(30') Seg 5 0cm	13.7	6240	0	1	0	1	0	0	7	0
CCB02-01	(30') Seg 5 5cm	13.75	6294	33	1	0	34	0	0	3	0
CCB02-01	(30') Seg. 5 15cm	13.85	6400	31	2	0	33	0	0	0	0
CCB02-01	(30') Seg 5 25cm	13.95	6773	39	11	0	50	0	0	0	0
CCB02-01	(30') Seg 5 35cm	14.15	6885	50	8	1	59	0	0	5	0
CCB02-01	(30') Seg 5 45cm	14.25	6984	35	2	0	37	0	0	3	1
CCB02-01	(30') Seg 5 55cm	14.35	7074	53	2	0	55	0	0	2	0
CCB02-01	(30') Seg 5 65cm	14.45	7119	41	3	2	46	0	0	3	0
CCB02-01	(30') Seg 5 75cm	14.55	7165	1	0	0	1	0	0	3	0
CCB02-01	(30') Seg 5 85cm	14.65	7255	0	1	2	3	0	0	2	0
CCB02-01	(30') Seg 5 95cm	14.75	7348	0	0	0	0	0	0	1	0
CCB02-01	(30') Seg 5 105cm	14.85	7444	0	0	2	2	0	0	4	0
CCB02-01	(35') Seg 6 0cm	15.4	7903	0	1	0	1	0	0	0	0
CCB02-01	(35') Seg 6 35cm	15.75	8019	0	0	0	0	0	0	0	0
CCB02-01	(35') Seg 6 40cm	15.8	8035	2	6	0	8	0	0	0	0
CCB02-01	(35') Seg 6 57cm	16	8085	7	1	0	8	0	0	0	0
CCB02-01	(35') Seg 6 65cm	16.1	8115	14	0	0	14	0	0	0	0
CCB02-01	(35') Seg 6 85cm	16.3	8168	56	4	0	60	0	0	0	0
CCB02-01	(35') Seg 6 95cm	16.4	8199	26	4	0	30	0	0	0	0
CCB02-01	(35') Seg 6 110cm	16.5	8226	24	15	0	39	0	0	0	0
CCB02-01	(40') Seg 7 10cm	16.8	8318	22	52	0	74	0	0	0	0
CCB02-01	(40') Seg7 30cm	17	8377	27	62	0	89	0	0	0	0
CCB02-01	(40') Seg. 7 50cm	17.2	8444	34	8	1	43	0	0	0	0
CCB02-01	(40') Seg. 7 70cm	17.4	8552	2	0	0	2	0	0	0	0
CCB02-01	(40') Seg 7 90cm	17.6	8648	1	1	0	2	0	0	0	3
CCB02-01	(40') Seg 7 110cm	17.8	8718	16	1	0	17	0	0	0	0
CCB02-01	(45-55') Seg 8 10cm	18.2	8862	44	1	0	45	0	0	12	3
CCB02-01	(45-55') Seg 8 30cm	18.5	8966	68	0	0	68	0	0	41	1
CCB02-01	(50') Seg 9 20cm	20	9531	14	0	0	14	0	0	13	2
CCB02-01	(50') Seg 9 40cm	20.2	9640	8	0	0	8	0	0	6	0
CCB02-01	(50') Seg 9 63cm	20.43	9742	6	0	0	6	0	0	10	0
CCB02-01	(50') Seg 9 80cm	20.6	9812	13	2	0	15	0	0	3	0
CCB02-01	(50') Seg 9 100cm	20.8	9899	9	0	0	9	0	0	2	0
CCB02-01	(50') Seg 9 120cm	21	9980	8	0	1	9	0	0	9	0
CCB02-01	(45-55') Seg 10 15cm	21.2	10067	4	0	0	4	0	0	2	0
CCB02-01	(45-55') Seg 10 25cm	21.3	10109	0	0	0	0	0	0	3	0
CCB02-01	(45-55') Seg 10 35cm	21.4	10147	9	0	0	9	0	0	0	0
CCB02-01	(45-55') Seg 10 45cm	21.5	10194	3	0	0	3	0	0	0	0
CCB02-01	(45-55') Seg 10 57cm	21.63	10248	2	0	0	2	0	0	0	0
CCB02-01	(60-65') Seg11 1cm	22.9	10720	1	0	0	1	0	0	0	0
CCB02-01	(60-65') Seg 11 20cm	23.1	10775	0	0	0	0	0	0	0	0
CCB02-01	(60-65') Seg 11 40cm	23.3	10826	3	0	0	3	0	0	0	0
CCB02-01	(60-65') Seg 11 54cm	23.45	10864	0	0	0	0	0	0	0	0
CCB02-01	(60-65') Seg 12 3cm	24.5	11150	1	0	0	1	0	0	6	0
CCB02-01	(60-65') Seg 12 17cm	24.63	11181	15	0	0	15	0	0	0	0
CCB02-01	(60-65') Seg 12 35cm	24.8	11226	22	0	0	22	0	0	0	0
CCB02-01	(60-65') Seg 12 52cm	24.97	11281	14	1	0	15	0	0	0	0

				Nonarboreal (Herbs/sedges/shrubs)										
Core (Anderson et al., 2008)	Sample ID Depth (cm)	Depth (mbsl)	Age (50% quantile)	Asteraceae	*Chenopodium*	*Galium*	Poaceae	*Ilex*	*Myrica*	Apiaceae	Onagraceae	*Utrica*	*Hippuris*	*Zea mays*
TBHD-5-1	260	3.21	988	12	22	1	17	7	0	0	0	0	0	0
TBHD-5-1	275	3.36	1032	15	24	0	20	2	1	0	0	0	2	0
TBHD-5-1	300	3.61	1112.5	7	16	2	21	4	0	0	0	0	0	0
TBHD-5-1	310	3.71	1171	12	18	0	24	8	0	0	0	0	0	0
TBHD-5-1	320	3.81	1218.5	21	14	0	24	8	1	0	0	0	0	0
TBHD-5-1	330	3.91	1265	3	36	1	24	7	10	0	0	3	0	1
TBHD-5-1	340	4.01	1308	6	15	1	16	7	3	0	0	5	0	0
TBHD-5-1	350	4.11	1352	2	12	0	24	4	0	0	0	0	0	1
TBHD-5-1	360	4.21	1399	12	15	0	14	7	0	0	0	0	0	0
TBHD-5-1	370	4.31	1445	12	18	0	15	7	1	0	0	0	0	0
TBHD-5-1	380	4.41	1490	26	25	0	26	6	0	0	0	0	0	0
TBHD-5-1	390	4.51	1537	11	21	0	13	3	0	0	0	0	0	0
TBHD-5-1	400	4.61	1582	15	22	0	22	7	0	0	0	0	0	1
TBHD-5-1	410	4.71	1632	19	41	0	20	5	0	1	0	0	0	0
TBHD-5-1	420	4.81	1744	15	24	0	33	5	0	0	0	0	0	0
TBHD-5-1	430	4.91	1892	9	37	0	33	7	3	0	0	0	0	0
TBHD-5-1	440	5.01	2041.5	30	67	0	33	12	0	0	0	1	0	0
TBHD-5-1	450	5.11	2187.5	26	49	0	40	7	1	0	0	1	0	0
TBHD-5-1	460	5.21	2331.5	22	37	0	39	6	0	0	0	0	0	0
TBHD-5-1	470	5.31	2484	26	45	0	39	5	0	0	0	0	0	0
TBHD-5-1	480	5.41	2641	37	59	0	23	2	1	1	1	0	0	0
TBHD-5-1	490	5.51	2872.5	10	52	0	25	9	1	1	0	0	0	0
TBHD-5-1	500	5.61	3116	23	39	0	31	7	0	0	0	0	0	0
TBHD-5-1	510	5.71	3361.5	16	41	0	50	1	1	0	0	1	0	0
TBHD-5-1	520	5.81	3604.5	25	45	0	30	3	0	0	0	0	0	0
TBHD-5-1	530	5.91	3836.5	17	51	0	37	10	0	1	0	0	0	0
TBHD-5-1	540	6.01	4056.5	36	76	0	28	7	0	0	0	0	0	0
TBHD-5-1	550	6.11	4287	50	94	0	39	8	2	2	0	1	0	0
TBHD-5-1	560	6.21	4462	39	97	0	32	7	0	0	0	1	0	0
TBHD-5-1	570	6.31	4621	34	59	0	52	12	1	0	0	0	0	0
TBHD-5-1	580	6.41	4768	52	85	0	50	20	0	0	0	0	0	0
TBHD-5-1	590	6.51	4914.5	76	131	0	49	11	0	0	0	0	0	0

				Arboreal (Trees)									Unknown
Core (Anderson et al., 2008)	Sample ID Depth (cm)	Depth (mbsl)	Age (50% quantile)	*Acer*	*Alnus*	*Carya*	*Juglans*	*Pinus*	*Quercus*	*Ostrya virginiana*	*Salix*	*Taxodium*	unk 6
TBHD-5-1	260	3.21	988	9	0	10	7	157	35	2	1	1	0
TBHD-5-1	275	3.36	1032	8	1	1	13	141	46	0	0	0	0
TBHD-5-1	300	3.61	1112.5	5	1	6	11	145	37	0	0	0	0
TBHD-5-1	310	3.71	1171	6	1	9	8	155	51	0	0	0	0
TBHD-5-1	320	3.81	1218.5	6	0	17	10	142	42	0	0	0	0
TBHD-5-1	330	3.91	1265	9	0	19	9	122	34	0	2	0	0
TBHD-5-1	340	4.01	1308	5	1	9	7	178	18	0	0	0	0
TBHD-5-1	350	4.11	1352	6	0	19	18	224	16	0	0	0	0
TBHD-5-1	360	4.21	1399	11	1	8	7	173	12	3	0	0	0
TBHD-5-1	370	4.31	1445	2	1	10	6	134	11	7	1	0	1
TBHD-5-1	380	4.41	1490	3	2	26	12	158	6	3	0	0	1
TBHD-5-1	390	4.51	1537	1	0	28	6	111	9	1	1	0	0
TBHD-5-1	400	4.61	1582	0	0	18	1	111	12	0	0	1	0
TBHD-5-1	410	4.71	1632	0	1	20	5	97	8	3	0	0	0
TBHD-5-1	420	4.81	1744	0	1	18	3	109	8	4	0	0	0
TBHD-5-1	430	4.91	1892	0	0	21	2	96	3	6	0	0	0
TBHD-5-1	440	5.01	2041.5	0	0	14	5	69	6	6	2	0	0
TBHD-5-1	450	5.11	2187.5	0	3	27	6	87	16	8	0	0	1
TBHD-5-1	460	5.21	2331.5	0	0	31	3	68	12	5	2	0	1
TBHD-5-1	470	5.31	2484	0	3	32	4	47	4	9	0	0	2
TBHD-5-1	480	5.41	2641	0	2	30	6	59	12	8	3	0	0
TBHD-5-1	490	5.51	2872.5	0	6	44	4	45	2	11	2	0	0
TBHD-5-1	500	5.61	3116	0	3	43	3	51	12	8	3	0	0
TBHD-5-1	510	5.71	3361.5	0	1	24	3	38	8	10	4	0	0
TBHD-5-1	520	5.81	3604.5	0	3	37	3	34	10	7	1	1	0
TBHD-5-1	530	5.91	3836.5	0	1	39	4	34	6	3	1	0	0
TBHD-5-1	540	6.01	4056.5	0	3	28	6	16	4	9	4	1	0
TBHD-5-1	550	6.11	4287	1	3	30	2	45	10	1	0	0	1
TBHD-5-1	560	6.21	4462	0	3	22	6	21	10	5	1	0	0
TBHD-5-1	570	6.31	4621	0	2	27	7	23	10	7	2	0	1
TBHD-5-1	580	6.41	4768	0	5	17	2	8	8	0	2	0	0
TBHD-5-1	590	6.51	4914.5	0	2	11	0	3	3	2	1	0	0

				Nonarboreal (Herbs/sedges/shrubs)										
Core (Anderson et al., 2008)	Sample ID Depth (cm)	Depth (mbsl)	Age (50% quantile)	Asteraceae	*Chenopodium*	*Galium*	Poaceae	*Ilex*	*Myrica*	Apiaceae	Onagraceae	*Utrica*	*Hippuris*	*Zea mays*
TV99-3	10	2.84	204	35	30	0	13	6	0	0	0	0	0	0
TV99-3	20	2.94	302.5	25	27	0	11	5	0	1	0	0	0	0
TV99-3	40	3.14	486	13	9	0	14	2	0	0	0	0	0	0
TV99-3	50	3.24	590	6	6	0	4	0	0	0	0	0	0	0
TV99-3	60	3.34	792	10	15	0	4	4	0	0	0	0	0	0
TV99-3	70	3.44	1019	5	23	0	7	4	0	0	0	0	0	0
TV99-3	80	3.54	1232.5	12	15	0	3	11	0	0	0	0	0	0
TV99-3	90	3.64	1428	2	11	0	8	7	0	0	0	0	0	0
TV99-3	100	3.74	1626	22	14	0	14	4	4	0	0	0	0	0
TV99-3	110	3.84	1819	24	15	0	14	10	1	0	0	0	0	0
TV99-3	120	3.94	2015	10	16	0	14	10	0	0	0	0	0	0
TV99-3	130	4.04	2220	13	19	0	16	8	1	1	0	0	0	0
TV99-3	140	4.14	2448.5	20	43	0	20	7	0	0	0	0	0	0
TV99-3	150	4.24	2532	22	44	0	44	12	0	0	0	1	0	0
TV99-3	160	4.34	2593.5	10	37	0	21	11	2	0	0	1	0	0
TV99-3	170	4.44	2659	16	30	0	43	16	0	0	0	0	0	0
TV99-3	180	4.54	2724.5	13	33	0	23	12	3	0	0	0	0	0
TV99-3	190	4.64	2781	17	42	0	42	9	1	1	1	0	0	0
TV99-3	200	4.74	2845.5	20	52	0	35	3	1	0	0	0	0	0

				Arboreal (Trees)									Unidentifiable	
Core (Anderson et al., 2008)	Sample ID Depth (cm)	Depth (mbsl)	Age (50% quantile)	*Acer*	*Alnus*	*Carya*	*Juglans*	*Pinus*	*Quercus*	*Ostrya virginiana*	*Salix*	*Taxodium*	unknown 6	Triporate 2
TV99-3	10	2.84	204	0	5	15	10	111	59	7	2	0	0	3
TV99-3	20	2.94	302.5	0	3	10	11	131	60	11	0	0	0	0
TV99-3	40	3.14	486	0	0	9	9	231	38	5	3	0	1	0
TV99-3	50	3.24	590	0	3	10	15	211	35	3	1	0	0	0
TV99-3	60	3.34	792	0	2	4	2	158	28	5	3	0	0	0
TV99-3	70	3.44	1019	0	0	23	6	298	44	5	0	0	0	0
TV99-3	80	3.54	1232.5	0	0	13	12	283	42	0	2	0	0	0
TV99-3	90	3.64	1428	0	2	12	10	259	71	2	2	0	0	0
TV99-3	100	3.74	1626	1	6	16	5	248	76	0	0	0	0	0
TV99-3	110	3.84	1819	5	6	9	7	101	100	0	0	0	1	0
TV99-3	120	3.94	2015	2	1	13	9	260	77	0	0	0	0	0
TV99-3	130	4.04	2220	4	3	19	9	246	60	0	0	1	2	0
TV99-3	140	4.14	2448.5	0	0	16	8	114	81	3	0	0	0	0
TV99-3	150	4.24	2532	0	1	28	6	249	133	3	4	0	0	0
TV99-3	160	4.34	2593.5	0	1	25	6	90	72	4	1	0	0	0
TV99-3	170	4.44	2659	0	2	26	8	50	94	6	1	0	0	0
TV99-3	180	4.54	2724.5	6	1	19	11	60	71	0	1	0	0	1
TV99-3	190	4.64	2781	4	1	34	7	40	68	4	0	0	3	0
TV99-3	200	4.74	2845.5	2	1	18	3	22	88	3	0	0	1	0

Supplementary Table B2. Full output of SIMPER analyses.

SIMPER

Corpus Christi Bay CCB02-01 Group A (green cluster) compared to Group B (blue cluster)					
Taxon	Av. Dissimilarity	Contrib. %	Cumulative %	Mean abund. 1	Mean abund. 2
Pinus	12.84	30.2	30.2	63.4	12
Quercus	10.98	25.84	56.04	78.7	35
Chenopodium	7.208	16.95	72.99	64.3	35.3
Asteraceae	4.148	9.756	82.75	32.2	16.3
Poaceae	1.706	4.012	86.76	12.6	13
Ilex	0.8888	2.091	88.85	5.38	2.67
Taraxacum officinale	0.8516	2.003	90.85	2.44	5
Helianthus	0.7989	1.879	92.73	3.36	2.67
Carya	0.7467	1.756	94.49	3.36	0.333
Alnus	0.7331	1.724	96.21	5.05	3
Carex	0.3885	0.9138	97.13	1.31	1
Apiaceae	0.3262	0.7674	97.89	1.33	0
Ephedra	0.3176	0.747	98.64	1.33	1.67
Acer	0.1965	0.4621	99.1	0.769	0
Onagraceae	0.1413	0.3323	99.44	0.564	0
Ulmus	0.1161	0.2732	99.71	0.462	0
Celtis	0.08135	0.1914	99.9	0.333	0
Juglans	0.04235	0.09961	100	0.154	0

Trinity Bay TBHD5-1 Group A (green cluster) compared to Group B (blue cluster)					
Taxon	Av. Dissimilarity	Contrib. %	Cumulative %	Mean abund. 1	Mean abund. 2
Pinus	10.53	39.68	39.68	157	105
Quercus	4.157	15.67	55.35	28	8
Chenopodium	2.322	8.753	64.1	19.5	29
Carya	2.061	7.768	71.87	12.2	21
Poaceae	1.637	6.171	78.04	20.5	24.2
Asteraceae	1.333	5.026	83.07	11.6	13.8
Juglans	1.286	4.848	87.91	9.82	3.4
Acer	1.251	4.715	92.63	6.36	0.2
Ostrya virginiana	0.5471	2.062	94.69	1.36	2.8
Ilex	0.4008	1.511	96.2	6.09	5.4
Myrica	0.3522	1.328	97.53	1.45	0.6
Utrica	0.1488	0.561	98.09	0.727	0
Alnus	0.1263	0.4761	98.57	0.727	0.4
Galium	0.09422	0.3551	98.92	0.455	0
Salix	0.09401	0.3543	99.28	0.364	0.2
Zea mays	0.0622	0.2344	99.51	0.182	0.2
Taxodium	0.05213	0.1965	99.71	0.0909	0.2
Apiaceae	0.04035	0.1521	99.86	0	0.2
Hippuris	0.03723	0.1403	100	0.182	0
Onagraceae	0	0	100	0	0

Trinity Bay TV99-3 Group A (green cluster) compared to Group B (pink cluster)					
Taxon	Av. Dissimilarity	Contrib. %	Cumulative %	Mean abund. 1	Mean abund. 2
Pinus	10.78	42.14	42.14	241	194
Quercus	6.003	23.46	65.61	47.7	90.2
Chenopodium	2.033	7.946	73.55	13.3	27.4
Poaceae	1.798	7.028	80.58	7.71	21.6
Asteraceae	1.301	5.087	85.67	10	17.8
Carya	1.011	3.953	89.62	12.4	17
Ilex	0.7329	2.865	92.48	4.57	9.4
Ostrya virginiana	0.5111	1.998	94.48	8.43	7.8
Juglans	0.3463	1.354	95.84	2.86	1.2
Alnus	0.3201	1.251	97.09	1.86	2.2
Acer	0.3125	1.222	98.31	0.143	2.2
Salix	0.2415	0.9441	99.25	1.57	0.8
Myrica	0.115	0.4496	99.7	0.571	0.4
Apiaceae	0.02679	0.1047	99.81	0	0.2
Taxodium	0.02679	0.1047	99.91	0	0.2
Utrica	0.02238	0.08748	100	0	0.2
Zea mays	0	0	100	0	0
Galium	0	0	100	0	0
Hippuris	0	0	100	0	0
Onagraceae	0	0	100	0	0

Corpus Christi Bay CCB02-01 Group B (blue cluster) compared to Group C (purple cluster)					
Taxon	Av. Dissimilarity	Contrib. %	Cumulative %	Mean abund. 1	Mean abund. 2
Asteraceae	10.58	25.54	25.54	16.3	61.5
Chenopodium	10.32	24.93	50.47	35.3	79.1
Quercus	4.879	11.78	62.25	35	48.4
Poaceae	4.443	10.73	72.98	13	30.3
Taraxacum officinale	3.706	8.951	81.93	5	18.3
Pinus	2.226	5.375	87.3	12	18.8
Apiaceae	1.289	3.113	90.41	0	5.42
Alnus	0.7397	1.786	92.2	3	5.17
Helianthus	0.7154	1.728	93.93	2.67	2.92
Ephedra	0.5617	1.357	95.29	1.67	3.5
*Ilex_*	0.5064	1.223	96.51	2.67	3.33
Carya	0.4499	1.086	97.59	0.333	1.92
Carex	0.4197	1.014	98.61	1	1.33
Onagraceae	0.3517	0.8494	99.46	0	1.42
Ulmus	0.131	0.3163	99.77	0	0.5
Juglans	0.0746	0.1802	99.95	0	0.333
Celtis	0.01915	0.04624	100	0	0.0833
Acer	0	0	100	0	0

Trinity Bay TBHD5-1 Group B (blue cluster) compared to Group C (purple cluster)					
Taxon	Av. Dissimilarity	Contrib. %	Cumulative %	Mean abund. 1	Mean abund. 2
Pinus	12	41.13	41.13	105	53.2
Chenopodium	4.493	15.39	56.52	29	48.5
Carya	2.931	10.04	66.56	21	32.1
Poaceae	2.852	9.772	76.33	24.2	34.7
Asteraceae	2.343	8.025	84.36	13.8	23.2
Ostrya virginiana	1.129	3.868	88.23	2.8	7.5
Quercus	0.9402	3.221	91.45	8	8.8
Ilex	0.7072	2.423	93.87	5.4	6.2
Alnus	0.4503	1.543	95.41	0.4	2.2
Juglans	0.4331	1.484	96.89	3.4	4.1
Salix	0.3863	1.323	98.22	0.2	1.8
Myrica	0.1908	0.6538	98.87	0.6	0.4
Apiaceae	0.08707	0.2983	99.17	0.2	0.3
Utrica	0.06663	0.2283	99.4	0	0.3
Taxodium	0.06067	0.2078	99.61	0.2	0.1
Acer	0.0468	0.1603	99.77	0.2	0
Zea mays	0.04625	0.1585	99.93	0.2	0
Onagraceae	0.02182	0.07474	100	0	0.1
Galium	0	0	100	0	0
Hippuris	0	0	100	0	0

Trinity Bay TV99-3 Group B (pink cluster) compared to Group C (red cluster)					
Taxon	Av. Dissimilarity	Contrib. %	Cumulative %	Mean abund. 1	Mean abund. 2
Pinus	20.61	60.96	60.96	194	52.4
Quercus	3.294	9.743	70.71	90.2	78.6
Chenopodium	2.598	7.683	78.39	27.4	38.8
Poaceae	2.396	7.086	85.48	21.6	32.8
Carya	1.484	4.389	89.86	17	24.4
Asteraceae	0.8986	2.658	92.52	17.8	15.2
Ilex	0.5948	1.759	94.28	9.4	10.2
Ostrya virginiana	0.4126	1.22	95.5	1.2	3.4
Acer	0.3795	1.122	96.62	2.2	2.4
Juglans	0.3723	1.101	97.73	7.8	7
Alnus	0.2771	0.8194	98.54	2.2	1.2
Myrica	0.1772	0.5242	99.07	0.4	1.4
Salix	0.1604	0.4744	99.54	0.8	0.6
Apiaceae	0.04866	0.1439	99.69	0.2	0.2
Utrica	0.04511	0.1334	99.82	0.2	0.2
Onagraceae	0.03067	0.0907	99.91	0	0.2
Taxodium	0.02991	0.08847	100	0.2	0
Zea mays	0	0	100	0	0
Galium	0	0	100	0	0
Hippuris	0	0	100	0	0

Corpus Christi Bay CCB02-01 Group C (purple cluster) compared to Group D (red cluster)					
Taxon	Av. dissim	Contrib. %	Cumulative %	Mean abund. 1	Mean abund. 2
Chenopodium	26.68	58.33	58.33	79.1	251
Asteraceae	5.04	11.02	69.35	61.5	34.4
Quercus	4.354	9.518	78.86	48.4	21.7
Poaceae	2.608	5.702	84.57	30.3	37.9
Taraxacum officinale	2.388	5.221	89.79	18.3	3.86
Pinus	1.162	2.541	92.33	18.8	16.6
Apiaceae	0.7333	1.603	93.93	5.42	3.43
Alnus	0.5602	1.225	95.15	5.17	1.71
Ephedra	0.4837	1.058	96.21	3.5	0.143
Ilex	0.4141	0.9052	97.12	3.33	1.43
Helianthus	0.3751	0.82	97.94	2.92	1.29
Carya	0.35	0.7651	98.7	1.92	0.857
Carex	0.2173	0.4752	99.18	1.33	0.429
Onagraceae	0.2167	0.4738	99.65	1.42	0
Ulmus	0.07847	0.1716	99.82	0.5	0
Juglans	0.04776	0.1044	99.93	0.333	0
Acer	0.02095	0.04579	99.97	0	0.143
Celtis	0.01219	0.02665	100	0.0833	0

Trinity Bay TBHD5-1 Group C (purple cluster) compared to Group D (red cluster)					
Taxon	Av. dissim	Contrib. %	Cumulative %	Mean abund. 1	Mean abund. 2
Chenopodium	8.711	28.52	28.52	48.5	90.3
Pinus	7.206	23.59	52.12	53.2	19.3
Asteraceae	5.124	16.78	68.9	23.2	47.8
Carya	2.515	8.234	77.13	32.1	22.5
Poaceae	2.405	7.875	85.01	34.7	41.7
Ilex	1.179	3.861	88.87	6.2	10.8
Ostrya virginiana	0.9115	2.985	91.85	7.5	4
Quercus	0.8846	2.896	94.75	8.8	7.5
Juglans	0.5223	1.71	96.46	4.1	3.83
Alnus	0.3522	1.153	97.61	2.2	3
Salix	0.2954	0.9674	98.58	1.8	1.67
Myrica	0.1302	0.4263	99.01	0.4	0.5
Apiaceae	0.1091	0.3574	99.36	0.3	0.333
Utrica	0.08985	0.2942	99.66	0.3	0.333
Taxodium	0.052	0.1703	99.83	0.1	0.167
Acer	0.03264	0.1069	99.93	0	0.167
Onagraceae	0.02014	0.06593	100	0.1	0
Zea mays	0	0	100	0	0
Galium	0	0	100	0	0
Hippuris	0	0	100	0	0

APPENDIX C
CHAPTER 4 SUPPLEMENTARY TABLES

Supplementary Table C1. Complete quantiles from age model.

Baffin Bay, TX Core BB07-11
Bchron Summary

Sample Core Depth (cm)	(m)	2.50%	10%	50%	90%	97.50%
1346	13.46	5566	5866	6303	6795	7014
1351	13.51	5580	5890	6326	6818	7039
1366	13.66	5656	5958	6395	6882	7104
1376	13.76	5696	6014	6435	6919	7144
1386	13.86	5736	6065	6488	6959	7205
1396	13.96	5779	6116	6537	6992	7238
1406	14.06	5844	6163	6583	7047	7280
1416	14.16	5882	6209	6631	7078	7317
1426	14.26	5918	6253	6678	7118	7357
1436	14.36	5946	6300	6728	7154	7390
1446	14.46	5992	6342	6776	7203	7416
1456	14.56	6068	6386	6833	7239	7448
1500	15.00	6284	6619	7058	7417	7601
1510	15.10	6351	6681	7109	7453	7636
1520	15.20	6460	6742	7163	7495	7676
1530	15.30	6587	6806	7217	7553	7720
1540	15.40	6678	6881	7288	7622	7784
1550	15.50	6755	6998	7368	7702	7866
1560	15.60	6883	7103	7469	7821	8019
1570	15.70	6964	7180	7540	7899	8074
1580	15.80	7065	7255	7605	7964	8148
1652	16.52	7530	7735	8070	8404	8575
1662	16.62	7604	7799	8143	8460	8647
1672	16.72	7717	7877	8210	8542	8736
1682	16.82	7810	7955	8290	8620	8808
1692	16.92	7918	8078	8399	8749	8931
1702	17.02	8094	8229	8543	8887	9058
1712	17.12	8191	8347	8691	9027	9233
1722	17.22	8281	8427	8827	9220	9497
1732	17.32	8375	8518	8983	9436	9683
1742	17.42	8434	8594	9063	9518	9926
1750	17.50	8472	8628	9101	9590	10020

Supplementary Table C2. Complete palynological counts.

Baffin Bay, TX Raw Counts		Sample Core Depth		Bchron Age	Herbs/Grasses/Sedges/Shrubs								
	Sample ID	(cm)	(m)	(50% quantile)	Asteraceae	*Chenopodium*	*Galium*	Poaceae	*Ilex*	*Ephedra*	Apiaceae	Onagraceae	*Carex*
BB07-11	44' 5cm	1346.00	13.46	6303	48	49	0	35	17	6	0	0	0
BB07-11	44' 10cm	1351.00	13.51	6326	28	23	0	41	3	1	0	1	1
BB07-11	44' 25cm	1366.00	13.66	6395	75	63	0	48	10	3	0	0	3
BB07-11	44' 35cm	1376.00	13.76	6435	73	56	0	43	13	2	1	0	3
BB07-11	44' 45cm	1386.00	13.86	6488	52	47	0	48	8	1	1	0	5
BB07-11	44' 55cm	1396.00	13.96	6537	45	62	0	36	11	1	0	0	6
BB07-11	44' 65cm	1406.00	14.06	6583	27	51	0	29	9	1	2	0	4
BB07-11	44' 75cm	1416.00	14.16	6631	54	62	0	39	18	1	0	0	9
BB07-11	44' 85cm	1426.00	14.26	6678	51	76	0	42	13	2	0	0	5
BB07-11	44' 95cm	1436.00	14.36	6728	52	65	0	47	6	1	0	0	3
BB07-11	44' 105cm	1446.00	14.46	6776	45	65	0	45	5	1	0	0	11
BB07-11	44' 115cm	1456.00	14.56	6833	39	66	0	48	7	3	2	0	8
BB07-11	49' 6cm	1499.50	15.00	7058	43	46	1	45	3	1	0	0	6
BB07-11	49' 16cm	1509.50	15.10	7109	33	32	1	46	3	0	0	0	6
BB07-11	49' 24cm	1519.50	15.20	7163	23	33	1	54	10	0	1	0	6
BB07-11	49' 36cm	1529.50	15.30	7217	61	54	0	78	10	0	0	0	9
BB07-11	49' 46cm	1539.50	15.40	7288	49	47	1	52	8	2	1	0	7
BB07-11	49' 56cm	1549.50	15.50	7368	32	33	1	71	3	1	1	0	8
BB07-11	49' 66cm	1559.50	15.60	7469	30	43	1	34	4	1	1	0	5
BB07-11	49' 76cm	1569.50	15.70	7540	22	22	0	26	2	2	1	0	4
BB07-11	49' 86cm	1579.50	15.80	7605	26	19	0	29	4	0	2	0	2
BB07-11	54' 6cm	1651.90	16.52	8070	26	67	0	36	4	1	0	0	6
BB07-11	54' 16cm	1661.90	16.62	8143	31	28	0	38	1	0	1	0	5
BB07-11	54' 26cm	1671.90	16.72	8210	23	41	0	20	6	4	0	0	4
BB07-11	54' 36cm	1681.90	16.82	8290	36	53	0	34	7	1	0	0	5
BB07-11	54' 46cm	1691.90	16.92	8399	48	39	0	32	4	0	0	0	4
BB07-11	54' 56cm	1701.90	17.02	8543	55	33	0	26	5	2	1	0	6
BB07-11	54' 66cm	1711.90	17.12	8691	64	54	0	31	10	4	4	0	2
BB07-11	54' 76cm	1721.90	17.22	8827	80	65	0	49	5	1	1	0	8
BB07-11	54' 86cm	1731.90	17.32	8983	74	78	1	69	9	2	0	0	9
BB07-11	54' 96cm	1741.90	17.42	9063	73	76	2	51	6	1	3	0	8
BB07-11	54' 104cm	1749.90	17.50	9101	70	70	1	46	8	2	3	0	17

Baffin Bay, TX
Raw Counts

	Sample ID	Sample Core Depth		Bchron Age	Trees											Spores	Pollen and Spore Total
		(cm)	(m)	(50% quantile)	*Acer*	*Alnus*	*Carya*	*Juglans*	*Pinus*	*Quercus*	*Salix*	*Taxodium*	*Ulmus*	*Myrica*	*Corylus*		
BB07-11	44' 5cm	1346.00	13.46	6303	8	14	3	0	42	55	0	0	1	2	1	0	281
BB07-11	44' 10cm	1351.00	13.51	6326	2	3	1	0	31	52	0	0	0	0	0	1	188
BB07-11	44' 25cm	1366.00	13.66	6395	5	9	2	0	40	70	2	0	0	0	0	0	330
BB07-11	44' 35cm	1376.00	13.76	6435	0	6	1	0	22	45	3	0	0	0	0	0	268
BB07-11	44' 45cm	1386.00	13.86	6488	4	8	0	1	27	59	0	0	0	0	0	1	262
BB07-11	44' 55cm	1396.00	13.96	6537	0	7	2	1	23	55	1	0	1	0	0	1	252
BB07-11	44' 65cm	1406.00	14.06	6583	3	1	0	0	28	69	0	0	2	0	0	1	227
BB07-11	44' 75cm	1416.00	14.16	6631	3	5	1	0	31	68	4	0	0	1	0	1	297
BB07-11	44' 85cm	1426.00	14.26	6678	0	9	0	0	40	81	5	0	0	0	3	1	328
BB07-11	44' 95cm	1436.00	14.36	6728	0	4	1	2	33	55	1	0	0	0	1	0	271
BB07-11	44' 105cm	1446.00	14.46	6776	0	4	0	0	22	65	6	0	0	0	0	0	269
BB07-11	44' 115cm	1456.00	14.56	6833	0	1	0	1	29	69	1	0	0	0	0	0	274
BB07-11	49' 6cm	1499.50	15.00	7058	0	0	1	0	18	36	0	0	0	0	0	0	200
BB07-11	49' 16cm	1509.50	15.10	7109	0	2	0	0	46	23	0	0	0	0	0	1	193
BB07-11	49' 24cm	1519.50	15.20	7163	0	2	0	0	12	33	0	0	0	0	0	0	175
BB07-11	49' 36cm	1529.50	15.30	7217	0	10	1	0	19	44	0	0	0	0	0	0	286
BB07-11	49' 46cm	1539.50	15.40	7288	0	4	0	0	12	27	0	0	0	0	0	0	210
BB07-11	49' 56cm	1549.50	15.50	7368	0	8	0	1	20	40	0	1	0	0	0	0	220
BB07-11	49' 66cm	1559.50	15.60	7469	0	5	0	3	7	28	0	0	0	0	0	0	162
BB07-11	49' 76cm	1569.50	15.70	7540	0	5	0	0	12	23	0	0	0	0	0	0	119
BB07-11	49' 86cm	1579.50	15.80	7605	0	2	0	0	9	13	0	0	0	0	0	0	106
BB07-11	54' 6cm	1651.90	16.52	8070	2	7	1	0	14	38	4	0	0	0	2	0	208
BB07-11	54' 16cm	1661.90	16.62	8143	0	2	0	0	13	33	0	0	0	0	0	0	152
BB07-11	54' 26cm	1671.90	16.72	8210	0	1	0	0	7	29	1	0	0	0	1	0	137
BB07-11	54' 36cm	1681.90	16.82	8290	0	4	0	0	12	40	3	0	0	0	0	1	196
BB07-11	54' 46cm	1691.90	16.92	8399	0	3	0	0	2	19	2	0	0	0	0	1	154
BB07-11	54' 56cm	1701.90	17.02	8543	0	7	0	0	11	46	0	0	0	0	0	0	192
BB07-11	54' 66cm	1711.90	17.12	8691	0	6	0	0	15	42	0	0	0	0	0	0	232
BB07-11	54' 76cm	1721.90	17.22	8827	0	4	1	0	23	53	0	0	0	0	1	0	291
BB07-11	54' 86cm	1731.90	17.32	8983	0	2	0	0	21	38	1	0	0	0	0	0	304
BB07-11	54' 96cm	1741.90	17.42	9063	0	4	0	0	30	51	1	0	0	0	0	0	306
BB07-11	54' 104cm	1749.90	17.50	9101	0	5	1	0	26	42	1	0	0	0	0	0	292

Baffin Bay, TX
Raw Counts

		Sample Core Depth		Bchron Age	Dinoflagellates						
	Sample ID	(cm)	(m)	(50% quantile)	*Polysphaeridium zoharyi*	*Spiniferites* spp.	*Nematosphaeropsis rigida*	*Lingulodinium machaerophorum*	*Tuberculodinium vancamppoae*	*Operculodinium centrocarpum*	Dinoflagellate Total
BB07-11	44' 5cm	1346.00	13.46	6303	45	8	3	0	0	0	56
BB07-11	44' 10cm	1351.00	13.51	6326	108	13	4	1	0	0	126
BB07-11	44' 25cm	1366.00	13.66	6395	66	4	5	2	0	1	78
BB07-11	44' 35cm	1376.00	13.76	6435	75	6	2	0	0	0	83
BB07-11	44' 45cm	1386.00	13.86	6488	90	12	0	3	1	1	107
BB07-11	44' 55cm	1396.00	13.96	6537	81	5	0	3	3	0	92
BB07-11	44' 65cm	1406.00	14.06	6583	73	10	0	3	3	1	90
BB07-11	44' 75cm	1416.00	14.16	6631	49	4	1	2	0	1	57
BB07-11	44' 85cm	1426.00	14.26	6678	23	11	0	0	0	1	35
BB07-11	44' 95cm	1436.00	14.36	6728	64	5	0	2	4	0	75
BB07-11	44' 105cm	1446.00	14.46	6776	43	4	0	1	1	0	49
BB07-11	44' 115cm	1456.00	14.56	6833	47	3	0	2	5	0	57
BB07-11	49' 6cm	1499.50	15.00	7058	98	5	0	1	3	0	107
BB07-11	49' 16cm	1509.50	15.10	7109	146	5	0	1	1	0	153
BB07-11	49' 24cm	1519.50	15.20	7163	110	21	0	8	9	0	148
BB07-11	49' 36cm	1529.50	15.30	7217	40	14	0	0	3	0	57
BB07-11	49' 46cm	1539.50	15.40	7288	77	26	0	4	13	0	120
BB07-11	49' 56cm	1549.50	15.50	7368	79	18	0	4	3	0	104
BB07-11	49' 66cm	1559.50	15.60	7469	135	18	0	16	1	0	170
BB07-11	49' 76cm	1569.50	15.70	7540	173	16	0	6	7	3	205
BB07-11	49' 86cm	1579.50	15.80	7605	175	21	0	13	5	2	216
BB07-11	54' 6cm	1651.90	16.52	8070	180	6	0	0	0	3	189
BB07-11	54' 16cm	1661.90	16.62	8143	155	9	0	2	2	2	170
BB07-11	54' 26cm	1671.90	16.72	8210	160	16	1	0	0	0	177
BB07-11	54' 36cm	1681.90	16.82	8290	140	16	0	0	0	1	157
BB07-11	54' 46cm	1691.90	16.92	8399	150	21	0	0	2	4	177
BB07-11	54' 56cm	1701.90	17.02	8543	115	15	0	2	2	2	136
BB07-11	54' 66cm	1711.90	17.12	8691	105	12	0	2	1	0	120
BB07-11	54' 76cm	1721.90	17.22	8827	32	15	0	1	1	0	49
BB07-11	54' 86cm	1731.90	17.32	8983	4	46	0	1	1	2	54
BB07-11	54' 96cm	1741.90	17.42	9063	4	11	0	2	0	0	17
BB07-11	54' 104cm	1749.90	17.50	9101	9	28	0	1	3	0	41

Baffin Bay, TX
Raw Counts

		Sample Core Depth		Bchron Age		Reworked		Concentration Data					
	Sample ID	(cm)	(m)	(50% quantile)	Palynomorph Total	Pollen	Dinoflagellates	Lycopodium counted	Dry sample weight (g)	Lycopodium tablet	Lycopodium tablet batch #3862	Pollen and Spore Absolute Abundance	Dinoflagellate Absolute Abundance
BB07-11	44' 5cm	1346.00	13.46	6303	337	39	2	231	4.7	1	9666	2502	499
BB07-11	44' 10cm	1351.00	13.51	6326	314	25	3	125	4.7	1	9666	3093	2073
BB07-11	44' 25cm	1366.00	13.66	6395	408	21	0	212	4.7	1	9666	3201	757
BB07-11	44' 35cm	1376.00	13.76	6435	351	15	0	178	4.7	1	9666	3096	959
BB07-11	44' 45cm	1386.00	13.86	6488	369	9	1	167	5.1	1	9666	2973	1214
BB07-11	44' 55cm	1396.00	13.96	6537	344	12	0	262	4	1	9666	2324	849
BB07-11	44' 65cm	1406.00	14.06	6583	317	10	1	265	4.7	1	9666	1762	698
BB07-11	44' 75cm	1416.00	14.16	6631	354	14	1	261	4.8	1	9666	2292	440
BB07-11	44' 85cm	1426.00	14.26	6678	363	7	1	215	5	1	9666	2949	315
BB07-11	44' 95cm	1436.00	14.36	6728	346	6	1	246	4.9	1	9666	2173	601
BB07-11	44' 105cm	1446.00	14.46	6776	318	11	1	176	5.9	1	9666	2504	456
BB07-11	44' 115cm	1456.00	14.56	6833	331	8	1	179	5.7	1	9666	2596	540
BB07-11	49' 6cm	1499.50	15.00	7058	307	5	0	155	3.3	1	9666	3779	2022
BB07-11	49' 16cm	1509.50	15.10	7109	346	5	2	227	3.3	1	9666	2490	1974
BB07-11	49' 24cm	1519.50	15.20	7163	323	8	2	274	2.5	1	9666	2469	2088
BB07-11	49' 36cm	1529.50	15.30	7217	343	9	1	279	3.4	1	9666	2914	581
BB07-11	49' 46cm	1539.50	15.40	7288	330	11	4	301	2.9	1	9666	2325	1329
BB07-11	49' 56cm	1549.50	15.50	7368	324	19	2	206	3.3	1	9666	3128	1479
BB07-11	49' 66cm	1559.50	15.60	7469	332	12	1	184	5	1	9666	1702	1786
BB07-11	49' 76cm	1569.50	15.70	7540	324	1	1	71	4.5	1	9666	3600	6202
BB07-11	49' 86cm	1579.50	15.80	7605	322	4	1	82	3.4	1	9666	3675	7489
BB07-11	54' 6cm	1651.90	16.52	8070	397	7	0	152	3.5	1	9666	3779	3434
BB07-11	54' 16cm	1661.90	16.62	8143	322	8	0	87	3.5	1	9666	4825	5396
BB07-11	54' 26cm	1671.90	16.72	8210	314	5	0	155	4.3	1	9666	1987	2567
BB07-11	54' 36cm	1681.90	16.82	8290	353	12	0	130	2.7	1	9666	5398	4324
BB07-11	54' 46cm	1691.90	16.92	8399	331	19	1	87	2.5	1	9666	6844	7866
BB07-11	54' 56cm	1701.90	17.02	8543	328	6	1	84	5.1	1	9666	4332	3069
BB07-11	54' 66cm	1711.90	17.12	8691	352	4	0	98	3	1	9666	7628	3945
BB07-11	54' 76cm	1721.90	17.22	8827	340	24	2	134	2.7	1	9666	7774	1309
BB07-11	54' 86cm	1731.90	17.32	8983	358	8	1	242	2.8	1	9666	4337	770
BB07-11	54' 96cm	1741.90	17.42	9063	323	12	1	239	5.3	1	9666	2335	130
BB07-11	54' 104cm	1749.90	17.50	9101	333	9	3	236	5.7	1	9666	2098	295

Supplementary Table C3. SIMPER results of clusters.

OVERALL 5-group SIMPER analysis

Taxon	Av. dissim	Contrib. %	Cumulative %	Mean abund. 1	Mean abund. 2	Mean abund. 3	Mean abund. 4	Mean abund. 5
Asteraceae	4.968	19.24	19.24	49.1	40.2	26.3	50.8	74.3
Quercus	4.913	19.03	38.28	61.9	33.8	27.3	36.8	46
Chenopodium	4.749	18.4	56.67	57.1	40.8	36.7	44.8	72.3
Poaceae	3.6	13.94	70.62	41.8	57.7	30.5	30.8	53.8
Pinus	3.228	12.5	83.12	30.7	21.2	10.3	10	25
Ilex	1.035	4.01	87.13	10	6.17	3.5	6.5	7
Carex	0.7845	3.039	90.17	4.83	7	4.33	4.25	10.5
Alnus	0.7454	2.888	93.06	5.92	4.33	3.67	5	3.75
Salix	0.3431	1.329	94.39	1.92	0	0.833	1.25	0.75
Ephedra	0.3093	1.198	95.58	1.92	0.667	1.33	1.75	1.5
Acer	0.2902	1.124	96.71	2.08	0	0.333	0	0
Apiaceae	0.2458	0.9521	97.66	0.5	0.5	0.833	1.25	1.75
Carya	0.1496	0.5794	98.24	0.917	0.333	0.167	0	0.5
Gallium	0.1259	0.4875	98.73	0	0.833	0.167	0	1
Juglans	0.1085	0.4203	99.15	0.417	0.167	0.5	0	0
Corylus	0.1001	0.3876	99.54	0.417	0	0.5	0	0.25
Ulmus	0.04649	0.1801	99.72	0.333	0	0	0	0
Myrica	0.03187	0.1234	99.84	0.25	0	0	0	0
Taxodium	0.01509	0.05845	99.9	0	0.167	0	0	0
Onagraceae	0.01341	0.05193	99.95	0.0833	0	0	0	0

Pairwise SIMPER analysis gr. 5 vs. 4

Taxon	Av. dissim	Contrib. %	Cumulative %	Mean abund. 5	Mean abund. 4
Chenopodium	5.667	23.49	23.49	72.3	44.8
Asteraceae	4.862	20.15	43.64	74.3	50.8
Poaceae	4.679	19.39	63.04	53.8	30.8
Pinus	3.117	12.92	75.95	25	10
Quercus	2.441	10.12	86.07	46	36.8
Carex	1.275	5.283	91.35	10.5	4.25
Ilex	0.4854	2.012	93.37	7	6.5
Alnus	0.3783	1.568	94.93	3.75	5
Apiaceae	0.3554	1.473	96.41	1.75	1.25
Salix	0.257	1.065	97.47	0.75	1.25
Ephedra	0.2519	1.044	98.52	1.5	1.75
Gallium	0.2027	0.8402	99.36	1	0
Carya	0.1035	0.4292	99.79	0.5	0
Corylus	0.05183	0.2148	100	0.25	0
Juglans	0	0	100	0	0
Acer	0	0	100	0	0
Myrica	0	0	100	0	0
Ulmus	0	0	100	0	0
Taxodium	0	0	100	0	0
Zea mays	0	0	100	0	0
Onagraceae	**0**	**0**	**100**	**0**	**0**

Pairwise SIMPER analysis gr. 4 vs. 3

Taxon	Av. dissim	Contrib. %	Cumulative %	Mean abund. 4	Mean abund. 3
Asteraceae	7.204	30.49	30.49	50.8	26.3
Chenopodium	5.188	21.96	52.46	44.8	36.7
Quercus	4.264	18.05	70.51	36.8	27.3
Poaceae	1.712	7.246	77.75	30.8	30.5
Pinus	1.398	5.918	83.67	10	10.3
Ilex	0.9284	3.93	87.6	6.5	3.5
Alnus	0.7449	3.153	90.76	5	3.67
Ephedra	0.4659	1.972	92.73	1.75	1.33
Salix	0.4454	1.885	94.61	1.25	0.833
Carex	0.4403	1.864	96.48	4.25	4.33
Apiaceae	0.3837	1.624	98.1	1.25	0.833
Juglans	0.1417	0.6	98.7	0	0.5
Corylus	0.1344	0.569	99.27	0	0.5
Acer	0.08353	0.3536	99.62	0	0.333
Gallium	0.04724	0.2	99.82	0	0.167
Carya	0.04177	0.1768	100	0	0.167
Myrica	0	0	100	0	0
Ulmus	0	0	100	0	0
Taxodium	0	0	100	0	0
Zea mays	0	0	100	0	0
Onagraceae	0	0	100	0	0

Pairwise SIMPER analysis gr. 3 vs. 2

Taxon	Av. dissim	Contrib. %	Cumulative %	Mean abund. 3	Mean abund. 2
Poaceae	7.483	28.65	28.65	30.5	57.7
Chenopodium	4.41	16.88	45.54	36.7	40.8
Asteraceae	4.011	15.36	60.9	26.3	40.2
Pinus	3.195	12.23	73.13	10.3	21.2
Quercus	2.822	10.8	83.93	27.3	33.8
Ilex	1.019	3.902	87.84	3.5	6.17
Alnus	0.9077	3.475	91.31	3.67	4.33
Carex	0.7525	2.881	94.19	4.33	7
Ephedra	0.3491	1.337	95.53	1.33	0.667
Gallium	0.2106	0.8065	96.34	0.167	0.833
Salix	0.2069	0.7923	97.13	0.833	0
Apiaceae	0.1917	0.734	97.86	0.833	0.5
Juglans	0.1652	0.6327	98.49	0.5	0.167
Corylus	0.1274	0.4879	98.98	0.5	0
Carya	0.1019	0.3902	99.37	0.167	0.333
Acer	0.07951	0.3044	99.68	0.333	0
Taxodium	0.04572	0.1751	99.85	0	0.167
Zea mays	0.03859	0.1477	100	0	0.167
Myrica	0	0	100	0	0
Ulmus	0	0	100	0	0
Onagraceae	0	0	100	0	0

Pairwise SIMPER analysis gr. 2 vs. 1

Taxon	Av. dissim	Contrib. %	Cumulative %	Mean abund. 2	Mean abund. 1
Quercus	5.853	23.89	23.89	33.8	61.9
Chenopodium	4.103	16.75	40.64	40.8	57.1
Asteraceae	3.493	14.26	54.89	40.2	49.1
Poaceae	3.321	13.55	68.45	57.7	41.8
Pinus	3.049	12.44	80.89	21.2	30.7
Ilex	1.106	4.513	85.4	6.17	10
Alnus	0.8808	3.595	89	4.33	5.92
Carex	0.7017	2.864	91.86	7	4.83
Acer	0.431	1.759	93.62	0	2.08
Salix	0.3824	1.561	95.18	0	1.92
Ephedra	0.294	1.2	96.38	0.667	1.92
Gallium	0.1789	0.7302	97.11	0.833	0
Carya	0.1783	0.7279	97.84	0.333	0.917
Apiaceae	0.1414	0.5773	98.42	0.5	0.5
Juglans	0.09861	0.4025	98.82	0.167	0.417
Corylus	0.08058	0.3289	99.15	0	0.417
Ulmus	0.07304	0.2981	99.45	0	0.333
Myrica	0.05025	0.2051	99.65	0	0.25
Taxodium	0.03422	0.1397	99.79	0.167	0
Zea mays	0.03006	0.1227	99.91	0.167	0
Onagraceae	0.02093	0.08543	100	0	0.0833

VITA

Shannon Ferguson was born in Georgia and attended Georgia Southern University to obtain her Bachelor of Science degree in Geology. There she was introduced to palynology by her undergraduate research advisor Dr. Fredrick Rich. Dr. Rich became an invaluable mentor and encouraged her to purse her M.S. degree. After completing her B.S. in Geology, she continued her academic studies as a M.S. student at Louisiana State University in Baton Rouge, Louisiana with Dr. Sophie Warny. Here she continued focusing on palynology with a new focus on dinoflagellate cysts. After completing her M.S. in Geology she was happy to stay in school a bit longer to pursue her Ph.D. at Louisiana State University this time combining her knowledge on pollen and dinoflagellate cysts. During her Ph.D. she interned with Homeland Security for two summers where she learned about forensic palynology and discovered that she really enjoyed the practical applications of the science. After completion of her Ph.D. program, she will begin work at the Homeland Security Laboratory as a Forensic Palynologist.